Volume 13, Number 5, 2022 ISSN 1847-6996

FERIT
FACULTY OF ELECTRICAL ENGINEERING, COMPUTER SCIENCE AND INFORMATION TECHNOLOGY **OSIJEK**

**IJECES** International Journal of Electrical and Computer Engineering Systems

# International Journal of Electrical and Computer Engineering Systems

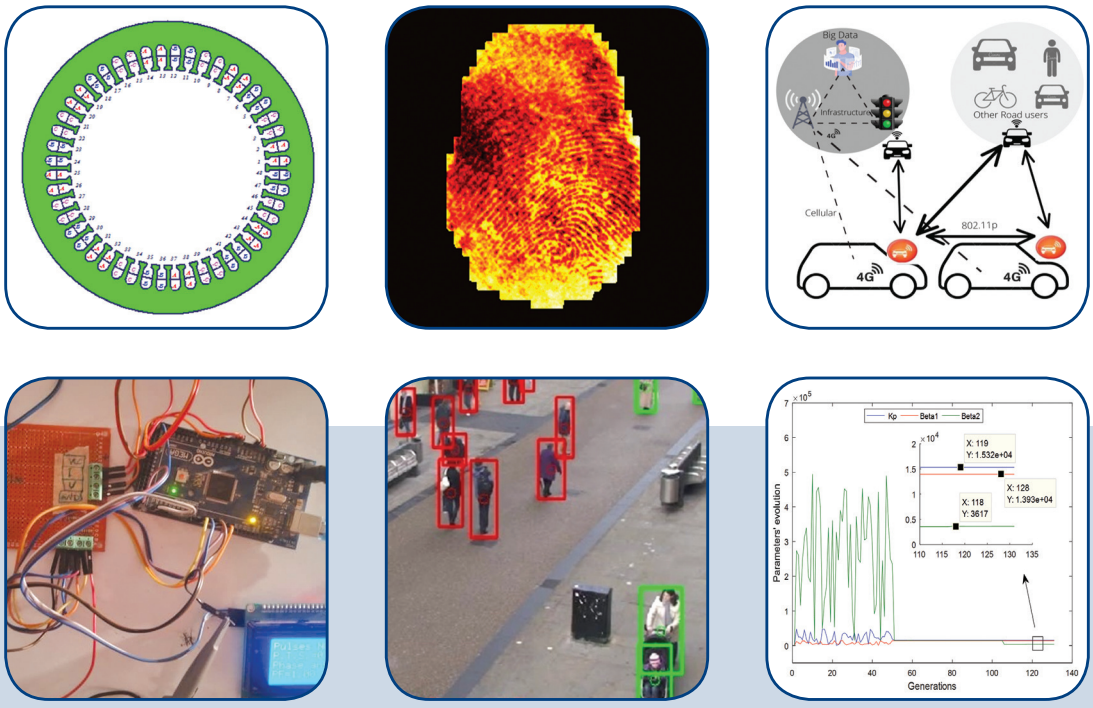

ISSN: 1847-6996

# INTERNATIONAL JOURNAL OF ELECTRICAL AND COMPUTER ENGINEERING SYSTEMS

Published by Faculty of Electrical Engineering, Computer Science and Information Technology Osijek, Josip Juraj Strossmayer University of Osijek, Croatia

Osijek, Croatia | Volume 13, Number 5, 2022 | Pages 331 - 415

The International Journal of Electrical and Computer Engineering Systems is published with the financial support of the Ministry of Science and Education of the Republic of Croatia

**CONTACT**

**International Journal of Electrical and Computer Engineering Systems (IJECES)**

Faculty of Electrical Engineering, Computer Science and Information Technology Osijek,
Josip Juraj Strossmayer University of Osijek, Croatia
Kneza Trpimira 2b, 31000 Osijek, Croatia
Phone: +38531224600, Fax: +38531224605
e-mail: ijeces@ferit.hr

**Subscription Information**

The annual subscription rate is 50€ for individuals, 25€ for students and 150€ for libraries.
Giro account: 2390001 - 1100016777,
Croatian Postal Bank



**Journal is referred in:**

- Scopus
- Web of Science Core Collection (Emerging Sources Citation Index - ESCI)
- Google Scholar
- CiteFactor
- Genamics
- Hrčak
- Ulrichweb
- Reaxys
- Embase
- Engineering Village

**Bibliographic Information**

Commenced in 2010.
ISSN: 1847-6996
e-ISSN: 1847-7003
Published: quarterly
Circulation: 300

**IJECES online**

https://ijeces.ferit.hr

# TABLE OF CONTENTS

# Enhanced convnet based Latent Finger Print Recognition

Original Scientific Paper

**R. Jhansi Rani**
Sathyabama Institute of Science and Technology,
Semmancheri, Chennai, Tamilnadu, 600119, India
jhansiranir12@gmail.com

**K. Vasanth**
Vidya Jyothi Institute of Technology,
Telangana, Hyderabad-500075, India
vasanthkpapers@gmail.com

***Abstract*** *– Latent finger print recognition plays an important role in forensic, criminal cases etc. The latent images will not be recognised easily since they are impartial images, which find difficult to match with the registered database. Due to noisy images, it is very difficult for recognition. Autoencoder plays an important role in pre-processing the latent image. ConvNetbased method is an efficient approach used for latent image recognition. For each minutiae extraction, ConvNet descriptor is performed. Both minutiae and texture matcher is considered for comparison. This technique is compared with existing methods which shows, that the proposed method provides a higher accuracy than the existing methods like CNN, skeleton approach nonlinear mapping and product quantization. The proposed method provides an accuracy of 76.4%, 80.4% and 86.4% for rank1,5 and 10 respectively.*

***Keywords****: convnet, autoencoder, texture template, minutiae extraction*

## 1. INTRODUCTION

Latent fingerprints, a kind of fingerprints which are taken from the finger skin impersonations at the criminality section, have been assumed to find distrusted convicts for a stretched time period. Real forensic cases, have greatly fewer sufficient result. Due to advanced technologies and experts, the difficulties present in recognition of finger prints is minimized. Quality of the image plays an important role in identification task. Latent prints are a minor section of entire finger print pattern. Latent images are taken from the surface using chemical reaction [2]. These latent prints, even if not of good quality, it is not possible for the expert to request the culprit for a clear print. Moreover, these latent prints are very much helpful in criminal investigations [6]. The fingerprint are captured using a camera from a distance. As a result, this fingerprint will be a zoomed image. It is necessary to enhance the image for further processing [20].

For enhancing the images, directional median filter [21] and an improved version called directional weighted median filter [22] is presented. Fourier transformation [23] is also used for enhancement. Hough transform [24] will provide the touchless technique of enhancing the image.

Latent recognition is done using physically pointed minutiae and region of interest [8]. The accuracy is improved using skeleton approach [9] and ridge flowing. But this technique consumes more time. Further the number of features used for mapping purpose is reduced and improvement is achieved using various techniques in [10], [11], [12]. A non-minutia latent fingerprint registration method, calculates the spatial transformation among two fingerprints [7]. Various feature extraction techniques are reviewed [5]. Latent fingerprint recognition algorithm uses Convolutional Neural Networks [4] to find out the templates for signifying the latent. Both rolled and slap images are taken and context switch is used for fusing the algorithms [1]. The physically marked structures [3], which consist of the Region of Interest (ROI), singular points, and minutiae is considered. Orientation field is calculated using the physically marked structures. Gabor filters plays an important role in enhancement. An approach using resemblance of learned demonstrations and interrelated patches is also provided. A deep learning network helps to study the optimized illustrations of latent im-

ages. CNN technique is used as a distance metric learning [13]. A round-robin technique [14] is used in examining the fingerprint data, resulting in good quality confidence scores.

From all the papers surveyed the following shortcomings are observed.

- Accuracy gets affected by more noise in images.
- The techniques consume more time.
- Accuracy will be affected when the patch size is varied.
- The contributions of the proposed work which overcomes these drawbacks are
- An auto encoder is used to improve the accuracy in extracting ridge flow and spacing.
- Minutiae template and ConvNet-based texture descriptor will increase the accuracy.
- Minutiae template and the texture descriptor are compared with the reference template which further reduces the computational complexity.

## 2. PROPOSED METHOD

The plan of the proposed latent fingerprint identification system is using an enhanced ConvNet based descriptor as shown in Fig. 1.

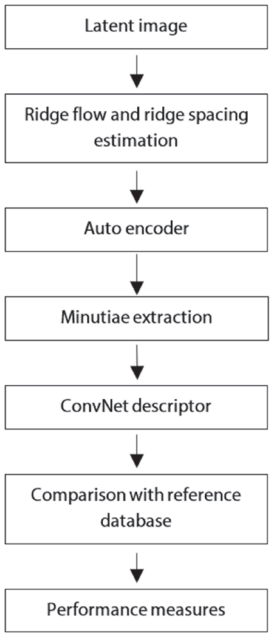


**Fig. 1.** Enhanced ConvNet based descriptor flow diagram

The latent image is subjected to ridge flow and ridge spacing estimation. The estimated ridge spacing is given to auto encoder. The output of auto encoder is subjected to minutiae extraction step. The extracted minutiae are given to ConvNet descriptor whose output is compared with reference database. Finally, the performance measures are estimated.

From the query latent image, the region of interest, ridge flow, ridge spacing are estimated as shown in Fig. 2.

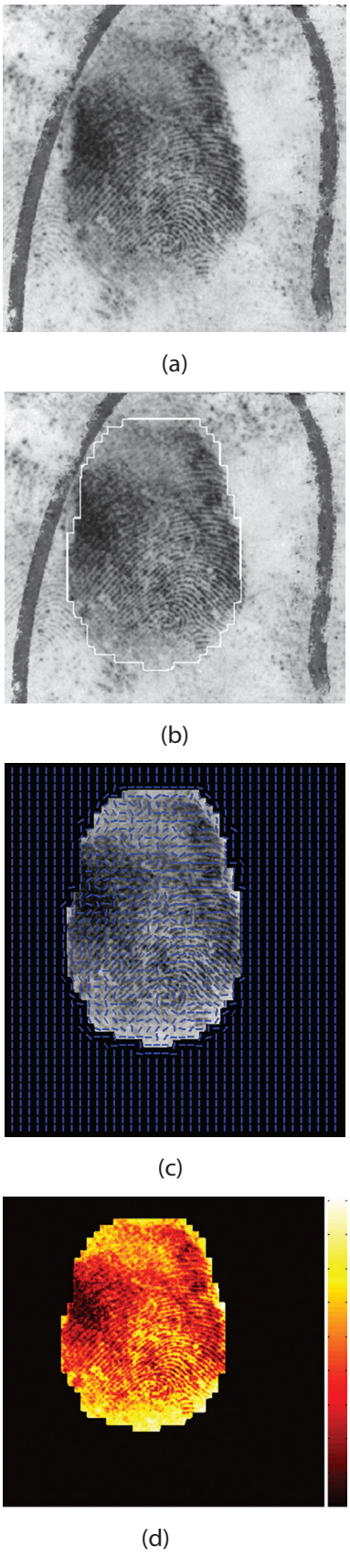

(a)

(b)

(c)

(d)

**Fig. 2.** Ridge quality, ridge flow and ridge spacing estimation (a) Latent finger print image, (b) RPI image (c) ridge flow and (d) ridge spacing shown as heat map

### 2.1 LATENT ENHANCEMENT VIA AUTOENCODER

First the latent image is enhanced to estimate ROI, ridge flow and ridge spacing accurately. The steps involved in latent enhancement is shown in Fig. 3. The ruined latent image is applied to encoder which has 5 convolutional layers, followed by decoder having 5 deconvolutional layer, resulting in enhanced finger print image.

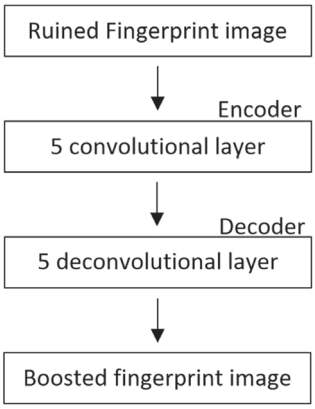


**Fig. 3.** A convolutional autoencoder for latent enhancement

From all the available latent finger print images the auto encoder will separate 3000 good quality fingerprint images (NFIQ 2.07 value > 70) for training purpose. Here the image is divided into overlapping patches each of size 128*128 pixels. Then Gaussian filtering is applied and finally enhanced image is obtained for training the auto encoder [16].

There are 5 layers of convolutional and deconvolutional layers in encoder and decoder respectively. Each layer is having a kernel window 4*4 and size 2. ReLU (Rectified linear Unit) is used in each layer except output layer. The rolled latent image does not provide good result while training the auto encoder. So, texture component of latent image is used in training phase of auto encoder [12]. Table 1 summarizes the architecture of the convolutional autoencoder.

**Table 1.** Summarizes the architecture of the convolutional autoencoder.

| Layer | Size in | Size Out | Kernel |
|---|---|---|---|
| Input | 128×128×1 | - | 4×4,2 |
| Conv 1 | 128×128×1 | 64×64×16 | 4×4,2 |
| Conv 2 | 64×64×16 | 32×32×32 | 4×4,2 |
| Conv 3 | 32×32×32 | 16×16×64 | 4×4,2 |
| Conv 4 | 16×16×16 | 8×8×128 | 4×4,2 |
| Conv 5 | 8×8×128 | 4×4×256 | 4×4,2 |
| DeConv 1 | 4×4×256 | 8×8×128 | 4×4,2 |
| DeConv 2 | 8×8×128 | 16×16×64 | 4×4,2 |
| DeConv 3 | 16×16×64 | 32×32×32 | 4×4,2 |
| DeConv 4 | 32×32×32 | 64×64×16 | 4×4,2 |
| DeConv 5 | 64×64×16 | 128×128×1 | 4×4,2 |

The boosted latents have expressively advanced ridge clarity than initial images

### 2.2 ESTIMATION OF RIDGE FLOW AND SPACING

In dictionary technique, entries of dictionary have various orientations and spacing. For calculating the ridge flow with ridge spacing, the output of the autoencoder is split into 32*32 with overlap of 16*16 pixels. The similarity $S_i$ and element $D_{iis}$ computed as $S_i$=$p.D_i$ $\|p\|+\alpha$ for every patch. In this the value of αis obtained as 200 which is the regularisation function. The dictionary entry which has the highest value of similarity $S_m$ is taken and its orientation and spacing are considered. The ridge quality is the summation of $S_{mand}$ the similarities between the patch with highest similarity and the patch whose ridge quality is to be estimated. The patch with larger ridge quality greater than 0.35 is taken as valid fingerprint patch.

### 2.3 MINUTIAE DETECTION VIA AUTOENCODER

In minutiae detection approach, two minutiae extractor models MinuNet reference and MinuNet Latent are trained. A set of reference minutiae is required to train the network for minutiae extraction. This is a challenging task in poor quality images. Experts can perform the minutiae markup easily. The editing involves, insert, delete and reposition of markup points.

For training MinuNet reference, around 400 fingerprint pairs involving both high and poor quality are taken from the MSP longitudinal fingerprint database [17]. A finger can be selected such that

$$(R_h - R_l) > 70 \quad (1)$$

Where $R_h$ is the highest NFIQ 2.0 value and $R_l$ is the lowest NFIQ 2.0 value. It is observed that from the same finger both low and high-quality image is obtained. To obtain the initial minutiae and its resemblance with the selected fingerprint image pairs, COTS SDK is used.

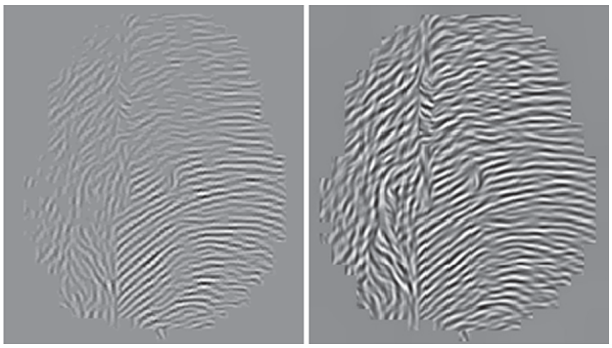

(a) (b)

**Fig. 4.** Latent Image processing: (a) STFT result (b) Autoencoder result

A minutia point $M$ is usually denoted as a triplet $M$ = ($X$, $Y$, $p$), where $X$ and $Y$ denote its location, and $p$ is its

orientation respectively. Using minutia cylinder-code [18], a minutiae set is encoded as a channel heat map and position the extraction of minutiae as a regression problem. For each point (*I, J, K*) response value m (*I, J, K*) calculated as $M(I,J,K) = \sum_{t=1}^{n} c_s\left(\left(X_t,Y_t\right),(I,J)\right).c_o(p_{t,}\frac{2k\pi}{12})$ where first and the second term are the spatial and orientation of minutia respectively.

The Euclidean distance between ($X_t$, $Y_t$), (*I, J*) is given by

$$c_s\left(\left(X_t,Y_t\right),(I,J)\right) = \exp\left(-\frac{\left\|(X_t,Y_t)-(I,J)\right\|^2}{2w_s^2}\right) \quad (2)$$

Here $w_s$ denotes the width of Gaussian. The function of difference in orientation value is given by

$$c_o\left(p_{t,}\frac{2k\pi}{12}\right) = \exp\left(\frac{-D\emptyset\left(p_t,\frac{2k\pi}{12}\right)}{2w_s^2}\right) \quad (3)$$

If $\emptyset_1$ and$\emptyset_2$ are two angles, then orientation difference between them is given as

$$D\emptyset\left(\emptyset_1,\emptyset_2\right) = |\emptyset_1 - \emptyset_2| if -\pi \le \emptyset_1 - \emptyset_2 < \pi \quad (4)$$

$$D\emptyset\left(\emptyset_1,\emptyset_2\right) = 2\pi - |\emptyset_1 - \emptyset_2| otherwise \quad (5)$$

The autoencoder applied for minutiae recognition and latent improvement are similar. The MinuNet reference and Latent, are trained for both the reference and latent images. In case of reference images and latent finger print images, the unprocessed fingerprint and short-time Fourier transform (STFT) are respectively used for training purpose. The model MinuNet Latent is a fine-tuned edition of the form MinuNet reference. Fig. 4. shows the latent image processing result.

Take an image of size $W \times H$ in the inference stage, a $W \times H \times 12$ minutiae map $N$ is obtained from a minutiae detection model. For each location (*I, J, K*) in $N$, if $N$(*I, J, K*) is larger than threshold value and if in its neighbouring it is local maximum a minutia is marked at this location. Minutiae orientation is calculated as

$$\mathrm{F(k-1)}.\frac{\pi}{6} = N(I,J,(K-1)\%12), \mathrm{F(c)}.\frac{\pi}{6} = N(I,J,K) \quad (6)$$

$$\mathrm{F(k+1)}.\frac{\pi}{6} = N(I,J,(K+1)\%12) \quad (7)$$

Where c%d represents c modulo d. Fig. 5. shows the minutiae detection result.

**Fig. 5.** Minutiae detection

### 2.4 MINUTIAE DESCRIPTOR

Based on the image features of neighbours there are numerous attributes in the descriptor. Conv net-based descriptor is used to train the fingerprint patches. Training a set of ConvNets using numerous image patches at changed scales and areas can knowingly increase the recognition performance. Numerous occurrences of areas take out for the same minutia are used to train 14 different ConvNets. Using bilinear interpolation all the patches are resized to 160* 160 pixels. For each and every ConvNet, output of the last layer which is 128-dimension has to be taken as a feature vector. Final descriptor output will be the concatenation of the all the feature vectors [15].

Here in case of training the patches, only the minutiae which have eight or more impressions from the same finger can be considered. The patches which are found locally to these minutiae is considered for ConvNet training. From all the 20 patches, the smaller patch can be resized to 160*160 pixels. In training certain shift and rotation pattern is selected in a random manner. From, the final layer a feature vector of 128-dimension is obtained. Thus, from all the 20 patches, 20 feature vector each of size 128 dimension is taken. The minutiae similarity is given as

$$S_{minutiae} = \sum_{I=1}^{N} De\ S(I_1,I_2) \quad (8)$$

Where DeS() is the descriptor similarity between two descriptors. Fig. 6. shows the minutiae descriptor result.

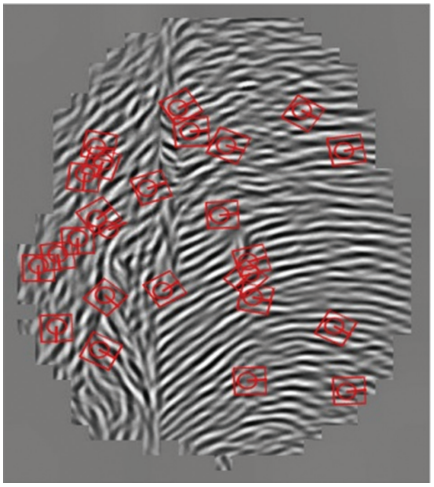

**Fig. 6.** ConvNet Minutiae descriptors

### 2.5 COMPARISON OF LATENT WITH ROLLED

Three comparison algorithms are framed:

(i) Algorithm for minutiae correspondence

(ii) Algorithm for power iteration in eigen value problem

(iii) Method to confirm one to one mapping

The detailed explanation of the algorithms is provided in section 3.

## 3. ALGORITHM

**Algorithm 3.1: Algorithm for minutiae correspondence**

**Step 1**: Latent and reference minutiae template having m_l andm_rminutiae respectively are obtained as inputs

**Step 2**: Minutiae correspondences are obtained as output.

**Step 3**: Estimate minutiae similarity matrix using below equation

$$sim(I1, I2) = \frac{1}{\sum_{p\in P} 1} \sum_{p\in P} \frac{DI1(p) - DI2(p)}{\|DI1(p)\|.\|DI2(p)\|} \quad (9)$$

Where $DI_1(p)$, $DI_2(p)$ is calculated based on the cosine function of the distance.

**Step 4:** Find out the top N minutiae correspondence from the matrix and design $h^2$

**Step 5**: Follow algorithm 2 and 4 and remove the false values and again construct $h^3$

**Step 6**: Once again remove the false correspondences and finally at the end show the minutiae correspondences.

Algorithm 3.2: Algorithm for power iteration in eigen value problem

**Step 1**: Provide $h^2$ value as input

**Step 2**: Principal eigen vector $y$, of $h^2$ is obtained as output.

**Step 3**: Initialize $y$

**Step 4**: Until convergence, perform the below rules,

$$\begin{aligned} y &\leftarrow hy \\ y &\leftarrow \frac{1}{\|y\|_2} y \end{aligned} \quad (10)$$

**Step5**: Finally find the power iteration for the third order eigen value problem.

$$y_i = \sum_{j,k} h^3{}_{i,j,k} y_j y_k \quad (11)$$

**Algorithm 3.3: Method to confirm one to one mapping**

**Step 1**: The eigen vector obtained from the above algorithm is given as input.

**Step 2**: Initialize threshold and minutiae pair.

**Step3**: Minutiae correspondence is taken as the output.

**Step 4**: Set flag as zero

**Step 5**: If maximum value of y is greater than threshold then flag is set as one and the loop continues.

**Step 6**: If the above condition is not satisfied then c. append= (I1, I2)

**Texture template similarity**

The algorithm used for minutiae comparison is used for texture template comparison. The texture template similarity is obtained by multiplying minutiae similarity with ridge flow similarity. A texture template for reference prints is presented in similar method as that for latent. The ROI is explained as the value of the gradient and the orientation each having a block size of 16 × 16 pixels. The block size can be preferred as 4 × 4, 8 × 8 and 16 × 16. But every block size will not provide good results for every quality of images. Preferably block size 16 × 16 will provide good results for even less quality of images. Only square shaped template is preferred since there is no loss in information. The intensity of the block is same as the intensity of image. The virtual minutiae nearby the mask boundary are left out. A 96-dimensional descriptor is first achieved and then lowered to 16 dimensions using product quantization.

**Similarity Score Fusion**

From the minutiae and texture template only one from each is taken as reference point. The similarity score is calculated as

$$S = \lambda_1 S_{minutiae1} + \lambda_2 S_{minutiae2} + \lambda_3 S_T \quad (12)$$

where $\lambda_1$, $\lambda_2$, $\lambda_3$ are the weights. $S_T$ is the texture template similarity.

## 4. EXPERIMENTAL RESULTS

In this paper, NIST SD27 [19] latent database is used to verify the performance of proposed method with existing method. This database has 258 latent finger print images and their reference images. For fingerprint of database manually marked ROI is used, but Finger net is applied for rolled ones. If background is clear, the Otsu's method [41] and morphological operations are used to obtain the ROI of each fingerprint. ROI is obtained by automatic cropping by providing boundary for the finger print in a query latent. The experiment is tested by varying the dimension of the descriptor as 100,80,30 for various ranks like 1,5,10 and accuracy of recognition is noted. Further the proposed technique is tested for various quantization factor such as 10,14,18 etc. Moreover, the technique has applied to two qualities of images like good and poor. Table2 shows the performance of proposed ConvNet method with the existing method like CNN, skeleton approach nonlinear mapping and product quantization for various ranks 1,5, and 10. The proposed ConvNet method provides an accuracy of 76.4%,80.4% and 82.4% respectively. The least performance is observed for nonlinear mapping which has an accuracy of 53.4%,62.2% and 73.2% for rank1, rank5 and rank10 respectively.

**Table 2.** Performance measure of proposed method in NIST SD database with CNN, skeleton approach, nonlinear mapping and product quantization

| Techniques | Rank 1 | Rank 5 | Rank 10 |
|---|---|---|---|
| ConvNet | 76.4% | 80.4% | 82.4% |
| CNN | 56.4% | 64.4% | 75.4% |
| Skeleton approach | 75.8% | 77.8% | 78.5% |
| Nonlinear mapping | 53.4% | 62.2% | 73.2% |
| Product quantization | 74.3% | 76.4% | 76.3% |

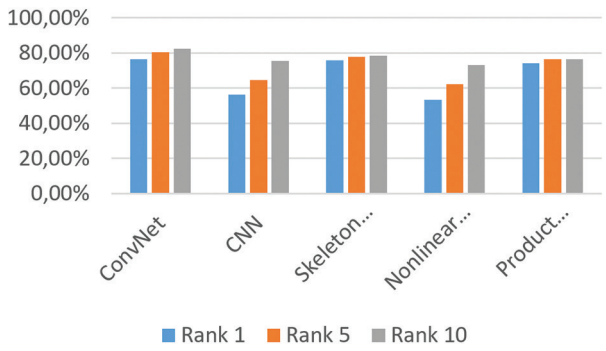


**Fig. 7.** Graphical plot of Table 2

Fig. 7. shows the performance plot of proposed method for various ranks compared with existing method as given in Table 2. From Fig. 7. it is observed that ConvNet provides good results in rank 1, rank 5 and rank10.Table 3shows that the technique is analysed with various quality of images like good, ugly, poor in rank 10. This proposed technique gives higher accuracy than the existing techniques like CNN, skeleton approach and local and global matching. Fig. 8. shows the graphical plot of Table 3. In poor quality image ConvNet provides an accuracy of 73.4% whereas least performance is nonlinear mapping which has an accuracy of 51.4%. For ugly image the ConvNet has an accuracy of 78.4% whereas nonlinear mapping has 61.2%. In good quality image higher and lower performance is for conv net and nonlinear mapping respectively. From Fig. 8., it is observed that ConvNet has good results for all the three types of images such as poor, ugly and good latent images.

**Table 3.** Comparison of proposed method with CNN, skeleton approach, nonlinear mapping and product quantization for various types of images in rank 10.

| Techniques | poor | ugly | good |
|---|---|---|---|
| Conv Net | 73.4% | 78.4% | 80.4% |
| CNN | 53.4% | 63.4% | 72.4% |
| Skeleton approach | 71.8% | 74.8% | 75.5% |
| Nonlinear mapping | 51.4% | 61.2% | 70.2% |
| Product quantization | 69.3% | 71.2% | 73.1% |

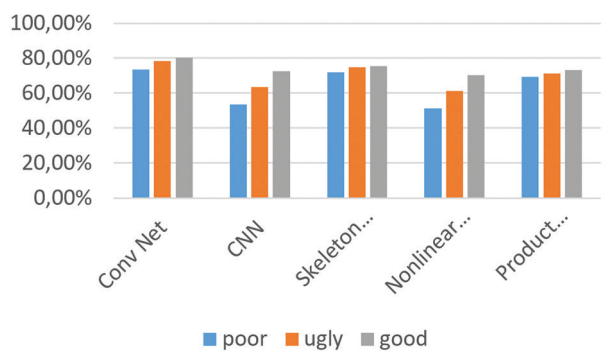


**Fig. 8.** Graphical plot of Table 3

## 5. CONCLUSION

Latent fingerprints comprise significant and broadly used sources of forensic data in forensic investigations. In midst of this plan and assemble accurate, robust, and entirely programmed latent fingerprint recognition systems have been restricted. In this paper latent image recognition is done using ConvNet method. Here minutiae template and texture template can be utilized, so that matching information can be obtained. Even though this latent image is not of good quality, it provides higher accuracy for various rank such as rank1, rank5 and rank10 for the NIST SD27 database compared to existing methods like CNN, skeleton approach nonlinear mapping and product quantization. In future work techniques has to be improved to enhance the speed of execution even after training large datasets.

6. REFERENCES:

[1] Sankaran, T. I. Dhamecha, M. Vatsa, R. Singh, "On Matching Latent to Latent Fingerprints", Proceedings of the 2011 International Joint Conference on Biometrics, Washington, DC, USA, 29 December 2011, pp. 1-6.

[2] D. Maltoni, D. Maio, A. K. Jain, S. Prabhakar, "Fingerprint Matching", Handbook of Fingerprint Recognition, pp. 131-171, Springer, New York, NY, 2003.

[3] A. A. Paulino, A. K. Jain, J. Feng, "Latent Fingerprint Matching: Fusion of Manually Marked and Derived Minutiae", Proceedings of the 23rd SIBGRAPI Conference on Graphics, Patterns and Images, Gramado, Brazil, 30 August - 3 September 2010, pp. 63-70.

[4] K. Cao, A. K. Jain, "Automated Latent Fingerprint Recognition", IEEE Transactions on Pattern Analysis and Machine Intelligence, Vol. 41, No. 4, 2019, pp. 788-800.

[5] D. Valdes-Ramirez, M. A. Medina-Pérez, R. Monroy, O. Loyola-González, J. Rodríguez-Ruiz, A. Morales, F. Herrera, "A Review of Fingerprint Feature Representations and Their Applications for Latent Fingerprint Identification: Trends and Evaluation", IEEE Access, Vol. 7, No. 1, 2019, pp. 48484-48499.

[6] X. Huang, P. Qian, M. Liu, "Latent Fingerprint Image Enhancement Based on Progressive Generative Adversarial Network", Proceedings of the IEEE/CVF Conference on Computer Vision and Pattern Recognition Workshops, China,14-19 June 2020, pp. 800-801.

[7] S. Gu, J. Feng, J. Lu, J. Zhou, "Latent Fingerprint Registration via Matching Densely Sampled Points", IEEE Transactions on Information Forensics and Security, Vol. 16, 2021, pp. 1231-1244.

[8] A. K. Jain, Jianjiang Feng, A. Nagar, K. Nandakumar, "On matching latent fingerprints", Proceedings of the IEEE Computer Society Conference on Computer Vision and Pattern Recognition Workshops, Anchorage, AK, USA, 23-28 June 2008, pp. 1-8.

[9] A. K. Jain, J. Feng, "Latent Fingerprint Matching", IEEE Transactions on Pattern Analysis and Machine Intelligence, Vol. 33, No. 1, 2011, pp. 88-100.

[10] H. Choi, M. Boaventura, I. A. G. Boaventura, A. K. Jain, "Automatic Segmentation of Latent Fingerprints", Proceedings of the IEEE Fifth International Conference on Biometrics: Theory, Applications and Systems, Arlington, VA, USA,23-27 September 2012, pp. 303-310.

[11] J. Zhang, R. Lai, C. J. Kuo, "Adaptive Directional Total-Variation Model for Latent Fingerprint Segmentation", IEEE Transactions on Information Forensics and Security, Vol. 8, No. 8, 2013, pp. 1261-1273.

[12] K. Cao, E. Liu, A. K. Jain, "Segmentation and Enhancement of Latent Fingerprints: A Coarse to Fine Ridge Structure Dictionary", IEEE Transactions on Pattern Analysis and Machine Intelligence, Vol. 36, No. 9, 2014, pp. 1847-1859.

[13] J. Ezeobiejesi, B. Bhanu, "Patch Based Latent Fingerprint Matching Using Deep Learning", Proceedings of the 25th IEEE International Conference on Image Processing, Athens, Greece, 7-10 October 2018, pp. 2017-2021.

[14] H. Guan, P. Lee, A. Dienstfrey, M. Theofanos, C. Lamp, B. Stanton, M. T. Schwarz, "Analysis, Comparison, and Assessment of Latent Fingerprint Image Preprocessing", Proceedings of the IEEE Conference on Computer Vision and Pattern Recognition Workshops, Hawai, USA, 21-26 July 2017, pp. 126-133.

[15] K. Cao, A. K. Jain, "Automated Latent Fingerprint Recognition", IEEE Transactions on Pattern Analysis and Machine Intelligence, Vol. 41, No. 4, 2019, pp. 788-800.

[16] K. Cao, D. L. Nguyen, C. Tymoszek, A. K. Jain, "End-to-End Latent Fingerprint Search", IEEE Transactions on Information Forensics and Security, Vol. 15, 2020, pp. 880-894.

[17] S. Yoon, A. K. Jain, "Longitudinal Study of Fingerprint Recognition", Proceedings of the National Academy of Sciences, Vol. 112, No. 28, 2015, pp. 8555-8560.

[18] R. Cappelli, M. Ferrara, D. Maltoni, "Minutia Cylinder-Code: A New Representation and Matching Technique for Fingerprint Recognition", IEEE Transactions on Pattern Analysis and Machine Intelligence, Vol. 32, No. 12, 2010, pp. 2128-2141.

[19] NIST Special Database 27, http://www.nist.gov/srd/nistsd27.cfm (accessed: 2018)

[20] V. Jain, A. K. Singh, R. Kumar, "An Efficient Approach for Latent Fingerprint Recognition," Proceedings of the Second International Conference on Computational Intelligence & Communication Technology, Ghaziabad, India,12-13 February, 2016, pp. 70-75.

[21] C. Wu, Z. Shi, V. Govindaraju, "Fingerprint image enhancement method using directional median filter", Biometric Technology for Human Identification, Vol. 5404, pp. 66-75.

[22] Y. Dong, S. Xu, "A New Directional Weighted Median Filter for Removal of Random-Valued Impulse Noise", IEEE Signal Processing Letters, Vol. 14, No. 3, 2007, pp. 193-196.

[23] A. M. Raičević, B. M. Popović, "An effective and robust fingerprint enhancement by adaptive filtering in frequency domain", Facta universitatis-series: Electronics and Energetics, Vol. 22, No. 1, 2009, pp. 91-104.

[24] A. Amrata, Khindre, V. A. More, "An Approach to Touchless Fingerprint Recognition Using Matlab," International Journal of Emerging Trends & Technology in Computer Science, Vol. 3, 2014, p. 4.

# SSDT: Distance Tracking Model Based on Deep Learning

Original Scientific Paper

**Chhaya Gupta**
Department of Computer Science & Applications
Maharshi Dayanand University, Rohtak
Haryana, India
chhayagupta.spm@gmail.com

**Nasib Singh Gill**
Department of Computer Science & Applications
Maharshi Dayanand University, Rohtak
Haryana, India
nasib.gill@mdurohtak.ac.in

**Preeti Gulia**
Department of Computer Science & Applications
Maharshi Dayanand University, Rohtak
Haryana, India
preeti.gulia81@gmail.com

***Abstract*** *– Coronavirus disease (COVID-19) is an infectious disease caused by the SARS-CoV-2 virus and population vulnerability increased all over the world due to lack of effective remedial measures. Nowadays vaccines are available; but in India, only 18.8% population has been fully vaccinated till now. Therefore, social distancing is only precautionary norm to avoid the spreading of this deadly virus. The risk of virus spread can be avoided by adhering to this norm. The main objective of this work is to provide a framework for tracking social distancing violations among people. This paper proposes a deep learning platform-based Smart Social Distancing Tracker (SSDT) model which is trained on MOT (Multiple Object Tracking) datasets. The proposed model is a hybrid approach that is a combination of YOLOv4 as object detection model merged with MF-SORT, Kalman Filter and brute force feature matching technique to distinguish people from background and provide a bounding box around these. Further, the results are also compared with another model, namely, Faster- RCNN in terms of FPS (frames per second), mAP(mean Average Precision) and training time over the dataset. The results show that the proposed model provides better and more balanced results. The experiment has been carried out in challenging conditions including, occlusion and under lighting variations with mAP of 97% and a real-time speed of 24 fps. The datasets provide numerous classes and from all the classes of objects, only people class has been used for identifying people in a closet. The ultimate goal of the model is to provide a tracking solution that will be helpful for different authorities to redesigning the layout of public places and reducing the risk. This model is also helpful in computing the distance between two people in an image and the results confirm that the proposed model successfully distinguishes between individuals who walk too close or breach the social distancing norms.*

***Keywords****: Deep Learning, COVID-19 Social Distancing, MF-SORT, Object Detection, People Detection, Bounding Box*

## 1. INTRODUCTION

COVID-19 was initiated from Wuhan, China and had affected many countries worldwide. WHO (World Health Organisation) had declared it as a pandemic [1]. Coronavirus is an infectious disease that causes acute respiratory syndrome. There are few more symptoms of this disease that are commonly found in people such as cold, cough, fever, trouble in breathing, body aches, loss of smell and taste. This virus spreads mostly when people come in contact with an infected person. This virus also spreads via air when an infected person sneezes or coughs. As per doctors and researchers, social distancing is an effective method for avoiding the spread of this

deadly virus. As there is an increase in death rate and active cases, it is mandatory to follow social distancing to avoid coming in contact with infected persons. This hybrid model is helpful in monitoring whether people are following the norms of social distancing or not.

"Social Distancing" the word itself is an important effort aiming to reduce the transmission of the virus. The norm of social distancing aims to minimise the physical contact between people. According to WHO, people must maintain a minimum distance of 6 feet among each other[2]. Many studies have shown that social distancing is an important measure to control the widespread of this deadly disease [3]. Fig. 1 shows the reduced peak of the pandemic when people follow social distancing norms[4]. It also shows that social distancing is one of the best ways to minimize the physical contact that causes a reduction in an increased rate of infection [5]. A lot of medicinal organizations and pharmaceutical companies are trying to develop medicines and vaccines for COVID-19 but there is no magic happened to date which can be considered as a treatment for this disease. Therefore, people must follow precautionary measures to limit the spread of the virus.

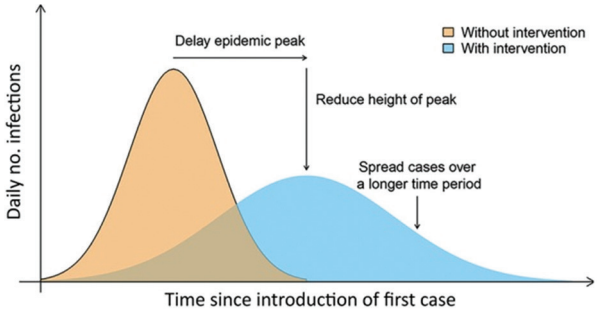


**Fig. 1.** Impact of Social Distancing on COVID-19 cases since the first case arrived

With an increasing number of cases and death counts, it is very important to maintain social distance and use masks to avoid the spread of coronavirus. The idea behind Social Distancing Tracker is to determine whether two people are following the social distancing norms or not. If two persons are following the social distancing norms then they are surrounded by a green bounding box and if they are too close to each other then they are surrounded by a red bounding box. This method works on the principle of measuring distances between people in pixels using different algorithms to compute the distance. The government has already specified the distance amongst two people i.e. 6 feet that need to be followed by everyone. The proposed hybrid model is developed using concepts of deep learning and image processing. It is compared with other object detection models used so far. The performance of object detection models has been compared to monitor the social distancing.

The rest of the paper is divided into the following sections: Section 2 provides a review of related literature in the field of study; section 3 provides knowledge on object detection tracking models and tracking techniques; section 4 presents the proposed SSDT model, section 5 discusses the implementation of SSDT model, section 6 presents results and discussions, and section 7 concludes the paper.

## 2. RELATED LITERATURE

In China, when Coronavirus arrived in December 2019, social distancing opted as a precautionary measure on January 23, 2020. Social distancing is an effective method to limit the transmission of the Covid-19 virus. The government has already specified the distancing rules to avoid the transmission of this deadly disease. A lot of work has been done by researchers to track the distance during this pandemic which is as follows:

Chhaya Gupta et al. [1] proposed a Deep learning-based CNN method for facemask detection. The idea behind their work is to determine whether a person is wearing a mask or not. If the person is not wearing a mask, then the person's face is surrounded by a red colour box and a label saying "without a mask" is also present.

Mahdi Rezaei et al. [4] proposed a hybrid computer vision and YOLOv4 based Deep Neural Network (DNN) for people detection in the crowd using common CCTV cameras. They have combined the model with the SORT tracking algorithm and inverse mapping technique to monitor social distancing. The proposed method was evaluated on the Oxford Town Centre dataset and the system provided 98% accuracy.

Dr S Syed Ameer Abbas et al. [6] founded a framework for human tracking and crowd management using Raspberry pi. They estimated the head tally and crowd is measured by contrasting the value and threshold value.

Prem K et al. [7] used synthetic location-specific contact patterns and produced matrices. They proposed an age-structured susceptible-exposed-infected-removed (SEIR) model for various social distancing measures. They found that social distancing measures were most effective in April and reduced the number of cases to 92%. They found that when restrictions were put on activities it helped in delaying epidemic peak.

Since coronavirus arrived, various countries take the help of technology to track movements of infected persons and tried to monitor their exposure to other people [8–10]. Many countries like India and South Korea used GPS tracking systems to track the movement of suspected persons among healthy people. The Indian government has also developed an Arogya Setu App to keep track of COVID-19 patients in surroundings [11]. The app uses Bluetooth and GPS tracking systems and helps healthy people to stay away from infected people. Many other departments have been using various other techniques like drones or surveillance cameras to identify gatherings and take required steps to disperse the crowd [12].

Ertem Zeynep et al. [13] proposed a decision analytical approach to estimate the effectiveness of social distancing methods. They proposed an age-structured compartmental simulation model to analyze computational results. The study shows that decision analytic tools help simulate different social distancing scenarios.

Su Jie et al. [14] proposed a visual social distancing (VSD) method for real-time social distancing measuring and analyzing the distance between pedestrians using CCTV videos in public areas. They proposed a multi-pedestrian tracking approach for Spatio-temporal trajectory. The method works on Euclidean distance between tracking objects but also considers discrete Frechet distance between trajectories. They worked on the MOT16 dataset.

Sreetama Das et al. [15] proposed a computer vision-based solution to encourage abidance with social distancing norms. The method provides options to choose between tool-based mode and automated mode of the camera. They have discussed various risk factors associated with social distancing violations.

Maria Fazio et al. [16] proposed an efficient and cost-effective indoor navigation system for moving people inside buildings. The method works on short-range wireless communication technology –IoT-based Bluetooth Low Energy (BLE) Beacons. The authors provide a new navigation system that recognizes user position according to information provided by beacons. This method reduces contagious risk and is very much helpful for the movement of people in smart cities during lockdowns. This method is really helpful for patients who want to travel from one ward to another. But this method is useful for people who have access to a smartphone which is a limitation.

Asif Hummam et al. [17] proposed a low confidence track filtering into simple online and Real-time tracking with a deep association metric (DeepSort) algorithm. The proposed method has shown improved results over the classic DeepSort algorithm with significant margins.

Narinder Singh Punn et al. [18] proposed a deep-learning-based framework using YOLOv3 merged with the DeepSort technique. The authors concluded that the proposed model showed better results when compared with different faster R-CNN models.

A lot of research has been done in the field for human detection and it is shown that human detection can be used in different applications. Despite the work done till now, there are a lot of limitations and hindrances that need to be investigated:

- Most of the work has been carried out with small datasets.
- The researchers have used pre-trained models via transfer learning for producing high accuracy results and it takes a lot of effort in changing the architecture of a pre-trained model and add something new to it.
- Most of the work has been done on available datasets and it is a task to work on real-time data.

To overcome the limitations, a hybrid approach using YOLOv4 merged with MF-SORT, Kalman Filter and Brute force feature matching technique has been proposed. The model in this paper does not work on real-time data as of now, but in future, it will be trained to work with real-time data.

## 3. OBJECT DETECTION TRACKING MODELS

Different object detection models have been used so far for detecting social distancing norms. The basic requirement for detecting objects in an image or any video is a bounding box that surrounds the object of interest. From the vast literature review, it has been observed that every object detection model uses bounding boxes for identifying multiple objects in an image [19]. The bounding box helps to identify each object independently and helps the object detection model to classify each object. The bounding boxes surround the images over different locations. The bounding boxes help the object detection model to predict the class of each bounding box and the object detection model helps to adjust the dimensions of the box to fit better. As there are many bounding boxes so one object can be associated with more than one bounding box and this problem is solved by evaluating the Intersection over Union (IoU) parameter [20] with the help of Non-Max Suppression (NMS) [21] helps in calculating ratios between overlapped regions and union of regions of various bounding boxes.

Every bounding box is assigned a label as positive or negative according to the associativity of the object of interest. For positive label 1 is used and for negative label 0 is used.

### 3.1. OBJECT DETECTION MODELS

Various object detection models have been used to detect social distancing norms which are as follows:

Faster R-CNN: This model was proposed by Ren et al. [22] from R-CNN and Fast R-CNN models and the architecture of this model is shown in Fig. 2. This model is composed of Region Proposal Network (RPN) module that is responsible for binary classification by which each object is classified. This model is an association of RPN and fast R-CNN models. Classification loss (Lcls) and regression loss (Lreg) for faster R-CNN are shown with the help of equations 1 and 2.

$$L_{cls}(p_i, p_i^*) = -p_i^* \log(\mathrm{p_i}) - (1 - p_i^*) \log(1 - p_i) \quad (1)$$

$$L_{reg}(t^u, v) = \sum_{x \epsilon x,y,w,h} L_1^{smooth}(t_i^u - v) \quad (2)$$

Where
tu = bounding box predicted corrections
pi= actual class
pi*= predicted class

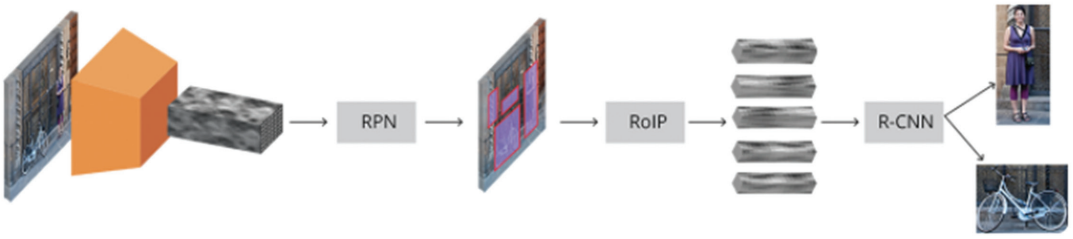


**Fig. 2.** The architecture of Faster R-CNN[22]

Single Shot Detector (SSD): This model is also used to detect people in videos. Faster R-CNN provides higher accuracy but has slow processing of frames and provides a low FPS rate. SSD improves the FPS rate and accuracy by using multiple scale features. It utilizes a feed-forward convolutional neural network that helps in associating objects with bounding boxes of fixed size and then the model follows the Non-Max Suppression (NMS) module to produce the final result. The complete model is categorized into three stages: in the first stage, a pre-trained network is used to extract feature maps, in the second stage multiple-scale feature is used and finally, the NMS module is used to provide the final result. The classification loss function and regression loss function for the SSD model is defined in equation 3 and 4. The architecture of this model is shown in Fig. 3[23].

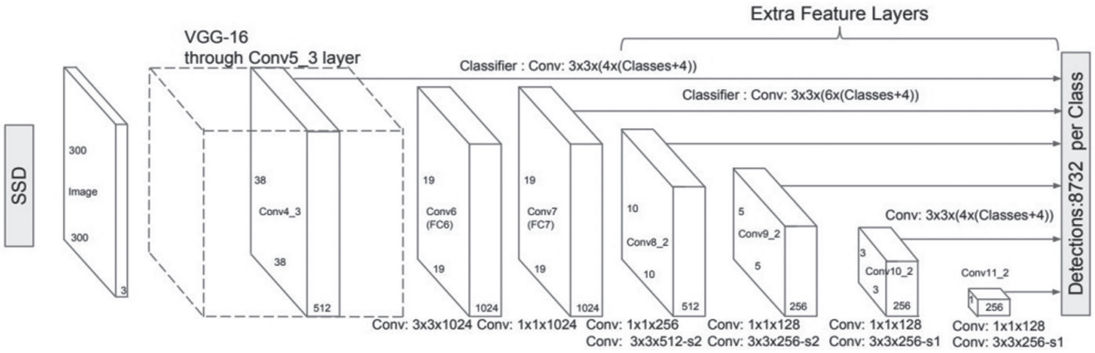


**Fig. 3.** The architecture of SSD[23]

$$L_{cls}(x,c) = -\sum_{i\in Pos}^{N} x_{ij}^{p} \log\left(\widehat{c_i^p}\right) - \sum_{i\in N\in g} \log(\widehat{c_i^o}) \quad (3)$$

$$L_{reg}(x,l,g) = \sum_{i\in pos}^{N} \sum_{m\in c_x,c_y,w,h} x_{ij}^{\kappa} \; smooth_{L_1}\left(l_i^m - \widehat{g_j^m}\right) \quad (4)$$

Where

l = predicted box

g = ground box

xij = it matches ith bounding box to jth ground box

cx and cy = offsets for bounding box

N = number of default matched boxes

YOLO: You Only Look Once (YOLO) can predict the location and type of object by just looking at the image once. It solves the problem of object detection by assuming it as a regression task rather than a classification task. In this model, only one convolutional network is used that helps to predict the bounding boxes. YOLO has many versions available like YOLOv1 [23] which is inspired from GoogleNet (or inception model) [24], YOLOv2 [25] which improves the accuracy provided by YOLOv1 and YOLOv3 performs multi-label classification. Equation 9 shows the loss function for YOLO is the mean average precision loss function for YOLO and the basic architecture of YOLO is represented in Fig.4 [26].

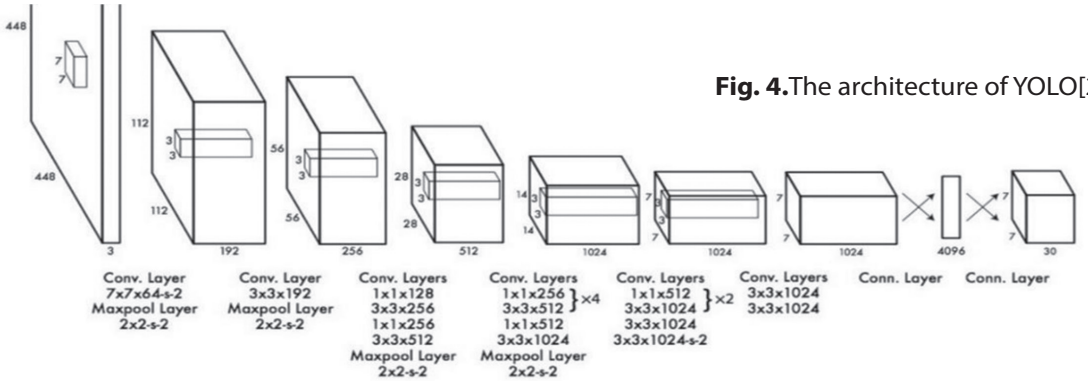


**Fig. 4.**The architecture of YOLO[26]

YOLOv4 outperforms the inference speed provided by other object detection models. It is a series of additions of computer vision methods. This method makes real-time object detection a priority. The ImageNet classification model forms the backbone for YOLOv4. This model also deploys the same bounding box detection steps as used by YOLOv3 and three steps of detection granularity. There are two threshold values taken in YOLO:

- IoU threshold: IoU is the ratio of the area of overlap of two images to the area of the union of two images. Equation 5 describes the IOU threshold value.

$$\text{IoU} = \frac{Area\ of\ Overlap}{Area\ of\ Union} \quad (5)$$

Confidence threshold: This value refers to the box confidence score which means, the minimum confidence the model has on the detected object.The equations to calculate the confidence scores are shown below:

$$\text{Box Confidence score} = P_r(\text{object}).\text{IoU} \quad (6)$$

$$\text{Conditionalclass probability} = P_r(\text{class}_i|\text{object}) \quad (7)$$

$$\text{Class confidence score} = P_r(\text{class}_i).\ \text{IoU} \quad (8)$$

Where,

$P_r$(object) = probability that box has an object

IoU = Intersection over Union between the predicted box and ground truth

$P_r(\text{class}_i|\text{object})$ = probability that object belongs to $\text{class}_i$ given an object is present.

$P_r(\text{class}_i)$ = probability that the object belongs to $\text{class}_i$.

If a box is detected then P(object) has value 1 otherwise 0. In this paper, the confidence score threshold is used.

$$\lambda_{coord} \sum_{i=0}^{s^2} \sum_{j=0}^{B} 1_{i,j}^{obj} \left((t_x - \hat{t_x}) + \left(t_y - \hat{t_y}\right)^2 + (t_w - t_w)^2 + (t_h - t_h)^2 + \sum_{i=0}^{s^2} \sum_{j=0}^{B} 1_{i,j}^{obj} \left(-\log\left(\sigma(t_0)\right) + \sum_{k=1}^{C} BCE(\hat{y_k}, \sigma(s_k))\right) + \lambda_{noobj} \sum_{i=0} \sum_{j=0}^{B} 1_{i,j}^{noobj} \left(-\log\left(1 - \sigma(t_0)\right)\right) \quad (9)$$

Where,

$\lambda_{coord}$ = weighted coordinator error

$s^2$ = number of grids in an image

B = number of bounding boxes per grid

$1_{i,j}^{obj}$ = 1 indicates that the objectresides in the jth bounding box in grid i.

Fig. 5 shows successful object detection of various models like Faster R-CNN [22], Fast YOLO [27], Single Shot Detector (SSD) [28] and YOLO [29] validated on COCO and PASCAL-VOC datasets, compared on their speed and accuracy which is dependent on many factors like input sizes, resolution of images, batch sizes etc.

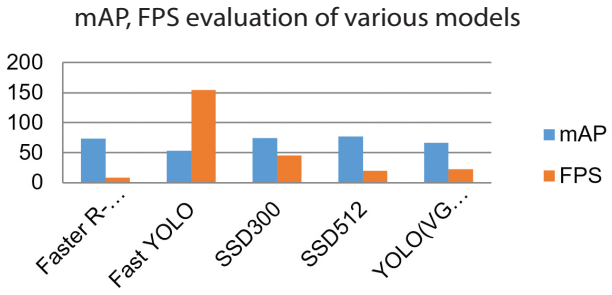


**Fig. 5.** Performance evaluation of various models

The models have been evaluated on the basis of mAP (mean Average Precision) [30] and FPS (Frames Per Second).

Table1 shows the performance evaluation of the above said models in terms of mAP, FPS, Batch size and Image resolution passed to models while testing them on PASCAL-VOC and COCO datasets.

**Table 1.** Performance of different Object Detection Models on various parameters.

| Method | mAP | FPS | Batch Size | Input Resolution |
|---|---|---|---|---|
| Faster R-CNN | 73.3 | 8 | 1 | 1000 X 600 |
| Fast YOLO | 52.8 | 154 | 1 | 448 X 448 |
| SSD300 | 74.5 | 45 | 1 | 300 X 300 |
| SSD512 | 77 | 20 | 1 | 512 X 512 |
| YOLO(VGG16) | 66.5 | 22 | 1 | 448 X 448 |

### 3.2. OBJECT DETECTION TRACKING TECHNIQUES

This section gives the idea about the basics of tracking. In a real-time environment, trackers need to be connected with a detector. Let us assume if the bounding box information for one ID in the frame is given then how to assign IDs in subsequent frames? This question is answered below:

Assigning ID based on Centroid: This is the simplest way to assign IDs. Centroids for each bounding box in one frame are calculated. After this, new centroids are calculated in the second frame (if any) and based on distance from previous centroids IDs are assigned. But this method fails when people come close to each other as this may switch IDs.

Particle-Filter: This method is being used widely in real-time object tracking. The main features of this filter are its simplicity and its flexibility. It is very easy to handle non-Gaussian and multimodality system models with this filter but it does not work well with gaussian systems, which is a drawback[31].

Kalman – Filter: This method is an improvement over the centroid method as this is based on the position and velocity of an object and thus helps in modelling track. It uses Gaussian scales to estimate the future position and velocity of an object. When a new reading is achieved, this method uses probability to assign

a measurement to its prediction and hence updates itself accordingly. It uses very less space and is effectively fast and shows better results than the centroid method. This method also helps in reducing unwanted noise by inaccurate detections. The current position of the object can be predicted by its previous moment position[32].

In addition, with Kalman filter, the proposed model also uses the brute force feature matching technique.

## 4. PROPOSED MODEL

A lot of challenges faced during the categorization and detection of objects in any image can be solved with the support of advanced computer vision and deep learning models. Computer vision focuses on various challenging aspects like segmentation, tracking and detection of objects. Deep learning is an artificial intelligence method that is useful for data processing and objects detection. Neural networks come into the picture in the late 1940s [33].

The main purpose of neural networks is to solve learning problems [19]. According to the literature survey, a robust model has been developed that can detect whether people are maintaining social distancing or not with the help of OpenCV and YOLO object detectors. OpenCV is an open-source computer vision programming library that accelerates the utilization of machine perception within the commercial product. The paper proposes a deep learning-based hybrid model SSDT (Smart Social Distancing Tracker) that helps to deal with social distancing violations and can reduce the number of COVID-19 cases. The proposed model uses YOLOv4 merged with MF-SORT[34], Kalman filter and Brute Force feature matching technique for computing social distancing violations in a video. The bounding boxes are colour coded which means if two persons are not following social distancing norms then the red colour bounding box surrounds both of them otherwise the colour of the bounding box is green. The workflow of the proposed framework is shown in Fig. 6.

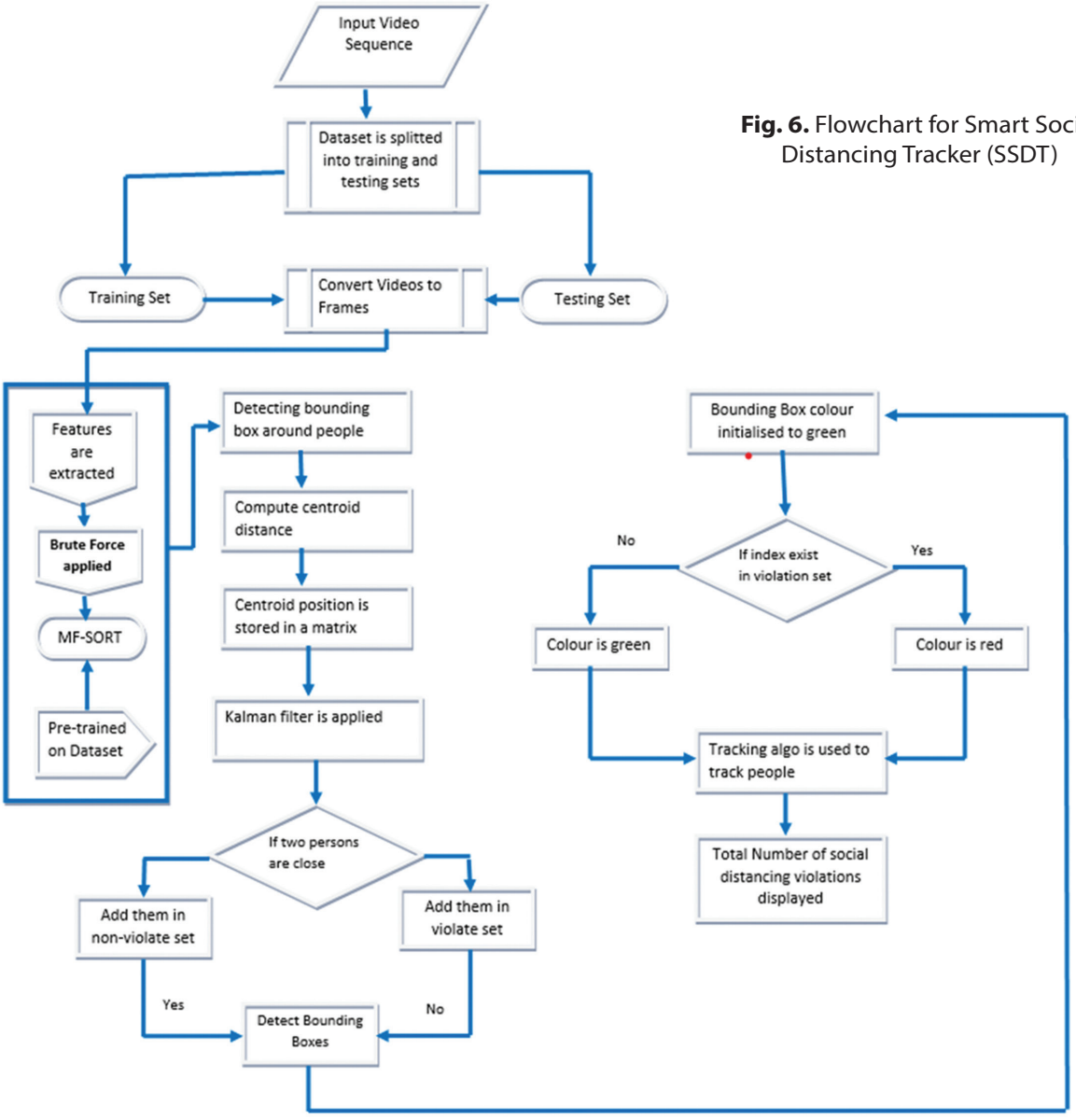


**Fig. 6.** Flowchart for Smart Social Distancing Tracker (SSDT)

## 5. IMPLEMENTATION OF SSDT MODEL

To develop the social distancing tracker, Computer vision and deep learning methods have been used. The hybrid model is based on YOLOv4 merged with MF-SORT (Simple Online and Real-time with motion features), Kalman-filter and brute force matching technique. The proposed model is implemented on MOT (Multiple Object Tracking) datasets[35] which is discussed as follows:

People Tracking – The first thing needed is a video and a tested model on it. The MOT dataset has been used for implementation which is a canonical dataset for computer vision people tracking. This dataset has many open-sourced clips having people's movements with different camera angles. Fig. 7 shows one of the frames from the clip.

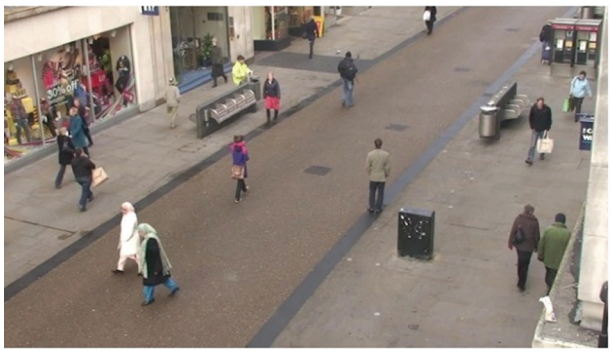

**Fig. 7.** Sample frame from MOT dataset

Person tracking is the task of providing an ID to a person detected in every frame and carrying their ID forward. Once the person has left a frame the ID is not reused and if a new person enters the frame, he/she is assigned a new ID. Tracking is a tedious task as people can look similar. People get occluded behind another person or any other object and they are assigned a new ID when they re-emerged. Deep learning helps in multi-object tracking. In this paper, the Kalman-filter method is used to track people and provide IDs. The hybrid model in this paper uses Simple Online and Real-time with motion features (MF-SORT) technique with Kalman filter and brute force matching techniques. Kalman filter helps in predicting human position at t+1 time based on present time t and this helps in identifying people in case of occlusion as well hence reducing occlusion. Brute force feature matcher compares two sets of keypoint descriptors and generates output. The output is a list of matches found. This technique is used to match the features of one image with the features of the second image, it takes a descriptor of the first image and matches it with all descriptors of the second image, then it takes the second descriptor of the first image and matches it with all the descriptors of the second image and so on[36]. It takes Euclidean distance or hamming distance depending on the type of detector but in this researchwork, brute force matcher is making use of distance calculated as per the centroid distances.

The state of each person in a frame is stated as,

$$x = [a, b, c, d, a', b', c']^T \tag{10}$$

Where (a,b) are horizontal and vertical position (centroids) of bounding box a and c is area and d is the aspect ratio of bounding box a',b',c' is predicted values by Kalman filter.

If an identified person is associated with a new observation, the present bounding box will be updated with this newly observed value. This is calculated by the Kalman filter based on the velocity and acceleration of the object.

After the detection and tracking process, a detection matrix Dt is defined that includes the location of n detected human in any image grid as,

$$D_t = \{P^t_{(x_n, y_n)}\} \tag{11}$$

Tracking Social distancing – There are different tracks in different frames and distance is measured between all the tracks. A bounding box with an ID is known as a track. Hence, the distance between bounding boxes is compared using the Euclidean Distance formula. The following steps have been performed for every frame:

Step 1: Pixel distances are compared between each track.

Step 2: If distance < proximity value (6feet) then, two people are walking very close to each other, hence changing the value of safe to 1 in the data frame for both the bounding boxes. The variable "safe" is used as a visualization variable later.

Step 3: To count the total breaches for each ID, so anytime distance <proximity value, a list of tracks is maintained that have come too near to each other. Many calculations are repeated many times to measure the distance between tracks and hence to save time, results are stored in a single pass which cuts the run time to half. One of the frames with results is shown below in Fig. 8.

**Fig. 8.** A sample frame showing results of social distancing violations between people

If a minimum of 2 persons are detected in a frame, then the following steps are performed:

Step 1: Euclidean distance is calculated between both persons.

Step 2: Loop over the upper triangular distance matrix.

Step 3: To check whether the distance is violating the minimum value. If two persons are extremely close then they are added to the violation set.

Step 4: The present index is verified if it is present in the violation set, if it is present in the violation set then the colour of the bounding box changes to red.

Step 5: The bounding box of each person in a frame is drawn. Every person is colour coordinated and hence now individuals can be verified whether they are nearby or not.

Step 6: Finally, the total number of violations is shown.

Fig. 9 shows one of the sample frames identifying the total number of social distancing violations being marked.

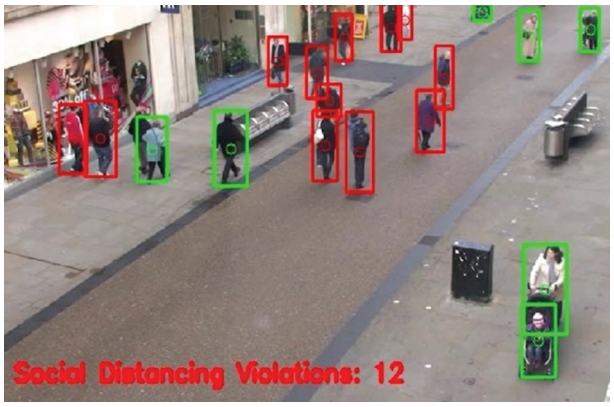


**Fig. 9.** A sample frame that shows the number of social distancing violations

## 6. RESULTS AND DISCUSSIONS

The proposed model has been trained on a video stream from the MOT dataset and various images. People are detected based on the distance between the pairs. The frames were also labelled as safe and unsafe and also the count of violations was made visible. The results are shown in Fig. 9. The red colour boxes around people indicate that they are not maintaining the social distancing and the green colour box indicates that the person is not violating any social distancing rule.

The is also compared with the Faster R-CNN model and YOLOv3 model[18]. Table-2 indicates the results of the models with the training time of each model, mean average precision (mAP) and frames per second (FPS) values. The result shows that Faster R-CNN achieves minimum loss when mAP is maximum but it also provides minimum FPS hence making it a non-suitable model for real-time object detection. The proposed hybrid model SSDT achieved much better results as compared to Faster RCNN in terms of mAP, FPS and training time. YOLOv3 and SSDT have similar training times but the big difference is in mean average precision values, hence concluding that SSDT is a better model over these two models. Fig. 10 shows the performance evaluation graphically.

**Table 2.** Performance comparison of SSDT and Faster R-CNN.

| Model | Training Time (s) | mAP | FPS |
|---|---|---|---|
| Faster R-CNN | 9765 | 0.964 | 3 |
| YOLOv3 | 5659 | 0.846 | 23 |
| SSDT | 5645 | 0.976 | 24 |

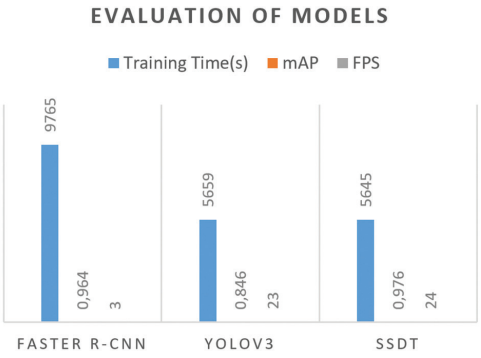


**Fig. 10.** Performance Evaluation of SSDT and Faster R-CNN

The proposed model is a hybrid social distancing tracker method but still, there are many challenging situations when it comes to implementing this type of model. Designing a system responsible for changes and flexible for all environments is a challenging task. This model can be deployed in many public areas to watch people and track social distancing violations. The proposed hybrid model works in challenging conditions such as occlusions, light conditions and hence it is an important method for different authorities to design public places with precautions as a measured thing to take care of in such difficult times.

## 7. CONCLUSION

The objective of this work is to identify a violation of social distancing norms for which a smart social distancing tracker (SSDT) has been proposed. If people are maintaining a safe distance between them then they will be marked with a green bounding box and if people are not following the social distancing laws then they will be marked with a red bounding box. The proposed model may be very helpful for cities, shops, restaurants, shopping malls etc. to assess public health risks. SSDT model is trained on MOT datasets and when compared with faster RCNN, and YOLOv3the SSDT model provides better and balanced results in terms of training time, mAP and FPS. The faster RCNN model provides minimum loss when it has maximum mAP but

has a very less FPS rate and takes more training time as compared to SSDT hence making it not a suitable model for real-time object detection. Although YOLOv3 and SSDT have similar results, the main difference is in mean average precision loss, YOLOv3 has lower mAP compared to SSDT. As the proposed model is efficient in detecting social distancing violations and is also able to remove occlusions between people successfully still there are several unaddressed issues like - it is not able to remove all the challenges of object detection like primitive illusions, low light visions, etc. but in future, this model may be deployed with an IoT based model along with deep learning methods to resolve the challenges of real-time object detection and also, the model is trained on video clips from MOT datasets, but in future, it will be trained and tested on real-time data.

## 8. REFERENCES:


[1] C. Gupta, N. S. Gill, "Coronamask: A face mask detector for real-time data", International Journal of Advanced Trends in Computer Science and Engineering, Vol. 9, No. 4, 2020, pp. 5624–5630.

[2] N. El-Guebaly, "COVID-19 and social distancing", Canadian Journal of Addiction, Vol. 11, No. 2, 2020, pp. 4–6.

[3] F. Ahmed, N. Zviedrite, A. Uzicanin, "Effectiveness of workplace social distancing measures in reducing influenza transmission: A systematic review", BMC Public Health, Vol. 18, No. 1, 2018, pp. 1–13.

[4] M. Rezaei, M. Azarmi, "Deepsocial: Social distancing monitoring and infection risk assessment in covid-19 pandemic", Applied Sciences, Vol. 10, No. 21, 2020, pp. 1–29.

[5] J. Pannu, "Nonpharmaceutical measures for pandemic influenza in nonhealthcare settings-international travel-related measures", Emerging Infectious Diseases, Vol. 26, No. 9, 2020, pp. 2298–2299.

[6] S. Syed Ameer Abbas, M. Anitha, X. Vinitha Jaini, "Realization of multiple human head detection and direction movement using Raspberry Pi", Proceedings of the International Conference on Wireless Communications, Signal Processing and Networking, Chennai, India, 22-24 March 2017, pp. 1160–1164.

[7] K. Prem et al., "The effect of control strategies to reduce social mixing on outcomes of the COVID-19 epidemic in Wuhan, China: a modelling study", The Lancet Public Health, Vol. 5, No. 5, 2020, pp. e261–e270.

[8] S. K. Sonbhadra, S. Agarwal, P. Nagabhushan, "Target specific mining of COVID-19 scholarly articles using one-class approach", Chaos, Solitons and Fractals, Vol. 140, 2020, p. 110155.

[9] N. S. Punn, S. Agarwal, "Automated diagnosis of COVID-19 with limited posteroanterior chest X-ray images using fine-tuned deep neural networks", Applied Intelligence, Vol. 51, No. 5, 2021, pp. 2689–2702.

[10] N. S. Punn, S. K. Sonbhadra, S. Agarwal, "COVID-19 epidemic analysis using machine learning and deep learning algorithms", medRxiv, 2020, pp. 1–10.

[11] "Covid-19 contact tracing app Aarogya Setu has alerted 1.4 lakh users: Official", https://www.livemint.com/news/india/covid-19-contact-tracing-app-aarogya-setu-has-alerted-1-4-lakh-users-official-11589226902816.html (accessed: 2021)

[12] M. Robakowska et al. "The use of drones during mass events", Disaster and Emergency Medicine Journal, Vol. 2, No. 3, 2017, pp. 129–134.

[13] Z. Ertem, O. M. Araz, M. Cruz-Aponte, "A decision analytic approach for social distancing policies during early stages of COVID-19 pandemic", Decision Support Systems, 2021, p. 113630.

[14] J. Su, X. He, L. Qing, T. Niu, Y. Cheng, Y. Peng, "A novel social distancing analysis in urban public space: A new online spatio-temporal trajectory approach", Sustainable Cities and Society, Vol. 68, 2021, p. 102765.

[15] S. Das, A. Nag, D. Adhikary, R. J. Ram, S. K. Ojha, G. M. Hegde, "Computer Vision-based Social Distancing Surveillance Solution with Optional Automated Camera Calibration for Large Scale Deployment", arXiv:2104.10891v1, 2021.

[16] M. Fazio, A. Buzachis, A. Galletta, A. Celesti, M. Villari, "A proximity-based indoor navigation system tackling the COVID-19 social distancing measures", Proceedings of the IEEE Symposium on Computers and Communications, Rennes, France, 7-10 July 2020.

[17] A. H. Rais, R. Munir, "Vehicle Speed Estimation Using YOLO, Kalman Filter, and Frame Sampling",

Proceedings of the 8th International Conference on Advanced Informatics: Concepts, Theory and Applications, Bandung, Indonesia, 29-30 September 2021.

[18] Z. Q. Zhao, P. Zheng, S. T. Xu, X. Wu, "Object Detection with Deep Learning: A Review", IEEE Transactions on Neural Networks and Learning Systems, Vol. 30, No. 11, 2019, pp. 3212–3232.

[19] H. Rezatofighi, N. Tsoi, J. Gwak, A. Sadeghian, I. Reid, S. Savarese, "Generalized intersection over union: A metric and a loss for bounding box regression", Proceedings of the IEEE/CVF Conference on Computer Vision and Pattern Recognition, Long Beach, CA, USA, 15-20 June 2019, pp. 658–666.

[20] J. Hosang, C. V May, "Learning non-maximum suppression", arXiv:1705.02950v2, 2017.

[21] S. Ren, K. He, R. Girshick, J. Sun, "Faster R-CNN: Towards Real-Time Object Detection with Region Proposal Networks", IEEE Transactions on Pattern Analysis and Machine Intelligence, Vol. 39, No. 6, 2017, pp. 1137–1149.

[22] X. Wang, X. Hua, F. Xiao, Y. Li, X. Hu, P. Sun, "Multi-object detection in traffic scenes based on improved SSD", Electronics, Vol. 7, No. 11, 2018.

[23] U. Handalage, L. Kuganandamurthy, "Real-Time Object Detection using YOLO: A review", 2021.

[24] P. Salavati, H. M. Mohammadi, "Obstacle detection using GoogleNet", Proceedings of the 8th International Conference on Computer and Knowledge Engineering, Mashhad, Iran, 25-26 October 2018 pp. 326–332.

[25] S. Gupta, T. U. Devi, "YOLOv2 based Real Time Object Detection", International Journal of Computer Science Trends and Technology, Vol. 8, No. 3, 2020, pp. 26–30.

[26] S. Shinde, A. Kothari, V. Gupta, "YOLO based Human Action Recognition and Localization", Procedia Computer Science, Vol. 133, 2018, pp. 831–838.

[27] M. J. Shaifee, B. Chywl, F. Li, A. Wong, "Fast YOLO: A Fast You Only Look Once System for Real-time Embedded Object Detection in Video", Journal of Computational Vision and Imaging Systems, Vol. 3, No. 1, 2017.

[28] W. Liu et al. "SSD Single Shot MultiBox Detector", arXiv:1512.02325v5, 2016.

[29] J. Redmon, S. Divvala, R. Girshick, A. Farhadi, "You Only Look Once: Unified, Real-Time Object Detection", arXiv:1506.02640v5, 2016.

[30] P. H. B, V. Ferrari, "End-to-End Training of Object Class Detectors for Mean Average Precision", Proceedings of the 13th Asian Conference on Computer Vision, Taipei, Taiwan, 20-24 November 2016, pp. 198–213.

[31] H. Chu, K. Wang, X. Xing, "Target Tracking via Particle Filter and Convolutional Network", Journal of Electrical and Computer Engineering, Vol. 2018.

[32] C. Urrea, R. Agramonte, "Kalman Filter: Historical Overview and Review of Its Use in Robotics 60 Years after Its Creation", Journal of Sensors, Vol. 2021, No. 1, 2021.

[33] W. Pitts, W. S. McCulloch, "How we know universals the perception of auditory and visual forms", The Bulletin of Mathematical Biophysics, Vol. 9, No. 3, 1947, pp. 127–147.

[34] H. Fu, L. Wu, M. Jian, Y. Yang, X. Wang, "MF-SORT: Simple Online and Realtime Tracking with Motion Features", Proceedings of the International Conference on Image and Graphics, Beijing, China, 23-25 August 2019, pp. 157–168.

[35] Y. Zhang et al. "ByteTrack: Multi-Object Tracking by Associating Every Detection Box", arXiv:2110.06864v3, 2022.

[36] A. Jakubović, J. Velagić, "Image feature matching and object detection using brute-force matchers", Proceedings of the International Symposium ELMAR, Zadar, Croatia, 16-19 September 2018, pp. 83–86.

# Labelled Classifier with Weighted Drift Trigger Model using Machine Learning for Streaming Data Analysis

Original Scientific Paper

**Gollanapalli V Prasad**
GNI Technical Campus,
Hyderabad, Telangana
prasad.venkata8@gmail.com

**S Krishna Mohan Rao**
Sidartha Institute of Enginiring Techology,
Hydeabad, Telangana
Krishnamohan6@yahoo.com

**Kapil Sharma**
Computer Science and Engineering,
Amity University,
Gwalior, India
ksharma@gwa.amity.edu

**Venkatadri M**
Amity School of Engineering & Technology (ASET)
Gwalior, India
vmarriboyina@gwa.amity.edu

**Rama Krishna B**
GNI Technical Campus,
Hyderabad, Telangana
ramakrishnabasude@gmail.com

***Abstract*** *– The term "data-drift" refers to a difference between the data used to test and validate a model and the data used to deploy it in production. It is possible for data to drift for a variety of reasons. The track of time is an important consideration. Data mining procedures such as classification, clustering, and data stream mining are critical to information extraction and knowledge discovery because of the possibility for significant data type and dimensionality changes over time. The amount of research on mining and analyzing real-time streaming data has risen dramatically in the recent decade. As the name suggests, it's a stream of data that originates from a number of sources. Analyzing information assets has taken on increased significance in the quest for real-time analytics fulfilment. Traditional mining methods are no longer effective since data is acting in a different way. Aside from storage and temporal constraints, data streams provide additional challenges because just a single pass of the data is required. The dynamic nature of data streams makes it difficult to run any mining method, such as classification, clustering, or indexing, in a single iteration of data. This research identifies concept drift in streaming data classification. For data classification techniques, a Labelled Classifier with Weighted Drift Trigger Model (LCWDTM) is proposed that provides categorization and the capacity to tackle concept drift difficulties. The proposed classifier efficiency is contrasted with the existing classifiers and the results represent that the proposed model in data drift detection is accurate and efficient.*

***Keywords***: *Data Clustering, Data Classification, Data Stream Mining, Streaming Data, Drift Detection, Drift Trigger Model, Labelled Classifier*

## 1. INTRODUCTION

With the help of Data Streaming Mining (DSM), knowledge structures can be gleaned from rapidly changing [1], continuous data streams. Streams of data can be read only once or a few times using limited computational and storage resources in many applications of data stream mining [2]. To forecast the class or values of new instances in a data stream, many common data mining applications rely on prior knowledge of class membership [3] or values of earlier data stream instances [4]. It is possible to learn this prediction model from labelled samples using machine learning techniques in an automated manner. Concepts from the incremental learning area are frequently used to deal with structural changes, online learning and real time requirements [5]. Non-stationary environments, where the distribution of instances or their labelling criteria may change over time [6], may need a change in the purpose of a prediction, such as which class to predict, or what target value to predict [7]. Concept drift is the name given to this phenomenon. Data stream mining relies heavily on the detection of concept drift. Additionally, when implementing machine intelligence to streaming data [8], there are other issues that need to be addressed, such as partially and delayed labelled data [9], concept drift recovery, and temporal dependencies [10].

Data repositories on the World Wide Web are expanding at a quicker rate than ever before, using real-time web applications [11]. Apps have started to use data mining techniques to analyse the massive amounts of data, in order to identify trends or patterns that may be used to make better business decisions [12], as the amount of data grows dramatically. Real-time decision making is becoming increasingly crucial in computer science and engineering, and data mining is becoming a major study topic. This is because of data mining techniques, which are able to successfully deal with the storage and processing constraints [13]. It has recently been proposed to use data mining techniques to handle streaming data, which is a difficult task. Data streams can be thought of as a continuous stream of training instances that arrive from one or more sources at a high rate of speed [14]. Mining continuous real-time streaming data with reasonable performance is a process known as data stream mining [15] [16].

Data stream mining is essential in a wide range of real-time applications, including detecting attacks, stock market monitoring, and web personalization [17]. It is challenging to build strategies for real-time mining of streaming data because it is so time-consuming [18]. One or more scans of the data may be required to convert it into information in traditional Online Analytical Processing systems (OLAP) [19]. Due to the particular properties of data stream mining, this is not possible. Because of this, standard data mining techniques must be reworked in order to manage data that is constantly flowing from several sources through the network [20]. It has become increasingly important in recent years to process data streams for uncover new information because such data is increasingly accessible via rich internet applications. In developing novel strategies to handle streaming data [21], there are two major obstacles. Fast mining methods for streaming data are the first problem, while the challenge today is to detect data distribution [22] and evolving concepts in an ever-changing environment. The process of streaming data drift detection is represented in Figure 1.

It is important to note that data mining is a significant part of data management. Offline data processing is at the heart of the majority of data mining systems [23]. It is common practice to train predictive models with a pair of data sets. Models trained on previously unseen data are used to anticipate the output of fresh data. It is impossible to handle streaming data concurrently because of the volume of data that is generated on a daily basis [24]. In order to fit all of this data into the machine's main memory, the only viable option is to use online data processing. It is possible to train predictive models by continuously updating them or by guaranteeing that the model retains its accuracy through the use of batches of data [25].

It's possible that the data distribution will shift over time, resulting in settings conducive to concept drift in ever-changing situations. Concept drift occurs when the conditional probability of varying output changes despite the input remaining unchanged [26]. A famous example of real concept drift is when a user's degree of interest shifts as they are following a news stream online [27]. For example, despite the fact that the distribution of a news item that is frequently shared may remain the same, the conditional probability [28] of interesting news items for the user may change. It is possible that the future predictions online are responding to idea drifts as a result of the adaptive learning process.

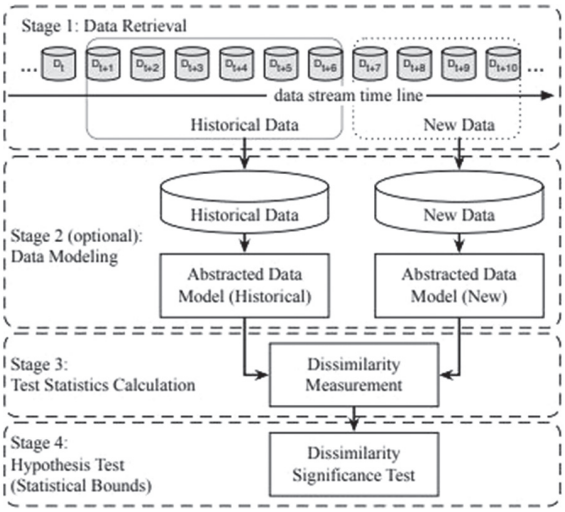


**Fig. 1.** Drift Detection Process

Predictive models that are able to effectively characterise the actual concepts concealed in data streams are the goal of DSM. As time goes on, new concepts are introduced, and rare data samples are discovered. This is the fundamental problem that arises during this process. The phenomena are referred to as notion drift. Class borders can be actual or virtual, depending on how the data is distributed in relation to those boundaries. Depending on how long it's been going on, data can be classified as either sudden or progressive. A continually changing environment necessitates that previously constructed models be constantly updated. There are two major ways to approach this task. As a blind adaptation, we constantly update our model independent of the stream's real condition.

A significant limitation on every unsupervised adaptive machine learning model, the restricted labelling plan could quickly make this technique unfeasible. Labelled instances are necessary for updating an algorithm that exists. It's impossible to expect that a corporation will have time or money to give annotations for all of the data that comes in, since collecting the accurate labels entails both a cost and time. There is no reason to waste time and money on fresh data points if there has been no change in the situation. The second strategy aims to update a system only when it is truly necessary, such as after a drift has occurred. A drift detector is a critical part of every such solution. In order to keep track of a stream's current condition, it monitors it using a model and alerts the user

when it changes. As a result, we have the ability to better manage our budget expenditure. The model can be kept stable, and we can use it when drift has been triggered and the model has become obsolete.

## 2. LITERATURE SURVEY

Khamassi et al. [1] proposed a model that take account a subcategory that includes unsupervised approaches, however none of those works are unique to unsupervised drift detection. Only unsupervised detection techniques are covered in their research. To put it another way, the proposed taxonomy is innovative because it focuses on features of detectors developed for unsupervised situations. The classification of autonomous drift detection systems given by Fernández et al. [2] is divided into three broad classes. In the first category, approaches that monitor error rates are considered, such as the Drift Detection Method (DDM), the Early Drift Detection Method (EDDM) and others. Distance measurements are used to estimate the resemblance between prior and present data distributions in the second class. There are further ways that employ several hypothesis tests to look for changes in an idea. No one class is specific to unsupervised methods but Cano et al. [3] presented an unstructured or semi-supervised approaches that fit into the last two classifications. According to the taxonomy established by Idrees et al. [5], autonomous detectors may fall within the two last categories.

According to Fernandez et al. [6], concept drift detection systems can be classified as either performance-based or data distribution-based. Some error-related parameter is continuously monitored in performance-based methods such as precision and recall. Generally speaking, a drop in an important statistic indicates a drift. These methods are inapplicable to unsupervised tasks since true labels are required to estimate mistakes. Distribution-based techniques, on the other hand, use metrics like location, density, and range to monitor distribution. This category includes both supervised and unsupervised methods. Barddal et al. [8] presented a categorization of approaches based on these two classes, and remark that this group contains these two methods.

Lin et al. [9] proposed classification approaches that are used under the guidance of an investigator. As a starting point, the techniques are divided into four main categories: statistical, window-based, and block-based methods, and incremental-based methods. For example, the Cumulative Average and the Page–Hinckley Test are examples of statistical detectors and drift detection methods are all part of this group. Approaches that monitor the accuracy of the classifier in a window are part of a second class that includes window-based methods. Methods based on monitoring ensemble classification accuracy differ in how data are processed as a response to drift, as shown by the last two classes. Methods in the class retrain classifications on chunks or blocks of examples, whereas methods in the last class retrain progressively with each new arrival of a new classifier.

"How are data processed?" "How is learning processed?" "How is concept drift monitored?" "How is concept drift handled?" and "What are the performance criteria?" are some of the questions posed by Junior et al. [11]. There are a number of different ways to answer this question, and they're categorised according the type of analysis they employ. The classification of unsupervised approaches is further refined into resemblance in time, similarities in space, and model complexity metrics by the authors. The first has to do with the differences in distribution between two timestamps, which are typically found using hypothesis testing, all used distance functions such Euclidean, Heterogeneous Euclidean-overlap, and Mahalanobis distances to monitor the evolution of data distribution in space. Changes in structural models and/or parameters are the focus of the last group.

According to Montiel et al. [12], there are just a few studies that take into account the temporal dependence of concept drift detection in the literature. This criterion is not included in our taxonomy because the author focused on the more modern aspects of supervised drift detection systems. Accordingly, all of the strategies mentioned here can be classified as belonging to the similarity-in-space category. Because of this, our taxonomy has been expanded to include more ways. Lastly, the final group is algorithm-dependent, but the works mentioned in this article can be produced using any machine learning technique

Even if conceptual evolution is solved, it still has a high false alarm rate for particular datasets and therefore can distinguish between distinct novel class problems. Pesaranghader et al. [15] came up with a way to deal with idea evolution induced by the emergence of new classes. Additional classifier sets are added to the main one. As soon as the primary classification set and the related classifier set establish that an incoming instance is an outlier, it is briefly kept in a buffer. The new class identification module is invoked for detection until there are enough examples in the buffer. An instance of a novel class will be indicated if it exists. According to the literature, the feature translation technique is proposed to handle the evolution of streaming data features. To address the issue of feature evolution in the data stream, the classic data stream integrating classifier is paired with a new class detection method.

Data mining relies on traditional learners, which are well-known classifiers, to meet their stream mining needs [16]. A forgetting process and other characteristics of an online learner are present. Naive Bayes, Neural network, and Decision tree rules are some of the techniques employed in [17]. When dealing with data that changes over time, a technique known a windowing technique may be used. There is a restriction on how many examples can be presented. FISH, ADWIN, and weighted windows are all examples of windowing strategies. Any learner can be adapted to evolving stream data using drift detector algorithms. When a conceptual model begins to stray, an alert goes off, prompting the learner to make corrections. It is

possible to discover drifts in conceptual thinking when utilizing DDM and EDDM [18].

A number of drift instances cannot be accommodated by the ensemble approach utilized in [19]. This problem can be better handled with adaptive classifiers. Recently, a number of studies have focused on adaptable learning methods using ELM-based single classifiers and ensembles for CD adaptation. A good example is Incremental Data Stream ELM, which trained its classifier in a gradual manner. A dynamic number of hidden neurons and the selection of certain Activation Layer enhances the model's performance in this method. This technique, on the other hand, soley considers stream data in the case of slow drift [20]. Current ML models aren't robust enough to operate in a nonstationary environment because of the necessity for significant improvements in accuracy and adaptability.

Researchers have focused on Concept Drift for the past decade since it has a wide range of vital applications. There are numerous studies on Concept Drift detection and adaptation that are well-researched, however there isn't any integrated information in the literature. Olorunnimbe et al. [21] provide an overview of Concept Drift Learning in a new survey, focusing on adaptation and detection strategies as well as CD datasets utilized in previous works. Researchers did not conduct a comparative examination of existing adaptation and detection tools or protective research directions for CD concerns in this study.

## 3. PROPOSED MODEL

Traditional machine learning applications use batch learning algorithms to analyse static datasets. Batch learning is a type of learning strategy in which all of the training data is available at once. Depending on the algorithm, the information may be disclosed once or numerous times. A variety of factors preclude batch learning from working with data streams. Since examples arrive sequentially and continually in a distributed method, common approaches have all of the data at their fingertips. A stream-mining algorithm must be built to function with just one pass of data, unlike batch and multi-pass instructional strategies.

The data distribution is assumed to be constant in classic machine learning approaches. An inherent property of a stream is that it is subject to change throughout time. This has rendered batch processing learning methods outdated. A data stream's distributing of instances is said to be 'drifting' when the term 'concept drift' is used. Over time, ideas evolve, but the speed at which they do so varies. Some instances can become obsolete because their dispersion no longer truly depicts their class classification; in other circumstances, it can be a problem. Models must be able to forget previous examples in order to keep up with new ideas once the concept has rambled.

The proposed classifier handles data drifts effectively. It is a classic learner modelled for stationary data mining that has the characteristics of an online learner mechanism. When it comes to classifier, a polling procedure is used to assemble the results. The classification accuracy is superior to that of a single classifier's combined decision. Adapting to new concepts is a natural process for them because of their modularity. Concept drift is a result of data distribution changing over time in dynamic or non-stationary situations. It is possible to fast adapt the concept drifts by saving concept descriptions, which may be re-examined and repurposed after words. Adopting an adaptive learning strategy bi therefore necessary when dealing with data in non-stationary settings. To maintain correctness, an existing model must be updated when conceptual drift is discovered.

An effective drift detector must be capable of distinguishing between real changes and false alarms, and this balance must be maintained. Using local output of feature subspace-based judgements, it is necessary to assess whether the entire data stream is affected by a concept drift. As long as the choice is made by a simple majority, it may not be as sensitive as one might prefer.

The drift data is considered for analysis and for detecting change of data. The records are initially analysed from the input and the initial analysis is performed as

The proposed model drift detection procedure is represented in Figure 2. The figure represents the flow of drift detection in streaming data.

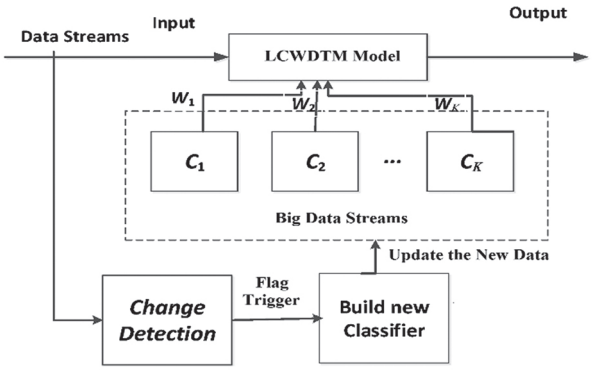


**Fig. 2.** Proposed Framework

$$Data\_Set[M] = \sum_{i=1}^{N} T_N\,(Record(row(i) + V_i^n(value)) \quad (1)$$

The data will be clustered based on the similarity values of the records and the cluster sets are monitored for drift detection by allocating labels to the determined attributes in the record set. The clustering process is applied as

$$Cluster\_Set(Data\_Set[M]) = \sum_{i=1}^{M} \max\left(\frac{sim(\mathrm{Re}\,cord(i), \mathrm{Re}\,cord(i+1)}{count(\mathrm{Re}\,cords(Data\_Set[M]))}\right) + \sum_{j=1}^{M} comp(V, V+j) \quad (2)$$

The record features are considered and then labelling is perfomed for each and every variable vector so

that change in the value will be triggered based on the label it is easy to identify the drift in the data. The labelling procedure of features are performed as

$$Labelled(Cluster_{Set[M]}) = \left( \sum_{i \in M} \sum_{i=1} \frac{\min(\text{Cluster\_Set(Record(i)}, \text{Cluster\_Set(Record(i+1)})}{\text{sizeof(Cluster\_Set[M])}} + random(V) \right) \quad (3)$$

The weights for the variables are assigned for accurate drift detection so that clusters sets are verified based on weights each cluster set is verified for drift data in sequence. The weights are allocated as

$$Weight\_Alloc(Labelled(R(M)))_N = \left( \frac{comp(\text{Prev}_{\text{Val(V)}}, \text{New}_{\text{val(V)}}) > (MDiff(Pev\_Val))^N}{\text{size(Labelled\_Set)}} \right) \quad (4)$$

Moving Average Convergence Divergence (MACD) is an indicator that shows the trend of the streaming data changes, and is based on Exponential Moving Average (EMA). MACD is calculated as

$$MACD(DSP) = EMA(Pr\,e\,v(V), New(V), L) \quad (5)$$

Here EMA signifies the more recent updated price based on the length L that represents the number of days values considered in the analysis of drift detection. Based on the MACD calculated, the EMA is updates as

$$EMA(New(V), L) = New(V) - Pr\,e\,v(V) + MACD \quad (6)$$

Relative Strength Index (RSI) is an oscillator-based indicator that focuses on the strengths and weaknesses of the data changes and updates weights to the variables. It is formulated as follows:

$$RSI = 100 - \frac{100}{1 + \frac{average\ gain}{average\ loss}} + \Sigma_{j=1}^{Q} weight\_alloc_j \left( \Sigma_{i=1}^{N} weight\_alloc(Cluster\_Set) \right) \quad (7)$$

The labelling is based on the weight drift trigger that automatically triggers the variable change prediction update based on the weights allocated for variables. The labelling is performed as

$$Labelling(W_{Ut}) = \frac{1}{MACD} \Sigma_{i=1}^{p} \left\{ max \left[ 0, \frac{1}{1 + abs\left(RSI(Pr\,ev\_Loss)_N^{EMA}\right)}, \frac{1}{1 + min\left(MDiff(Ut(i,j))\right)_{Dt}^{Pr\,ev\_Loss}} \right] \right. \quad (8)$$

The drift detection is performed and the drift identified set of clusters are maintained for considering the updated drift dataset that is used for further analysis. The updated drift detected set is maintained as

$$Drift\_Detect - Set(Labelled(\text{Re}\,cord(M))) = \frac{\max(RSI) + \min(Labelled(Weight\_Alloc(i)) + \max(MACD)}{size(Labelled\_Set(M)} \quad (9)$$

## 4. RESULTS

The proposed stock market prediction model is implemented using python and evaluated in Google Colab. The dataset is available from the link https://www1.nseindia.com/products/content/equities/indices/historical_index_data.htm. This dataset provides historical information as well as real time data based on the time range provided. The Proposed Labelled Classifier with Weighted Drift Trigger Model (LCWDTM) is compared with the traditional Machine Learning Algorithm for Continuous Concept Drift Detection (MLA-CCDD) Model. The proposed model is compared with the traditional models in terms of Data Records Analysis Time Levels, Data Clustering Accuracy Levels, Drift Detection Time Levels, Drift Trigger Accuracy Rate, Classifier Accuracy for Drift Detection and Error Rate.

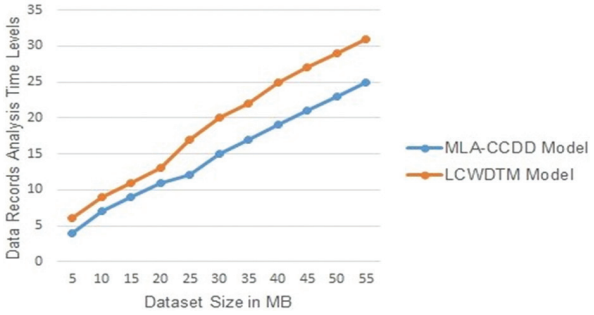


**Fig. 3.** Data Records Analysis Time Levels

Analysing raw data is the act of identifying and synthesising useful information and drawing conclusions from it. It's during this phase that a dataset is organised, transformed and modelled by an investigator or data analyst. In the proposed model, streaming data is considered and the data records are analysed for detection of drift in data. The data records analysis time levels of the proposed and traditional models are shown in Figure 3.

Data Clustering is a machine learning technique for discovering and grouping related data points in huge datasets without regard for the outcome. Clustering is a technique for organising data into patterns that are easier to comprehend and manipulate. Clustering is the process of splitting a population or set of data points into many groups so that measured values in the same category are more similar than data points in other groups. The goal is to separate groups with similar characteristics and assign them to clusters. The data clustering of streaming data accuracy levels of the proposed and existing models are represented in Figure 4.

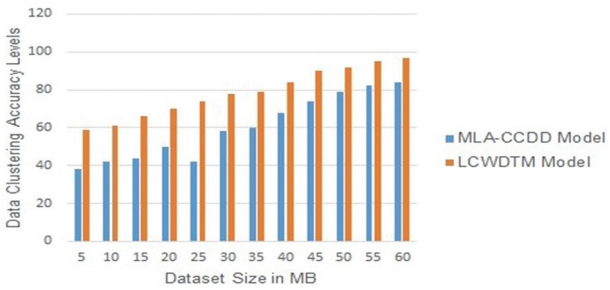


**Fig 4:** Data Clustering Accuracy Levels

To determine whether a data real configuration has drifted from its expected configuration, drift detection is an essential tool. By monitoring the statistical features of data, the model's predictions and their relationship with other parameters, one can detect data drifts. Modern data architectures result in unforeseen and unrecorded changes in data format, interpretation, and infrastructure. However, data drift has the potential to uncover new avenues for data utilisation. The drift detection time levels of the proposed and traditional models are indicated in Figure 5.

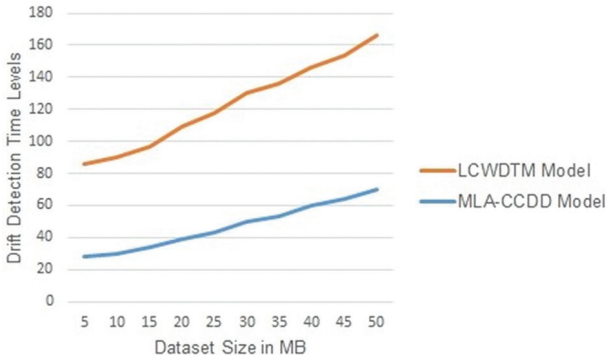


**Fig. 5.** Drift Detection Time Levels

Prescriptive modelling and machine learning might suffer from "concept drift," which refers to a change in statistical features of the target variable. As time passes, the accuracy of the projections deteriorates, which is problematic. The proposed model triggers a flag when there is a data drift observed. The drift trigger accuracy levels of the proposed model is high compared to existing model. The drift trigger accuracy rate of the proposed and traditional models are represented in Figure 6.

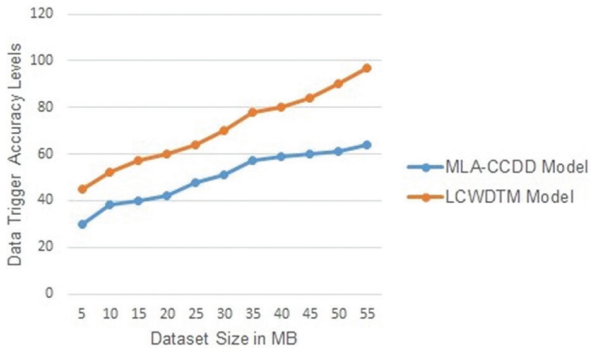


**Fig. 6.** Drift Trigger Accuracy Rate

A data stream is a collection of data that comes from a variety of sources. Real-time analytics necessitates the ability to analyse data as it moves through a system. Traditional mining methods have been ineffective since the nature of data has changed. Data streams have additional hurdles, such as memory and running time limits, as well as a single scan of the data. When a dataset's notion or distribution changes over time, it is referred to as "concept drift".

Due to idea drift even when data is stationary, dealing with this problem becomes more difficult for models and classifiers in data streams. The classifier designed will effectively detects data drifts in handling big streaming data. The proposed classifier achieves an accuracy of 98% in drift detection that represents that the proposed model is efficient that the traditional methods. The classifier accuracy of the proposed and traditional models are shown in Figure 7.

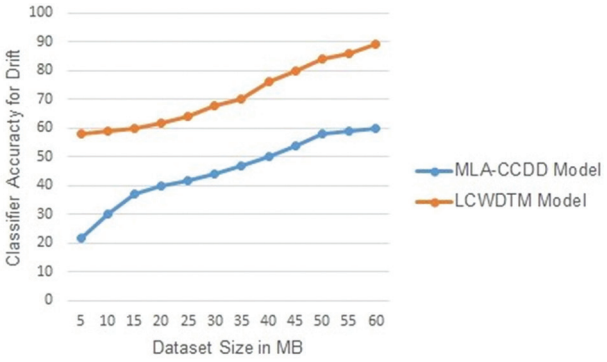


**Fig. 7.** Classifier Accuracy for Drift Detection

The average number of times we get our target's class classification wrong is known as the error rate. True positives and true negatives divided by the total number of true positives, true negatives, false positives, and false negatives is the true positive/negative ratio. The Error rate of the proposed model is high that represents that the performance of the proposed model is high. The error rate of the proposed and traditional models ate shown in Figure 8.

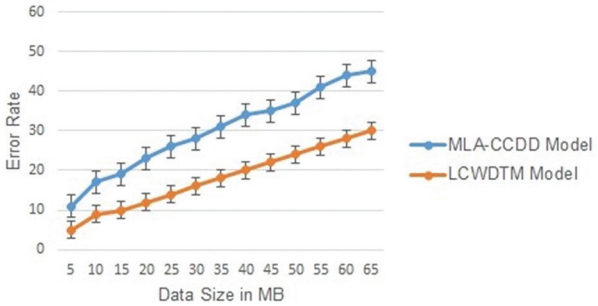


**Fig. 8.** Error Rate

## 5. CONCLUSION

In industrial and commercial applications, stream mining is a tough problem, but it has valuable poten-

tial yields. Data streams are an untapped supply of descriptive and analytical information that might be used in a variety of ways to improve the profitability and efficiency of enterprises. Machine learning approaches are difficult to implement because of the unrestricted size, uncertain pace, and variable features of data streams. Concept drift complicates the difficulty of developing online classifiers that can interpret streaming input. For data classification techniques, a Labelled Classifier with Weighted Drift Trigger Model is proposed that provides categorization and the capacity to tackle concept drift difficulties. Streams of evolving data with idea drift have a distribution that changes over time and at variable rates of severity. If a stream is observed, its core is always shifting, which can lead to a phenomena known as notion drift. Conventional machine learning models based on historical data may no longer be valid when employing streaming data to solve predictive problems. Stream-drifting demonstrated to be ideal for adaptive models provided with methods to reflect changes in the data. The proposed model trigger will be activated if there is any change observed in the data. The proposed classifier achieves an accuracy of 98% in drift detection that represents that the proposed model is efficient than the traditional methods. Another critical deficiency is the unavailability of test datasets for evaluation. Many researchers use generators since there aren't any real-world benchmark datasets available to them. There are a lot of generators available, and each one relies on a different set of user-specified parameters. It's up to the individual to decide which generator and settings are best suited for a given task. Next-generation research should focus on creating gold-standard datasets that can be used for experimentation.

## 6. REFERENCES


[1]. I. Khamassi, M. Sayed-Mouchaweh, M. Hammami, K. Ghédira, "A new combination of diversity techniques in ensemble classifiers for handling complex concept drift", Learning from Data Streams in Evolving Environments, Vol. 41, 2018, pp. 39–61.

[2]. A. Fernández, S. García, M. Galar, R. C. Prati, B. Krawczyk, F. Herrera, "Learning from imbalanced data sets", Springer, Berlin, 2018.

[3]. A. Cano, B. Krawczyk, "Kappa updated ensemble for drifting data stream mining", Machine Learning, Vol. 109, 2020, pp. 175–218.

[4]. Z. H. Ghaderi, H. Altınçay, "Imbalance learning using heterogeneous ensembles", Expert Systems with Applications, Vol. 142, 2020, p. 113005.

[5]. M. M. Idrees, L. L. Minku, F. Stahl, A. A. Badii, "Heterogeneous online learning ensemble for non-stationary environments", Knowledge-Based Systems, Vol. 188, No. 4, 2020, p. 104983.

[6]. J. L. Fernandez-Aleman, J. M. Carrillo-De-Gea, M. Hosni, A. Idri, G. Garcia-Mateos, "Homogeneous and heterogeneous ensemble classification methods in diabetes disease: a review", Proceedings of the Annual International Conference of the IEEE Engineering in Medicine and Biology Society, 2019.

[7]. H. M. Gomes, A. Bifet, J. Read, J. P. Barddal, F. Enembreck, B. Pfharinger, G. Holmes, T. Abdessalem, "Adaptive random forests for evolving data stream classification", Machine Learning, Vol. 106, No. 9-10, 2017, pp. 1469–1495.

[8]. J. P. Barddal, H. M. Gomes, F. Enembreck, B. Pfahringer, "A survey on feature drift adaptation: definition, benchmark, challenges and future directions", Journal of Systems and Software, Vol. 127, No. 1, 2017, pp. 278–294.

[9]. C. C. Lin, D. J. Deng, C. H. Kuo, L. Chen, "Concept drift detection and adaption in big imbalance industrial IoT data using an ensemble learning method of offline classifiers", IEEE Access, Vol. 7, 2019, pp. 56198–56207.

[10]. A. V. Luong, T. T. Nguyen, A. V. Liew, "Streaming active deep forest for evolving data stream classification", arXiv:2002.11816v1, 2020.

[11]. B. Junior, M. D. C. Nicoletti, "An iterative boosting-based ensemble for streaming data classification", Information Fusion, Vol. 45, 2019, pp. 66–78.

[12]. J. Montiel, R. Mitchell, E. Frank, B. Pfahringer, T. Abdessalem, A. Bifet, "Adaptive XGBoost for evolving data streams", arXiv:2005.07353v1, 2020.

[13]. D. Brzezinski, J. Stefanowski, "Ensemble diversity in evolving data streams", Proceedings of the International Conference on Discovery Science, Bari, Italy, October 19–21, 2016, pp. 229–244.

[14]. J. Large, J. Lines, A. J. Bagnall, "The heterogeneous ensembles of standard classification algorithms (HESCA): the whole is greater than the sum of its parts", Data Mining and Knowledge Discovery, Vol. 33, 2019, pp. 1674–1709.

[15]. A. Pesaranghader, H. Viktor, E. Paquet, "Reservoir of diverse adaptive learners and stacking fast

hoeffding drift detection methods for evolving data streams", Machine Learning, Vol. 107, 2018, pp. 1711–1743.

[16]. C. T. Li, M. K. Shan, S. H. Jheng, K. C. Chou, "Exploiting concept drift to predict popularity of social multimedia in microblogs", Information Sciences, Vol. 339, 2016, pp. 310–33.

[17]. S. Liu, L. Feng, J. Wu, G. Hou, G. Han, "Concept drift detection for data stream learning based on angle optimized global embedding and principal component analysis in sensor networks", Computers and Electrical Engineering, Vol. 58, No. 8, 2017, pp. 327–336.

[18]. Y. Y. Lo, W. Liao, C. S. Chang, Y. C. Lee, "Temporal matrix factorization for tracking concept drift in individual user preferences", IEEE Transactions on Computational Social Systems, Vol. 5, No. 1, 2018, pp. 156–168.

[19]. D. Marrón, E. Ayguadé, J. R. Herrero, A. Bifet, "Resource-aware elastic swap random forest for evolving data streams", arXiv:1905.05881v1, 2019.

[20]. J. Montiel, J. Read, A. Bifet, T. Abdessalem, "Scikit-multiflow: a multi-output streaming framework", Journal of Machine Learning Research, Vol. 19, No. 72, 2018, pp. 1–5.

[21]. M. K. Olorunnimbe, H. L. Viktor, E. Paquet, "Dynamic adaptation of online ensembles for drifting data streams", Journal of intelligent information Systems, Vol. 50, No. 2, 2018, 291–313.

[22]. S. Ren, B. Liao, W. Zhu, Z. Li, W. Liu, K. Li, "The gradual resampling ensemble for mining imbalanced data streams with concept drift", Neurocomputing, Vol.286, 2018, pp. 150–166.

[23]. D. Ruano-Ordás, F. Fdez-Riverola, J. R. Méndez, "Concept drift in e-mail datasets: an empirical study with practical implications", Information Sciences, Vol. 428, 2018, pp. 120–135.

[24]. O. Sagi, L. Rokach, "Ensemble learning: a survey", Data Mining and Knowledge Discovery, Vol. 8, No. 5, 2018, p. e1249.

[25]. J. N. Van Rijn, G. Holmes, B. Pfahringer, J. Vanschoren, "The online performance estimation framework: heterogeneous ensemble learning for data streams", Machine Learning, Vol. 107, 2018, pp. 149–176.

[26]. S. Wang, L. L. Minku, X. Yao, "A systematic study of online class imbalance learning with concept drift", IEEE Transactions on Neural Networks and Learning Systems, 2018.

[27]. J. Zenisek, F. Holzinger, M. Affenzeller, "Machine learning based concept drift detection for predictive maintenance", Computers and Industrial Engineering, Vol. 137, 2019, p. 106031.

[28]. B. Krawczyk, L. L. Minku, J. Gama, J. Stefanowski, and M. Wozniak, "Ensemble learning for data stream analysis: A survey," Information Fusion, Vol. 37, 2017, pp. 132–156.

# Improved control for DFIG based wind power system under voltage dips using ADRC optimized by genetic algorithms

Original Scientific Paper

**Noureddine Elmouhi**
Mohammed V University in Rabat,
Ecole Nationale Supérieure d'Arts et Métiers (ENSAM),
Research Center in Sciences and Technologies of Engineering and Health (STIS)
Institut supérieur d'ingénierie et des affaires (ISGA Rabat),
Laboratory of Innovation in Management and Engineering for Enterprise (LIMIE), Rabat, Morocco.
n.elmouhi@gmail.com

**Ahmed Essadki**
Mohammed V University in Rabat,
Ecole Nationale Supérieure d'Arts et Métiers (ENSAM),
Research Center in Sciences and Technologies of Engineering and Health (STIS), Rabat, Morocco
Ahmed.essadki1@gmail.com

**Hind Elaimani**
Mohammed V University in Rabat,
Ecole Nationale Supérieure d'Arts et Métiers (ENSAM),
Research Center in Sciences and Technologies of Engineering and Health (STIS)
Institut supérieur d'ingénierie et des affaires (ISGA Rabat),
Laboratory of Innovation in Management and Engineering for Enterprise (LIMIE), Rabat, Morocco.
h.elaimani@gmail.com

***Abstract*** *– Many countries have focused on the study of the electrical energy production using wind generators. These studies include maintaining the production under disturbed conditions at the grid connection point of wind farms, and maintaining production during voltage dips. Electrical grid operators have established different requirements for connecting renewable energy production systems to electrical grids. In this research paper, we are interested in the study of the wind power system based on the Doubly Fed Induction Generator during a voltage dip. We are also developing a control approach based on Active Disturbance Rejection Control and Genetic Algorithms, which aims to control the stator flux variations which should be taken into account during the current controllers computing. This control strategy will allow the wind power system to remain connected to the grid under voltage dips, and to resume the normal operation after the fault disappearance. The model of the wind power system and the proposed control strategy, are tested in the MATLAB-Simulink software.*

***Keywords****: ADRC, DFIG Control, wind turbine, MPPT, wind energy, genetic algorithm, voltage dips*

## 1. INTRODUCTION

In wind turbine-based power generation stations, the Doubly-fed Induction Generator (DFIG) is the most adopted and installed configuration by leaders in wind turbine construction around the world. Indeed, it has many advantages due to its ability to supply energy at constant voltage and frequency for a variable rotor speed, which allows maximum power extraction regardless of the wind speed [1], [2].

The configuration of wind power system based on DFIG is presented in figure 1. As shown in this structure, the stator is directly connected to the grid and the rotor is connected by means of two converters, a grid filter and a transformer [2,3,4].

The electrical energy produced must correspond to the expectations of consumers, producers and grid managers. Among the main criteria for measuring the level of the energy produced quality, we find the sensitivity to voltage dips and the quality of the injected signal (harmonic distortion rate).

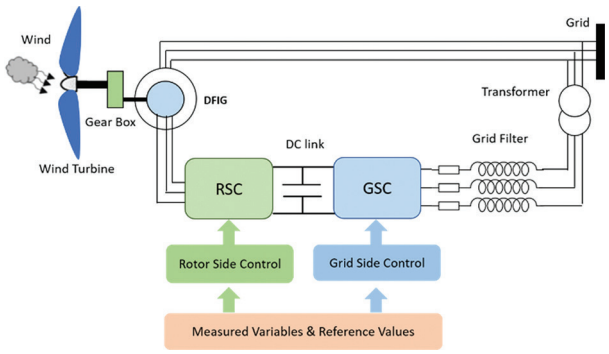


**Fig. 1.** Variable speed wind turbine structure

The DFIG presents many difficulties with regard to compliance with the conditions for connection to the electricity grid imposed by the electrical grid managers. Indeed, it is very sensitive to electrical faults, in particular voltage dips in the grid [5]. During voltage faults, the wind power system is destabilized and the internal protection system intervenes to its disconnection from the grid. This disconnection reinforces the imbalance in voltage and frequency. However, wind turbines are forced to remain connected after voltage dips [3,4].

The use of the DFIG is based on the power converters as an interface with the grid, this interface generates harmonic currents liable to induce harmonic voltages in the grid, which requires the limitation of these harmonic currents.

For the problem related to voltage dips, some research [6,7,8] has proposed an approach which is based on PI controllers for the command adaptation in the voltage dips event. However, this solution does not present the robustness against the internal parameters change of the DFIG. Especially since the synthesis of these regulators is based on these parameters.

Other authors, in other works [9,10], has proposed to use synchronous static compensators to participate in voltage setting during voltage dips. The problem of this solution is that it presents a very high implementation cost.

The authors in [11] propose a method for better attenuation of switching harmonics. This method is based on linear Active Disturbances Rejection Control ADRC while providing compensation of resonant poles in the LCL filter via zero pole cancellation [11]. This strategy is effective under the grid impedance uncertainty, and ensures the filtering of the parameter's uncertainties without adjustment of control. This approach has shown good performance compared to control by conventional PI regulators.

In [12] and [13], the work is focused on the use of an LCL filter and the problem of interactive resonance which is triggered by the interaction between inverters, this causes a mutual current in the grid. For this disturbance, considered as external, the authors propose a control approach to estimate and then cancel these disturbances by using ADRC technique [12]. This technique is introduced first for an L filter and then for an LCL. The results of this approach showed that the resonance and antiresonance peaks present in the LCL filter, with the current on the inverter side, are damped using the pole-zero cancellation technique [13].

In this paper, the work is focused on the study and the analysis of the DFIG behavior in the case of the first criterion relating to the electrical energy quality, mentioned above, which is the sensitivity to voltage dips. In effect, the drop in stator voltage leads to:

- A decrease in the electromagnetic torque which causes an increase in the speed of rotation.
- A drop in the magnetic flux and consequently the demagnetization of the machine.
- An increase in the stator and rotor current as well as the DC link voltage. This increase triggers the protection circuits and consequently the wind turbine disconnection.

The objective is to establish a robust control method using ADRC and genetic algorithms, which allows to keep the wind turbine connected to the grid. Indeed, the ADRC, with the proposed adaptation in this paper, makes it possible to resume normal operation after the fault disappearance, while ensuring robustness against changes in the internal parameters system. The genetic algorithm makes it possible to find an optimal adjustment of the different controllers used in this approach.

This article is structured as follows: the first part will be devoted to the development of the dynamic model of the wind power system, then we will develop the Active Disturbance Rejection Control of converters. The second part will be entirely devoted to the study of the system behavior during the voltage fault, and to the adaptation of the DFIG command. The final section of this paper will be devoted to presenting and interpreting simulation results using the MATLAB / Simulink environment.

## 2. DYNAMIC MODEL OF WIND POWER SYSTEM

### 2.1. WIND TURBINE MODEL

A wind turbine is characterized by an aerodynamic torque, which is given by the following expression [10]:

$$T_{aer} = \frac{P_{extr}}{\Omega_t} = \frac{1}{2.\Omega_t} \rho \, \pi \, R^2 \, v^3 C_p(\beta, \lambda) \tag{1}$$

$P_{extr}$ is the maximum power that can be extracted which is given by [3,14]:

$$P_{extr} = \frac{1}{2} \rho \, \pi \, R^2 \, v^3 C_p(\beta, \lambda) \tag{2}$$

$C_p$ is a power coefficient turbine, which depends on λ, the velocity ratio, and the pich angle β [3]. It is expressed by:

$$C_p(\lambda, \beta) = \frac{1}{2}\left(116\left(\frac{1}{\lambda+0.08\beta} + \frac{0.035}{1+\beta^3}\right) - 0.4\beta - 5\right) e^{-21\left(\frac{1}{\lambda+0.08\beta} + \frac{0.035}{1+\beta^3}\right)} + 0.0068\lambda \tag{3}$$

The mechanical speed is expressed by the following expression [3,15]:

$$J.\frac{d\Omega_{mec}}{dt} = T_{mec} \tag{4}$$

$$J = \frac{J_{Turbine}}{G^2} + J_g \tag{5}$$

$$J\frac{d\Omega_{mec}}{dt} + f\Omega_{mec} = T_g - T_{em} \tag{6}$$

### 2.2. DFIG MODELLING

The equations of DFIG model in the Park reference dq and the electromagnetic torque are given by the following expressions [16]:

$$\begin{cases} \Phi_{sd} = L_s i_{sd} + L_m i_{rd} \\ \Phi_{sq} = L_s i_{sq} + L_m i_{rq} \\ \Phi_{rd} = L_r i_{rd} + L_m i_{sd} \\ \Phi_{rq} = L_r i_{rq} + L_m i_{sq} \end{cases} \tag{7}$$

$$\begin{cases} V_{sd} = R_s i_{sd} + \frac{d\Phi_{sd}}{dt} - \omega_s \Phi_{sq} \\ V_{sq} = R_s i_{sq} + \frac{d\varphi_{sq}}{dt} + \omega_s \Phi_{sd} \\ V_{rd} = R_r i_{rd} + \frac{d\varphi_{rd}}{dt} - \omega_r \Phi_{rq} \\ V_{rq} = R_r i_{rq} + \frac{d\varphi_{rq}}{dt} + \omega_r \Phi_{rd} \end{cases} \tag{8}$$

$$T_{em} = p\frac{L_m}{L_s}(i_{rd}\Phi_{sq} - i_{rq}\Phi_{sd}) \tag{9}$$

The expressions of active and reactive powers are:

$$\begin{cases} P_s = V_{sd} i_{sd} + V_{sq} i_{sq} \\ Q_s = V_{sq} i_{sd} - V_{sd} i_{sq} \end{cases} \tag{10}$$

$$\begin{cases} P_r = V_{rd} i_{rd} + V_{rq} i_{rq} \\ Q_r = V_{rq} i_{rd} - V_{rd} i_{rq} \end{cases} \tag{11}$$

For a medium and high power DFIG, the stator resistance Rs can be neglected [17]. The previous equations can be simplified by directing the stator flux in accordance with d-axis:

$$T_{em} = -\frac{3}{2}p\frac{L_m}{L_s} i_{rq}\Phi_s \tag{12}$$

$$P_s = -V_{sq}\frac{L_m}{L_s} i_{rq} \tag{13}$$

$$Q_s = -\frac{V_{sq}\Phi_s}{L_s} - V_{sq}\frac{L_m}{L_s} i_{rd} \tag{14}$$

### 2.3. POWER CONVERTERS

The connection of the DFIG to the grid is made through a converter connected to the rotor, and a converter linked to the grid with a grid filter and transformer [14,15,18,19]. This structure is shown in figure 2:

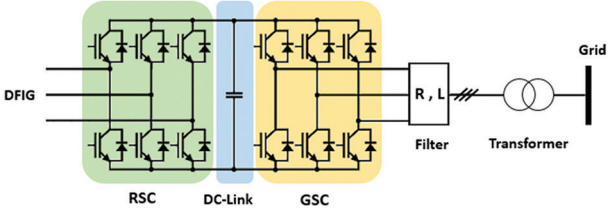


**Fig. 2.** Bloc diagram of RSC, DC link and GSC

The RSC ensures the active and reactive powers control so that they follow their references, and the GSC controls the DC link voltage [20].

## 3. ACTIVE DISTURBANCE REJECTION CONTROL STRATEGY

The Active disturbances rejection control is a robust command based on the extension of the model system by a use of a «Extended State Observer (ESO)» to estimate and cancels internal and external disturbances [3,4,8,21]. Figure 3 and 4 shows the basic structure of ADRC controller and the ESO [22]:

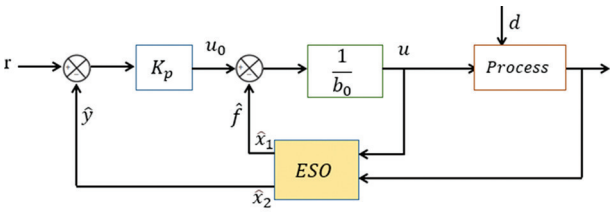


**Fig. 3.** Structure of the first-order ADRC controller

The extended state observer gains are theoretically defined by [23] : $\beta_1=2\omega_0$ *and* $\beta_1=\omega_0^2$

Where $\omega_0$ is determined as a function of the closed-loop system poles to ensure both fast observer dynamics and minimal sensitivity to noise.

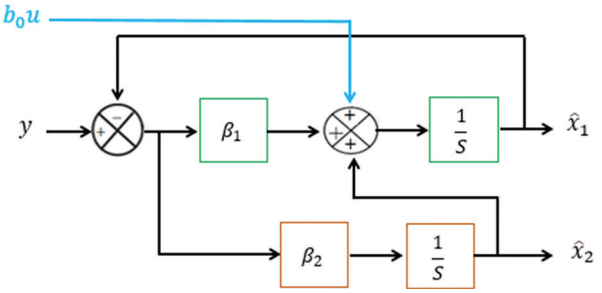


**Fig. 4.** Extended State Observer ESO

### 3.1. ROTOR SIDE CONVERTER CONTROL RSC

By adopting the assumptions relating to the choice of the park reference and to the stator resistance, the rotor currents expressions can be rearranged to be in the following form [24]:

$$\frac{di_{rd}}{dt} = -\frac{R_r}{\sigma L_r} i_{rd} + \omega_r . i_{rq} + \frac{1}{\sigma L_r} V_{rd} \tag{15}$$

$$\frac{di_{rq}}{dt} = -\frac{R_r}{\sigma L_r} i_{rq} - \omega_r . i_{rd} - \omega_r \frac{L_m}{\sigma L_r L_s}\Phi_s + \frac{1}{\sigma L_r} V_{rq} \tag{16}$$

Where $\sigma = 1 - \frac{L_m^2}{L_s L_r}$ represent the dispersion coefficient. We put these expressions in the following form:

$$\frac{di_{rd}}{dt} = f_d(i_{rd}, d, t) + b_0 u(t) \tag{17}$$

$$\frac{di_{rq}}{dt} = f_q(i_{rq}, d, t) + b_0 u(t) \tag{18}$$

Where:

$$\begin{cases} f_d = -\frac{R_r}{\sigma L_r} i_{rd} + \omega_r . i_{rq} + (\frac{1}{\sigma L_r} - b_0) V_{rd} \\ u = V_{rd} \quad , \quad b_0 = \frac{1}{\sigma L_r} \end{cases} \tag{19}$$

$$\begin{cases} f_{dq} = -\frac{R_r}{\sigma L_r} i_{rq} - \omega_r . i_{rd} - \omega_r \frac{L_m}{\sigma L_r L_s} \Phi_s + (\frac{1}{\sigma L_r} - b_0) V_{rq} \\ u = V_{rq} \quad , \quad b_0 = \frac{1}{\sigma L_r} \end{cases} \tag{20}$$

$f_d$ and $f_q$ represent the disturbances impacting respectively affecting the direct and quadratic rotor currents. Vrd and Vrq represent the control set points of the current's loops. The gain parameter b0 represent the known part of the system parameters [24]. It is opted as:

$$b_0 = \frac{1}{\sigma L_r}$$

The reference current $i_{rqRef}$ makes it possible to regulate the electromagnetic torque to its imposed reference by the maximum power point tracker (MPPT) bloc [24]. Its expression is given by the equation 21:

$$i_{rqRef} = \frac{-2L_s}{pL_m \Phi_{sq}} T_{emRef} \tag{21}$$

The reference rotor current $i_{rdRef}$ is determined in order to control the reactive power provided or absorbed by the DFIG [15,25]. Its expression is given by the equation 22. The diagram of the RSC is presented in figure 5.

$$i_{rdRef} = \frac{\Phi_s}{L_m} - \frac{L_m}{V_s L_m} Q_{sref} \tag{22}$$

The parameters $K_p$, $\beta_1$ and $\beta_2$ of the ADRC controllers are determined so that the rotor currents follow their reference $i_{rqRef}$ and $i_{rdRef}$ [26]. This is obtained using genetic algorithms which make it possible to have an optimum response.

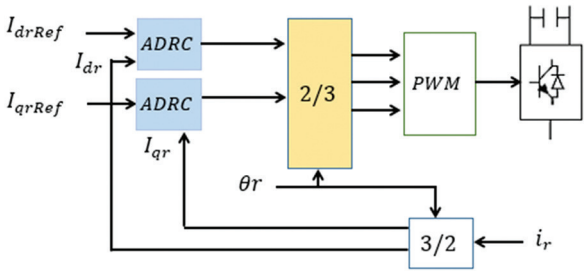


**Fig. 5.** Block diagram of the RSC

### 3.2. CONTROL OF GSC

The grid filter currents $i_{qf}$ and $i_{df}$ are given by the following expressions [27]:

$$\frac{di_{df}}{dt} = \frac{1}{L_f} V_{sd} - \frac{R_f}{L_f} i_{df} - w_s i_{qf} - \frac{1}{L_f} V_{df} \tag{23}$$

$$\frac{di_{qf}}{dt} = \frac{1}{L_f} V_{sq} - \frac{R_f}{L_f} i_{qf} - w_s i_{df} - \frac{1}{L_f} V_{qf} \tag{24}$$

According to the ADRC structure, these expressions can be rearranged to be in the following form:

$$\frac{di_{df}}{dt} = f_{df}(i_{df}, d, t) + b_0 u(t) \tag{25}$$

Where:

$$\begin{cases} f_{df} = \frac{1}{L_f} V_{sd} - \frac{R_f}{L_f} i_{df} - w_s i_{qf} + (\frac{1}{L_f} - b_0) V_{df} \\ u = V_{df} \quad , \quad b_0 = -\frac{1}{L_f} \end{cases} \tag{26}$$

$$\frac{di_{qf}}{dt} = f_{qf}(i_{qf}, d, t) + b_0 u(t) \tag{27}$$

Where:

$$\begin{cases} f_{qf} = \frac{1}{L_f} V_{sq} - \frac{R_f}{L_f} i_{qf} - w_s i_{df} + (\frac{1}{L_f} - b_0) V_{qf} \\ u = V_{qf} \quad , \quad b_0 = -\frac{1}{L_f} \end{cases} \tag{28}$$

The *iqf* and *idf* currents can follow their references by making a good adjustment of the ADRC controller parameters. The gain parameter b0 is opted as:

$$b_0 = -\frac{1}{L_f}$$

The block diagram of the GSC is given in figure 6:

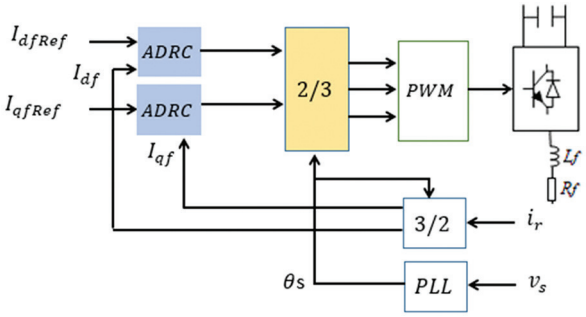


**Fig. 6.** Diagram for the GSC

## 4. CONTROL STRATEGY OF DFIG DURING A VOLTAGE DIP

During a voltage dip, the electromagnetic torque of the generator decreases, which leads to an increase in the rotation speed. This increase is more important as the voltage dip is deeper [20,28]. The stator is directly connected to the grid, which causes the stator flux decrease. When the fault disappears, the DFIG risks re-magnetizing itself suddenly, which causes a strong current to be drawn in and subsequently a system disconnection [25]. However, the dynamics of the stator flux should not be neglected during sizing of the current controller.

The voltage dip also provokes an increase in stator current. This high current passes through the rotor and the converters on the rotor side [22,29]. Which also leads to an increase in the DC-link voltage and consequently the destruction of the power converters [30,31].

The concern during the voltage dip is to keep the wind turbine connected during the fault and to ensure a restart after the disappearance fault. We are also interested to keep the electrical and mechanical quantities of the system under the threshold values trigger-

ing the protection systems [4,32]. Without neglecting the flux dynamics stator flux.

The proposed method to keep the wind turbine connected, consists in taking into account the stator flux variations, during the generation of the command voltages $V_{rd}$ and $V_{rq}$, which are necessary for the rotor side control. Consequently, the neglected terms in the ADRC control equations without voltage dips must be taken into account, and the expressions of the control quantities must be recalculated, as well as the structure of the ADRC control which must be adapted.

The stator currents are given from equation 8:

$$i_{sd} = \frac{\Phi_{sd} - L_m i_{rd}}{L_s} \quad (29)$$

$$i_{sq} = \frac{\Phi_{sq} - L_m i_{rq}}{L_s} \quad (30)$$

From equation 9, the rotor flux is given by:

$$\varphi_{rd} = \sigma L_r i_{rd} + \frac{L_m}{L_s}\Phi_{sd} \quad (31)$$

$$\varphi_{rq} = \sigma L_r i_{rq} + \frac{L_m}{L_s}\Phi_{sq} \quad (32)$$

From the previous equations, the stator voltages can be given by the following expressions:

$$V_{sd} = \frac{R_s}{L_s}\Phi_{sd} - \frac{R_s}{L_s} i_{rd} + \frac{d\Phi_{sd}}{dt} \quad (33)$$

$$V_{sd} = \frac{R_s}{L_s}\Phi_{sd} - \frac{R_s}{L_s} i_{rd} + \frac{d\Phi_{sd}}{dt}$$

So, by replacing the flux expressions in the rotor voltages expressions, we obtain:

$$V_{rd} = R_r i_{rd} + \sigma L_r \frac{di_{rd}}{dt} - \omega_r \sigma L_r i_{rq} - \omega_r \frac{L_m}{L_s}\Phi_{sq} + \frac{L_m}{L_s}\frac{d\Phi_{sd}}{dt}$$
$$V_{rq} = R_r i_{rq} + \sigma L_r \frac{di_{rq}}{dt} + \omega_r \sigma L_r i_{rd} + \omega_r \frac{L_m}{L_s}\Phi_{sd} + \frac{L_m}{L_s}\frac{d\Phi_{sq}}{dt} \quad (34)$$

$$V_{rd} = R_r i_{rd} + \sigma L_r \frac{di_{rd}}{dt} + e_q + e_{\Phi_d}$$

$$V_{rq} = R_r i_{rq} + \sigma L_r \frac{di_{rq}}{dt} + + e_d + e_{\Phi_q}$$

Where:

$$e_d = \omega_r \sigma L_r i_{rd}$$
$$e_q = -\omega_r \sigma L_r i_{rq}$$
$$e_{\Phi_d} = \frac{L_m}{L_s}\left(-\omega_r \Phi_{sq} + \frac{d\Phi_{sd}}{dt}\right)$$
$$e_{\Phi_q} = \frac{L_m}{L_s}\left(\omega_r \Phi_{sd} + \frac{d\Phi_{sq}}{dt}\right)$$

We can so present a DFIG control block by ADRC adapted in the voltage dip event (figure 7):

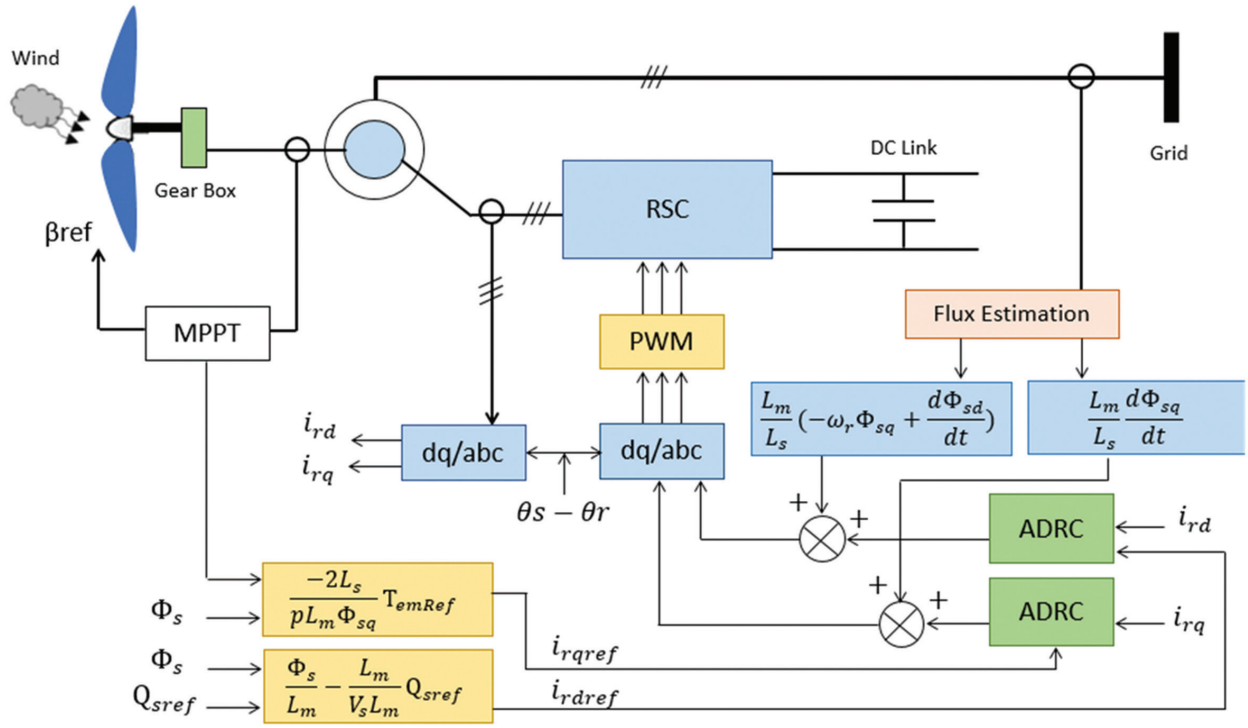


**Fig. 7.** Block diagram of DFIG control in the voltage dip event

The proposed method, which consists in taking into account the dynamics of the stator flux during a voltage dip, can be further improved by using an LCL filter instead of an L filter. Indeed, the results presented by the authors in [11-13] show that this higher order filter allows a better attenuation and reduction of the current harmonics absorbed by the power converters. The resonance effect in this filter will be damped using zero pole cancellation. This allows to keep preserved dynamic performance and a higher stability margins.

## 5. GENETIC ALGORITHM

The genetic algorithm GA is an optimization method based on theories of natural selection [9]. In the litera-

ture, this technique is recognized to be very effective and efficient in finding optimal solutions to optimization problems. It makes it possible to avoid local minima constituting a major problem in the case of nonlinear systems [33,34].

In this technique, the solutions to an optimization problem are represented as chromosomes from an initial population to evolve to an optimal solution with repeated modification [34].

The application of the algorithm is done in three stages: selection, crossing and mutation. these three steps are applied to create new individuals and subsequently assess their performance against the previous ones using a fitness function. [34].

To have the optimal solution, represented by the best individuals, this algorithm must be repeated for many generations and finally stops when it reaches these chromosomes [34]. In figure 8, we present the genetic algorithm optimization diagram to be established to have the ADRC controllers' parameters.

In our case, genetic algorithm is used to optimize the DFIG control in the voltage dip event. the procedure used is as follows:

For each individual belonging to the real population, the objective function is calculated. Therefore, the parameters of the ADRC controller can be decoded, and then the DFIG model is simulated to obtain the objective function value.

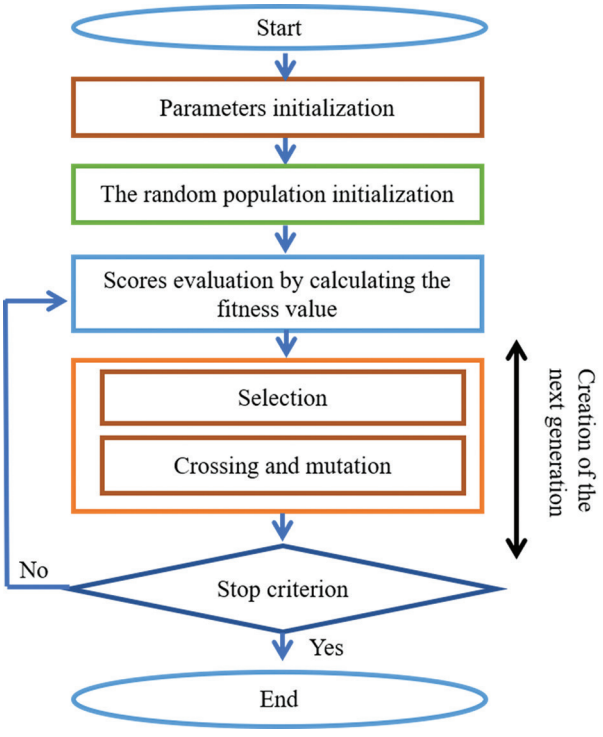


**Fig. 8.** Genetic Algorithm optimization diagram

In our case, genetic algorithm is used to optimize the DFIG control in the voltage dip event. the procedure used is as follows:

For each individual belonging to the real population, the objective function is calculated. Therefore, the parameters of the ADRC controller can be decoded, and then the DFIG model is simulated to obtain the objective function value.

The following population is generated based on the operators of the genetic algorithm, namely selection, crossing and mutation. These two steps are repeated from generation to generation until a final population with optimal values is obtained.

This algorithm is used in our case to adjust the parameters $K_p$, $\beta_1$ and $\beta_2$ so as to obtain the optimal performance in terms of dynamics, robustness and disturbance rejection. The objective function is chosen so that the difference between the reference power and the measured power is as small as possible.

The types of the GA operations used in this work, and the parameters' initialization are listed in Table 1 and 2 below:

**Table 1.** Types of the GA operations used

| Property | Type |
|---|---|
| Selection | GA default selection function |
| Mutation | Uniform |
| Crossover | Arithmetic |

**Table 2.** Genetic algorithm parameters

| Property | Value | |
|---|---|---|
| | Backstepping | ADRC |
| Number of variables | 2 | 3 |
| Population size | 50 | 50 |
| Maximum number of generations | 500 | 500 |
| Mutation fraction | 0.01 | 0.01 |
| Crossover fraction | 0.08 | 0.08 |
| Tolerance | 500 | 500 |

The best score value and mean score versus generation for the ADRC method are represented in the following figure (figure 13):

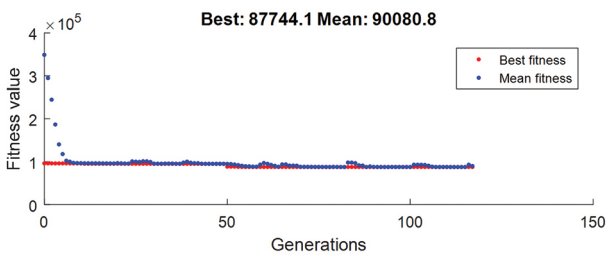


**Fig. 9.** ADRC Fitness value

Using the previous optimization diagram, the Parameters' evolution during the generation is presented in figure 10 and their values obtained bay GA are listed in table 3:

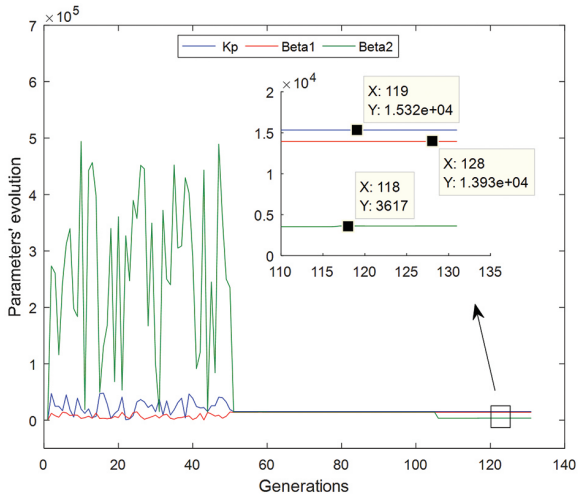


**Fig. 10.** Parameters' evolution during the generation

**Table 3.** ADRC controller parameters

| Parameter | Symbol | Value |
|---|---|---|
| Currents controller gain | $k_p$ | 15320 |
| Extended state observer gains | $\beta_1$ | 13930 |
| | $\beta_2$ | 3617 |

## 6. SIMULATION RESULTS

To study the DFIG behavior in the voltage dip event and the performance of the proposed strategy, we consider a voltage dip with a depth of 50% that lasts 600ms.

The duration of the considered voltage dip is relatively short compared to the wind speed variations and fluctuations. Therefore, we can study with a constant wind speed equal to 12 m.s-1. The DFIG parameters as well as the parameters of DC link and filter are summarized in table 4 and table 5 in appendix. Immediately after the fault appears at t = 1s, the generator voltage drops, as shown in figure 11:

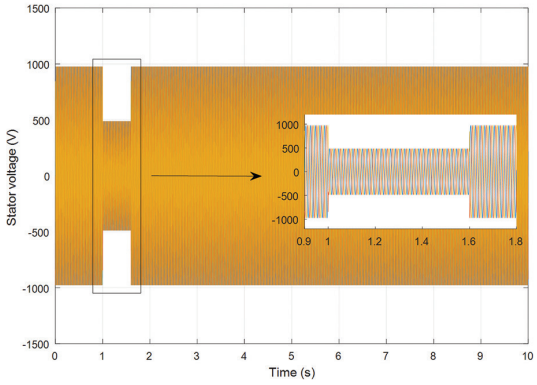


**Fig. 11.** Stator voltages

In next figures, 12 and 13, we present the stator currents with the conventional method and the adapted control strategy.

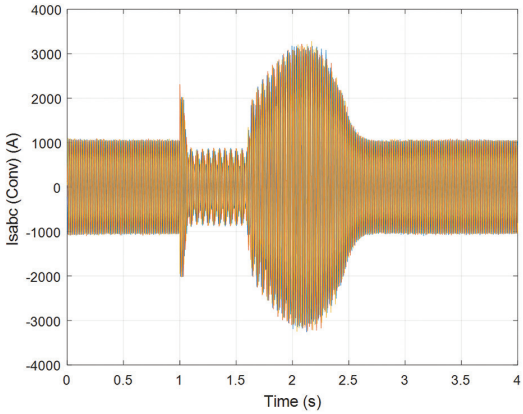


**Fig. 12.** Stator currents with the conventional strategy

From these two figures, we notice that by taking into account the stator flux dynamics, the modified control strategy generates less oscillations compared to the classical method which presents large oscillations and an unbalance after the fault disappearance. The current peak, that occurs when the voltage dip occurs, is due to the additional power introduced into the system during the drop of the transmitted power to the grid. Therefore, the protection circuits responsible for disconnecting the wind turbine from the grid will not be triggered. the system can therefore resume normal operation after the fault disappearance

In figure 14, we present the stator active power transferred to the grid. When the fault occurs, it can be noted that, in the classical method, the active power is completely cancelled out and shows a very remarkable additional overshoot after the fault disappears. This is due to the instability in the torque evolution and the rotation speed, which leads to the disconnection of the turbine by the internal protection systems. In the case of the modified strategy, this power is non-zero during the fault, which shows that the proposed method allows the generator magnetization during the voltage dip. The generation of active power resumes after the fault disappears and recapture its initial value, without exhibiting many oscillations or a large overshoot of the reference value which causes the activation of the protection circuits.

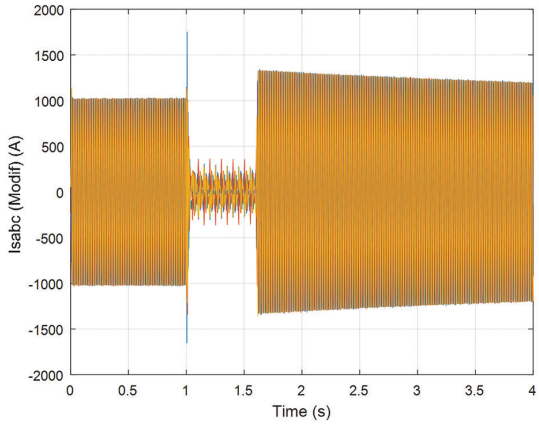


**Fig. 13.** The stator currents with the modified strategy

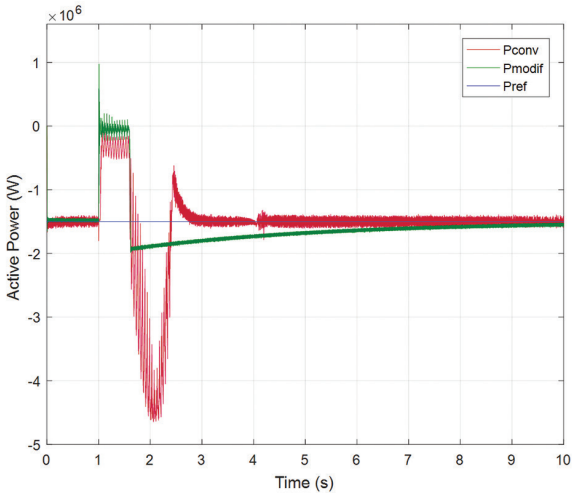


**Fig. 14.** Active stator power

Figure 15 shows the evolution of the stator reactive power. This power must be normally null to ensure a unitary power factor. When the fault occurs, for the proposed strategy, we note that this power presents some oscillations during a transient state and returns to its value after the fault. In the case of the conventional method, this power is not zero during the fault and presents a large overshoot after the fault disappearance.

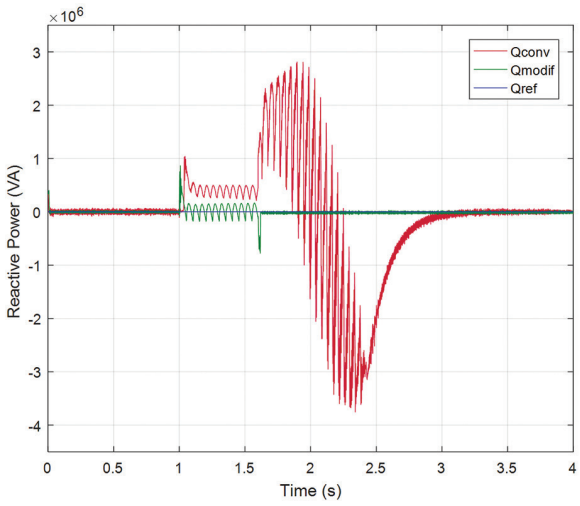


**Fig. 15.** Reactive stator power

In Figures 16 and 17, we present the rotor currents before, during and after the voltage dip. From these figures, we notice that these currents increase after the appearance of the fault. A high rotor current can damage the rotor side converter, which can be avoided by protecting with an additional circuit called Crowbar. Its role is to limit the rotor current and the DC link voltage.

From these figures it can be seen that in the case of the conventional control method, the currents are completely disturbed after the appearance of the voltage dip and present an imbalance after the fault. For the modified strategy, the currents return more quickly to their normal values before the fault appearance without remarkable overshoot.

It can therefore be noted that the proposed approach makes it possible to improve the DFIG behavior during a voltage dip, by limiting the stator and rotor currents, consequently keeping the wind turbine connected after the fault disappearance.

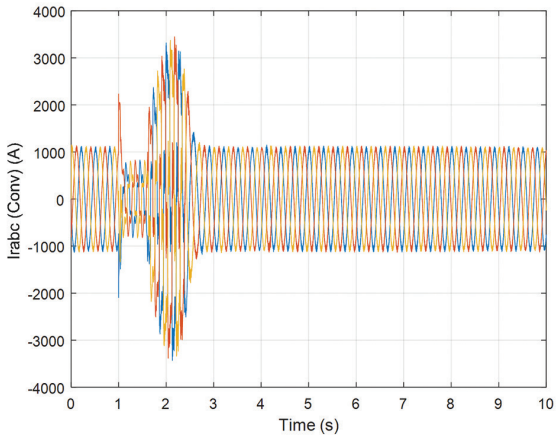


**Fig. 16.** Rotor currents with the conventional strategy

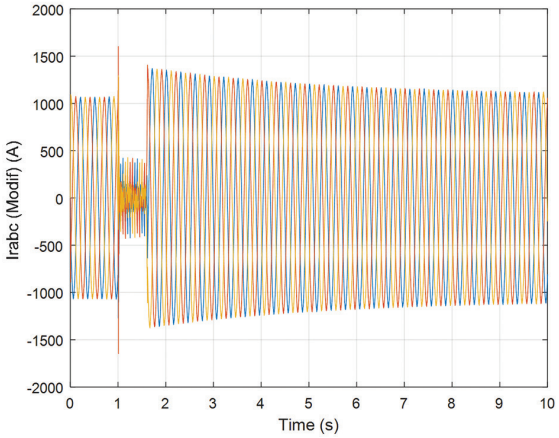


**Fig. 17.** Rotor currents with the modified strategy

## 7. CONCLUSION

In this research paper, we have dealt with the dynamic modeling and control of the wind energy conversion system based on DFIG, using active disturbance rejection control. We are interested in evaluating the dynamic performances of this system in the voltage dip event, and in developing a modified control strategy, which makes it possible to keep the DFIG connected to the power grid during this fault.

The voltage dip causes the stator flux decrease. To ensure the magnetization of the generator during and after the voltage dip, the stator flux dynamics must not be neglected and must be considered in the controller computing.

The simulation results were presented to ensure the validity and performance of the proposed control strategy based on ADRC and genetic algorithms, which allowed the production system to stay connected during the voltage dip and regain it's the normal operation after the fault has disappeared.

As a perspective, the quality of the generated power can be further improved by integrating a higher order link filter, with an eliminating method of the resonance effect. This will eliminate harmonic distortion in the currents. We can also focus the study on the impact of the uncertainty of the grid impedance on the control performances.

## 8. NOMENCLATURE

- R turbine radius
- ρ Air density
- $v$ Wind speed
- $\Omega_t$ Turbine speed
- $C_p$ Power coefficient
- λ Velocity ratio
- β Pich angle
- J Total inertia
- $J_{Turbine}$ Turbine inertia
- $J_g$ Generator inertia
- f Coefficient of viscous friction
- G Gain multiplier
- $\Phi_{sdq}$ dq axis Stator fluxes
- $\Phi_{rdq}$ Rotor fluxes
- $V_{sdq}$ Stator voltages according to dq axis
- $V_{rdq}$ Rotor voltages according to dq axis
- $i_{sdq}$ Stator currents according to dq axis
- $i_{rdq}$ Rotor currents according to dq axis
- $\omega_s$ Rotor angular frequency
- $\omega_r$ Stator angular frequency

## 9. APPENDIX

**Table 4**. DFIG Parameters

| Parameter | Symbol | Value |
|---|---|---|
| Rated power | $P_s$ | 1.5 M |
| Stator resistance | $R_s$ | 8.9 mΩ |
| Rotor resistance | $R_r$ | 13.7 mΩ |
| Stator inductance | $L_s$ | 13.7 mH |
| Rotor inductance | $L_r$ | 13.67 mH |
| Mutual cyclic inductance | $L_m$ | 13.5 mH |
| Number of pole pairs | p | 2 |
| Optimal tip speed ratio | $\lambda_{opt}$ | 8.1 |
| Maximal power coefficient | $C_{pmax}$ | 0.48 |

**Table 5.** Parameters of the RL filter and the DC bus

| Parameter | Symbol | Value |
|---|---|---|
| Filter resistance | $R_t$ | 0.25 Ω |
| Filter inductance | $L_t$ | 0.005 H |
| DC link Capacitor | C | 0.0044 F |
| DC link voltage | $U_{dc}$ | 1200 V |

## 10.REFERENCES:


[1] I. Kharchouf, A. Essadki, M. Arbaoui, T. Nasser, "Modeling and PI Control Strategy of DFIG Based Wind Energy Conversion Systems", Proceedings of the International Renewable and Sustainable Energy Conference, Tangier, Morocco, 4-7 December 2017.

[2] M. Nadour, A. Essadki, M. Fdaili, T. Nasser, "Advanced Backstepping Control of a Wind Energy Conversion System Using a Doubly-Fed Induction Generator", Proceedings of the International Renewable and Sustainable Energy Conference, Tangier, Morocco, 4-7 December 2017.

[3] R. Chakib, A. Essadki, M. Cherkaoui, "Modeling and control of a wind system based on a DFIG by active disturbance rejection control", International review on modelling and simulations, Vol. 7, No. 4, 2014, pp. 626-637.

[4] A. Boukhris, "Robust Control by ADRC of The Wind Turbine Based on The Double Fed Induction Generator", Ph.D. Thesis, 2015.

[5] M. Smaili, "Modeling and Control of a Double Fed induction Generator for Simulation of Cogeneration Problems", Master thesis, 2013.

[6] I. Kharchouf, A. Essadki, T.Nasser, "Wind System Based on a Doubly Fed Induction Generator: Contribution to the Study of Electrical Energy Quality and Continuity of Service in the Voltage Dips Event", International Journal of Renewable Energy Research, Vol.7, No.4, 2017.

[7] J. Lopez, E. Gubia, E. Olea, J. Ruiz, L. Marroyo, "Ride through of wind turbines with doubly fed induction generator under symmetrical voltage dips", IEEE Transactions on Industrial Electronics, Vol. 56, No. 10, 2009, pp. 4246-4254.

[8] A. Lazrak, A. Abbou, "An Improved Control Strategy of DFIG Wind Turbine of Ride-Through Voltage Dips", Proceedings of the 6th International Renewable and Sustainable Energy Conference, Rabat, Morocco, 5-8 December 2018.

[9] L. Zhou, J. Liu, F. Liu, "Design and implementation of STATCOM combined with series dynamic breaking resistor for low voltage ride through of wind farms", Proceedings of the IEEE Energy Conversion

Congress and Exposition, Atlanta, GA, USA, 12-16 September 2010, pp. 2501-2506.

[10] M. S. El-Moursi, B. Bak-Jensen, M. Abdel-Rahman,."Novel STAT COM controller for mitigating SSR and damping power system oscillations in a series compensated wind park", IEEE Transactions on Power Electronics, Vol. 25, No. 2, 2009, pp. 429-441.

[11] M. Saleem, K. Y. Choi, R. Y. Kim, "Resonance damping for an LCL filter type grid-connected inverter with active disturbance rejection control under grid impedance uncertainty", Electrical Power and Energy Systems, Vol. 109, 2019, pp. 444-454.

[12] M. Saleem, B. S. Ko, S. H. Kim, S. Kim, B. S. Chowdhry, R. Y. Kim, "Active Disturbance Rejection Control Scheme for Reducing Mutual Current and Harmonics in Multi-Parallel Grid-Connected Inverters", Energies, Vol. 12, 2019, p. 4363.

[13] M. Saleem, M. H. A. K. Khushik, H. Tahir, R.Y. Kim, "Robust L Approximation of an LCL Filter Type Grid-Connected Inverter Using Active Disturbance Rejection Control under Grid Impedance Uncertainty", Energies, Vol. 14, 2021, p. 5276.

[14] S. El Aimani. "Towards a Practical Identification of a DFIG Based Wind Generator Model for Grid Assessment", Energy Procedia, Vol. 14, 2012, pp. 1677-1683.

[15] N. Elmouhi, A. Essadki, H. Elaimani, R. Chakib, "Participation of a DFIG Based Wind Energy Conversion System in Frequency Control", Proceedings of the 5th International Conference on Renewable Energies for Developing Countries, Marrakech, Morocco, 29-30 June 2020.

[16] S. Mensou, A. Essadki, I. Minka, T. Nasser, B. Bououlid Idrissi."Backstepping Controller for a Variable Wind Speed Energy Conversion System Based on a DFIG", Proceedings of the International Renewable and Sustainable Energy Conference, Tangier, Morocco, 4-7 December 2017.

[17] N. El Mouhi, A. Essadki. "Active and Reactive Power Control of DFIG used in WECS using PI Controller and Backstepping", Proceedings of the International Renewable and Sustainable Energy Conference, Tangier, Morocco, 4-7 December 2017.

[18] H. Elaimani, A. Essadki, N. Elmouhi, R. Chakib, "The Modified Sliding Mode Control of a Doubly Fed Induction Generator for Wind Energy Conversion During a Voltage Dip", Proceedings of the International Conference on Wireless Technologies, Embedded and Intelligent Systems, Fez, Morocco, 3-4 April 2019.

[19] S. El Aimani, B. François, B. Robyns, E. De Jaeger, "Dynamic Behaviour of Two Stator Flux Control Systems of a Doubly Fed Induction Generator-Based Grid-Connected Wind Turbine During Voltage Dips", Proceedings of the International Conference on Electricity Distribution Turin, Italy, 6-9 June 2005.

[20] H Elaimani, A Essadki, N Elmouhi, R Chakib, "Comparative Study of the Grid Side Converter's Control during a Voltage Dip", Journal of Energy 2020, Vol. 2020, 7892680, 11 pages.

[21] A. Boukhriss, T. Nasser, A. Essadki, A. Boualouch. "Active Disturbance Rejection Control for DFIG Based Wind Farms Under Unbalanced Grid Voltage", International Review on Modelling and Simulations, Vol. 7, No. 1, 2014.

[22] L. Xu, "Coordinated Control of DFIG's Rotor and GridSide Converters During Network Unbalance", IEEE Transactions on Power Electronics, Vol. 23, No. 3, 2008, pp. 1041-1049.

[23] A. Radaideh, M. Bodoor, A. Al-Quraan, "Active and Reactive Power Control for Wind Turbines Based DFIG Using LQR Controller with Optimal Gain-Scheduling", Journal of Electrical and Computer Engineering, Vol. 2021, 1218236.

[24] A. Boukhriss, A. Essadki, A. Bouallouch, T. Nasser, "Maximization of generated power from wind energy conversion systems using a doubly fed induction generator with active disturbance rejection control ", Second World Conference on Complex Systems, Agadir, Morocco, 10-12 November 2014.

[25] R. Rouabhi, "Control of the powers generated by a variable speed wind power system based on a doubly fed induction generator", PhD thesis, University of Batna, Faculty of Technology 2016.

[26] I. Minka, A. Essadki, S. Mensou, T. Nasser, "Power Control of a DFIG Driving by Wind Turbine: Com-

parison Study Between ADRC and PI Controller", Proceedings of the International Renewable and Sustainable Energy Conference, Tangier, Morocco, 4-7 December 2017.

[27] R. Chakib, A. Essadki, M. Cherkaoui, "Modeling and control of a wind system based on a DFIG by active disturbance rejection control", International review on modelling and simulations, Vol. 7, No. 4, 2014, pp. 626-637.

[28] A. G. Abo-Khalil, W. Alharbi, A. Al-Qawasmi, M. Alobaid, I. Alarifi, "Modeling and control of unbalanced and distorted grid voltage of grid-connected DFIG wind turbine", International Transactions on Electrical Energy Systems, Vol. 31, No. 5, 2021.

[29] S. Mensou, A. Essadki, T. Nasser, B. Bououlid Idrissi, "A direct power control of a DFIG basedWECS during symmetrical voltage dips", Protection and Control of Modern Power Systems, Vol. 5, No. 5, 2020.

[30] L. Xu, "Dynamic Modeling and Control of DFIG-BasedWindTurbines Under Unbalanced Network Conditions", IEEE Transactions on Power Systems, Vol. 22, No. 1, 2007, pp.314-323.

[31] M.B.C Salles, A.J.S Filho and A.P.Grilo, "A Study on the Rotor Side Control of DFIG-based Wind turbine during Voltage Sags without Crowbar System" Proceedings of the International Conference on Renewable Energy Research and Applications, Nagasaki, Japan, 11-14 November 2012.

[32] A. Cheriet, A. Bekri, H. Gouabi, A. Hamed, "Nonlinear backstepping control optimized by genetic algorithm for the control of a wind turbine" International Journal of Industrial Electronics and Electrical Engineering, Vol. 7, No. 6, 2019, pp. 3-7.

[33] A. Boulmane, Y. Zidani, D. Belkhayat, and M. Bouchouirbat, "A GA-based adaptive mechanism for sensorless vector control of induction motor drives for urban electric vehicles", Turkish Journal of Electrical Engineering & Computer Sciences, Vol. 28, No. 3, 2020, pp. 1731-1746.

[34] K. E. Okedu, M. Al Tobi, S. Al Araimi, "Comparative Study of the Effects of Machine Parameters on DFIG and PMSG Variable Speed Wind Turbines During Grid Fault", Frontiers in Energy Research, 2021.

# Management System of Smart Electric Vehicles Using Software Engineering Model

Original Scientific Paper

**Muayad Sadik Croock**
University of Technology-Iraq,
Department of Control and System Engineering
Baghdad, Iraq
muayad.s.croock@uotechnology.edu.iq

**Sahar Salman Mahmood**
University of Technology-Iraq,
Department of Civil Engineering
Baghdad, Iraq
sahar.s.mahmood@uotechnology.edu.iq

***Abstract*** *– In this paper, a management system for smart electric vehicle is introduced using software engineering models and installed Sensor Network (SN). Two software engineering models are proposed to construct the information exchange and available resource management algorithms, in which the required performance of vehicles is obtained. The resource management algorithm adopts the LeNet-5 deep-learning model in choosing the best driving mode amongst suggested five modes. The dataset is achieved from the simulated SN. The results show the satisfactory performance of the electric cars in terms of information exchange and resource management. The Message Queuing Telemetry Transport (MQTT) broker server is employed for monitoring the information exchange between the sensors, actuators and controller. The delay time is measured to be less than 1 sec for transmitting 1000 message. The proposed system saves energy by 1-8 kWh and a storage capacity by 9-95 MB for driving 100 km.*

***Keywords****: Software Engineering, Electric Car, Sensor Network, Deep-Learning*

## 1. INTRODUCTION

The changing of energy resources from oil based ones to the renewable energy resources forces the car factories to turn up with the electric cars. These cars face different challenges that should be tackled to accommodate the industry in right way. These challenges include the consuming of the electrical energy and related factors that affect the performance of cars. Moreover, the presented cars should come up with smart technique in managing them throughout different circumstances. The Sensor Networks (SN)s are utilized to offer the smart touch in addition to the real-time monitoring to the surrounding circumstances of the cars. The use of these techniques provide the electric car with smart management in terms of reading the sensors and taking the suitable actions. Moreover, the Artificial Intelligent techniques, such as machine learning and deep-learning are widely used with the SN for optimizing the solutions [1]-[5].

The energy saving in the electric car represents an important point of well industry. This is due to the limitation of used batteries in energy abilities. Therefore, different research works were introduced to propose numerous methods in energy reduction. The energy reduction methods focus on the common point, which is the reducing of facilities and properties of the car and the actuation actions [6].

The information exchange between the car sensors, actuators, and controllers is allocated at the high priority consideration. It should be controlled by a suitable protocol, such as Message Queuing Telemetry Transport (MQTT). In addition to the used protocol, an algorithms are also built to manage the readings scheduling and the processing procedures [7]. At the other hand, the software engineering models are widely used in the designed systems for increasing different factors, including reliability, expandability, and so on. In the car system, it is important to design the management algorithm based on the software engineering models to guarantee the mentioned parameters above. Moreover, the proposed algorithms consider the required conditions that should be available as well as the actuation actions in the electric cars [8]-[10].

In this paper, software engineering models are presented to be adopted in designing the data exchange and resource management algorithms for electric cars based on SN. The SN is installed in wired connection over the parts of electric cars throughout the controller. The data exchange algorithm manages the reading and actuation actions exchange over the SN. While the proposed resource management algorithm focuses on minimizing the consumed energy and storage capacity through the work of electric cars. This is done by applying the proposed software engineering model and driving modes that are varied from economy to costly. The deep-learning model is used in selecting the suitable driving mode based on the sensor readings. This model is trained using a dataset, achieved from the SN simulation using MATLAB. The achieved results show the efficiency of the proposed algorithms and the effect of software engineering model on the system performance. There are noticed enhancements in the data exchange, as well as the consumed energy and storage capacity.

## 2. RELATED WORK

Due to the importance of developing the industry of electric cars, numerous researchers interested in providing models that tackled different visions of facing problems. The authors of [11] presented a deep review study on the provided energy management methods for hybrid electric vehicles. Moreover, different optimization algorithms have been studied to point out the solutions for the appeared issues. In [12], a real-time energy management system for hybrid electric vehicles using Adaptive Equivalent Consumption Minimization Strategy. The designed controller collected the information for trips and concluded the optimal way in consuming the energy for each trip in future. The system was evaluated and compared with the traditional methods, such as charge depleting charge sustaining, and the results showed the superior performance of the proposed system. Whilst, a comprehensive review has been presented in [13] to cover the solutions for the energy management of electric cars. These solutions included the artificial intelligent tools and other optimization methods. The review focused on two points: review on energy management systems, and optimal solutions, introduced based on the facing problems.

In [14], the authors also introduced a review on the problems of energy optimization in the electric cars as well as the solutions and presented algorithms. In addition, the simulation prototype for energy management of electric cars has been proposed in [15] using dynamic programming and receding horizon. The controller in the simulation obtained a partial information of each planned trip from the user and the old information for similar trips to evaluate the required amount of charging and fuel. This could reduce the consumed energy by 10% according to the simulation results. The authors of [16] proposed a fuzzy logic based controller that minimized the consumed energy of the Hybrid cars using instantaneous Degree of Hybridization. The proposed controller balanced between the electric and fuel engines in driving the cars. The results were studied for different modes of driving to clarify the effects of the proposed controller on the energy consuming.

In [17], mathematical and simulated models have been proposed for designing the controller that managed the consumed energy by the electric cars. The analysis of the proposed models proved the well management of the system of the available resources. In [18], a trade-off formulation was presented in controlling the fuel amount and energy required for driving hybrid cars in specific routs. Different optimization algorithms have been employed in producing the car system for economy driving mode. The authors of [19] proposed a gateway convertor between Alternating Current (AC) and Direct Current (DC) power that controlled the charging and discharging batteries as well as the balancing between power generating and consuming. The simulation results showed the recorded efficiency of the proposed system in terms of batteries charging/discharging and power consumption management. A dynamic programming method was adopted in presenting an optimized rule-based strategy for reducing the consumed power of electric cars [20]. The optimization method adopted the collected data from the cars to decide the optimal way of saving the power with satisfactory level of driving. Moreover, numerous optimization methods have been used in [21] to reduce the consumed power in hybrid vehicles. All these methods were employed in real-time environment to compensate the drawbacks of the traditional methods.

In [22], an education based platform of electric cars was proposed. It was built based on software engineering models. This model was designed for minimizing the consumed power in electric cars using optimization methods. The authors of [23] presented the challenges that faced the designing of electric cars in terms of the used embedded and software systems. One of the most tackled challenges was the batteries life-time and charging capacity. Additionally, it considered the unexpected problems that might appeared throughout the performance and driving of the cars.

In [24], five preconditions were presented for obtaining the best data management in the electric cars. The data management was important to control the changes in the car system due to the surrounding circumstances including the land shape and modes of driving. The authors of [25] introduced a review on the analysis of data in the electric cars. These data covered the internal and external environments. The internal dealt with the monitoring data of power, fuel, engine, etc. While the external data included the infrastructure of the system, such as power stations, road data, trip data, etc. In the same way, the authors of [26] adopted the data management for different applications to achieve the required aim in efficient approach

## 3. PROPOSED RESOURCE MANAGEMENT SYSTEM

The propose resource management system for electric cars has been built using different techniques including the software engineering models that is used for designing the software algorithms for data and resource management. The SN is adopted in the proposed system to monitor the parts and behavior of electric car. It contains sensors to measure temperature of engine and weather, acceleration, weather moisture, air pressure, energy, Ultra Violet (UV) detection, around car detection, and speed. Weather temperature and moisture are used for providing this information to the driver. Moreover, a Raspberry Pi4 can be used as a controller due to its ability in performing the algorithms in sufficient and reasonable real-time. The core frequency of Raspberry Pi4 reaches 1.8 GHz that provides the system with high speed processing, which is satisfied to the proposed prototype. In addition, the consumed energy of this component is suitable (3.8-4 W) for designing the proposed system.

Figure 1 explains the block diagram of the proposed system in terms of SN. From this figure it can be seen that the SN is based on the central control with planned distribution of sensors. The sensors with their functions are represented in the block diagram and they are connected to the central controller. At the same time, the sensors are connected together to pass the data throughout the gateway of each sensor node. This connectivity between sensors offers the guarantee of delivering the data for each sensor to the controller in case of a faults appeared in communication of such sensor. Each sensor is a node with processor, memory, battery, and communication unit (gateway).

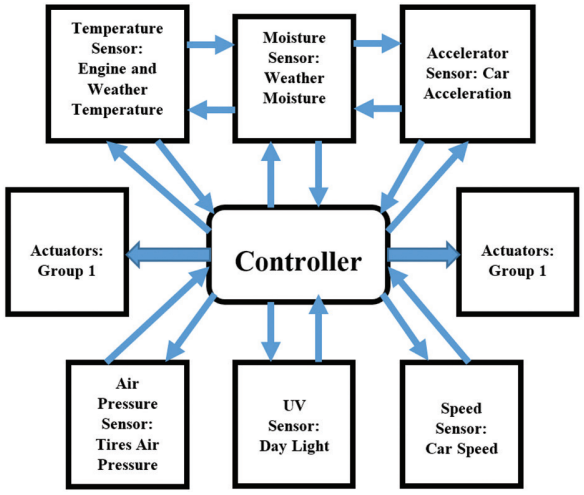


**Fig. 1.** SN structure

In order to ease the reading flow, this section is divided into two main parts as follows.

### 3.1. SOFTWARE ENGINEERING MODEL FOR DATA EXCHANGE

As mentioned above, the SN is adopted in sensing the change in the surrounding circumstances of the electric car. Due to the use of SN, there is a need for managing the data exchange between sensor nodes and the controller. Basically, the MQTT protocol is adopted in managing the data transmission over the SN. Meanwhile, there is another need for managing the work of each node that can be presented in Figure 2 as a software engineering model using state diagram for data exchange between a sensor node with another one or controller as well as the required actuators. From Figure 2, the software engineering model manages the following points:

- ***Sensor Node***: The presented model represents the state of each sensor node that prepares the data message of the readings from the sensor to be sent for the controller every 30 sec. This time is selected as we assume that there no risky change in readings within it. The readings in the data message are exchanged with the controller and the near nodes that works as gateways for double check that the readings are safely received by controller. The exchange is done in two ways (transceiver) for sending the data messages and receiving acknowledgments, represented as feedback arrows, from controllers or any other orders of turning ON/OFF or repeating the readings. Each sensor node has its own feedback for correcting the faulted readings and ensuring the validity of data message.
- ***Controller***: It is the main part of managing the electric car. It receives the data messages from all sensor nodes throughout the MQTT routes and manages this process for preventing any loss in the sent data messages. This data is processed and then the required actions are decided by the controller to be sent for actuators or sensor nodes. The controller has a self-feedback for correcting the produced decisions based on the received data. This can guarantee the validity and availability of the resources in the management system of the electric cars.
- ***Actuators***: This part is responsible on performing the decisions, come from controller, in an efficient way. The cycle loop between the actuator and controller can prevent any error in actuating the decisions.

It is important to note that the software engineering model offers further features to the data exchange algorithm rather than using just MQTT protocol. This model provides the algorithm with availability, integrity, and validity. These features increase the reliability of the algorithm and reduce the faults.

### 3.2. SOFTWARE ENGINEERING MODEL FOR RESOURCE MANAGEMENT ALGORITHM

In electric car systems, the available energy and storage size are considered as important resources that should be managed well. The reducing of the consumed energy provides the cars with longer battery life that can reflect positively on the crossed driving

distances. At the other hand, the data storage capacity is tackled due to importance of storing the sensor readings for a specific period of time for system evaluation purpose. In this paper, the software engineering model is proposed to design the resource management algorithm that addresses the issues of consumed energy and storage. Figure 3 represents the proposed software engineering model for the resource management algorithm using state diagram. The working steps of the proposed algorithm can be summarized as:

- ***Energy Source:*** In the electric car, the battery unit provides the energy to all parts of cars, including sensor nodes, engine, lights, and so on.

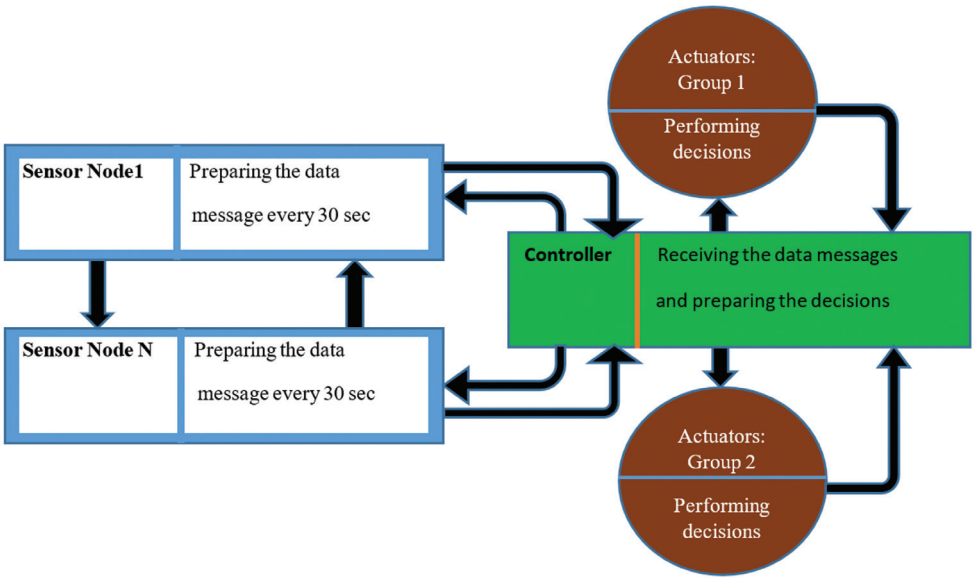


**Fig. 2.** The proposed data exchange algorithm represented as a software engineering state model

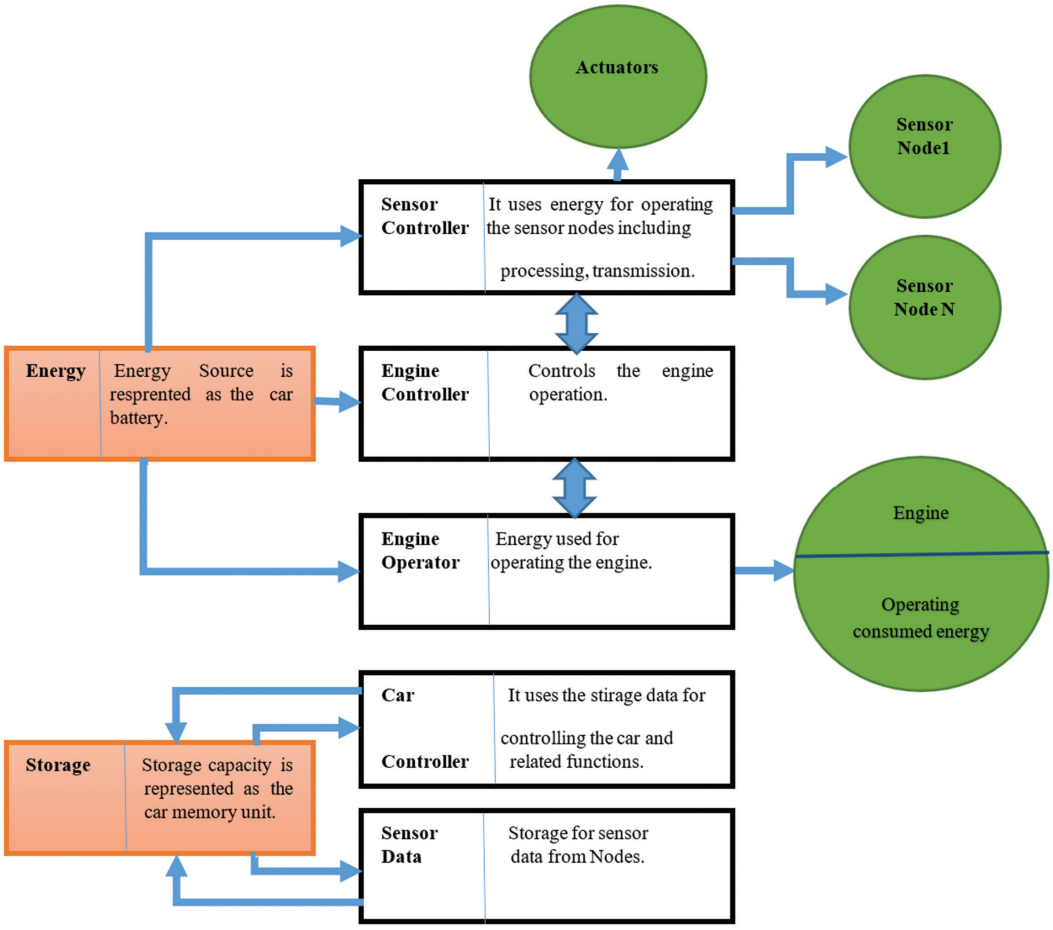


**Fig. 3.** Software engineering model for resource management algorithm

- ***Sensor Controller***: It is a part of the main controller of electric car. To control the operating of sensor nodes, each one has a controller that manages the operation, storage, processing and data transmission. This reflects on the amount of consumed energy, which is the results of readings flow process of the sensors. The sensor is turned on/off depending on the need of the system to avoid the continuous working and consuming energy, as it requires processing storage and transmission. The same procedure is applied on actuators, such as lights, glass wiper motors, and so on. The need of operating sensors depends on the current case. For example, the lights should not turn on in a day time and the wipers as well in a sunny day. In addition, the transmission of data is performed in different period based on the circumstances to prevent keep sending the same data. The decision of sending readings (data) to the main controller is taken when a change to them is occurred. This can save a valuable energy amount as the data transmission consumes most of available energy for sensors.
- ***Engine Controller***: It is a part of the main controller of electric car. This unit provide the engine with operation statuses. These statuses include the driving mode, speed, acceleration, and load balancing. The control signals are sent to the next unit that is engine operator.
- ***Engine Operator***: As a part of the main controller, it is responsible on operating the engine by generating a pulse width modulation based signal to the major engine motors.
- ***Storage Capacity***: Each electronic part of the electric car system contains a memory unit. All these units are combined in the storage capacity that saves the reading of sensor nodes and the decisions of the car controller for a period of time, in this case one weak. After that, the new data is over written on the old stored information.

### 3.3. INTELLIGENT DECISION MAKING MODEL

The main controller takes important decisions regarding the status of managing the electric cars. The deep-learning model is employed to obtain the right driving mode of the car. This model is performed in the main controller unit of the electric car. Each selected driving mode controls the operating of all cars including engine, sensor nodes, and actuators. The deep-learning model classifies the collected sensor reading into decisions (classes) of driving modes. This model is trained using the collected dataset from the sensor network of a car that includes 2.52 million records as explained in the next section.

The deep-learning model of LeNet-5 architecture [27] is adopted. This model is shown in Figure 4 that explains the deep-learning stages and layers, such as convolutions, subsampling, full connection and Gaussian connections. Some changes have been done on the LetNet-5 in terms of changing the two dimensions input to one dimension to be compatible with the dataset of the adopted sensor network of electric car.

In this paper, six driving modes are adopted to be as classes in deep-learning model. These modes are explained in Table 1. From this table, it is shown that the modes explode the sensors and actuators in different ratios. Each mode uses the sensors and related actuators depending on the weather, time, and land shape and varies from 0% to 100%.

In mode A, the car is turned off and all parts of car are powered off. Mode B is the economy one that offers the basic conditions of driving the car in safe in day time with suitable weather and land conditions. The difference between mode B and mode C is that the last considers the acceleration property that provide the car with more engine horse energy. This is used for speedy drive and hell land shapes. Mode D represents the driving in mode C in summer time, where the air conditioner is on. This mode needs more energy for operating the related sensors and actuators. In Mode E, the driving is in night time with good weather condition and hell land. This mode consumes more energy due to the use of lights. Mode F is the most consumed energy one due to the use of all properties of electric car with raining and bad land shape. The selection of the suitable mode is based on the readings of sensor nodes that are sorted in upper and lower thresholds for each. Table 2 lists the considered thresholds of each mode.

## 4. DATASET

As mentioned in the early section, the deep-learning model is trained using the prepared dataset. It is prepared by collecting the data readings of sensors from the constructed sensor network of the electric car, shown in Figure 1. The dataset represents the run work of the network that is simulated using MATLAB environment. The MQTT protocol is adopted in this sensor network for managing the data exchange. The reading data of each sensor is considered as a feature for the deep-learning model. Therefore, six features are the input of dataset to the model. Different case studies have been employed for covering the possible changes in the car system, surrounding circumstances, and energy consuming. Table 3 is the summary to the collected dataset that is represented in different numbers of records for each mode. Some of records are not valid in terms of data structure of sensor readings due to delays, data corruption, and packet loss. Thus, these records are excluded from the valid dataset. The dataset is divided into training by 70% and test by 30% samples. Validation Ratio is computed as:

$$Validation\ Ratio = \frac{No.of\ Valid\ Records}{No.of\ Records} \quad (1)$$

It is important to keep in mind that each driving mode is formulated as a class in deep-learning model that is used later in selecting the suitable mode that can save more energy and storage capacity rather than exhausting the resources in single one.

## 5. RESULTS

The proposed resource management system for electric car is simulated in MATLAB environment to be tested under different case studies to measure the obtained energy saving and storage capacity by employing the proposed software engineering model based resource management algorithm that adopts the deep-learning model in selecting the suitable driving mode. Moreover, the data exchange between the sensors and controllers is managed using the proposed software engineering model based data exchange algorithm.

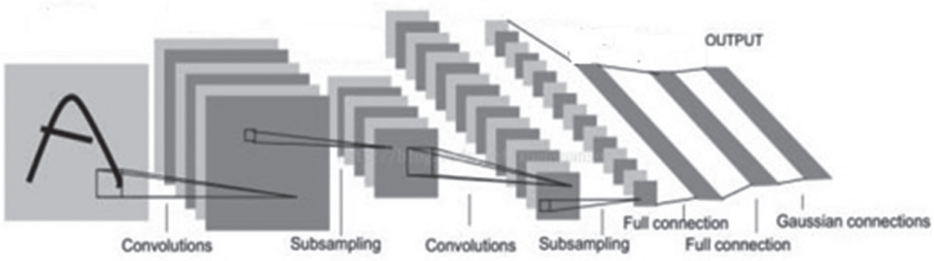


**Fig. 4.** The LeNet-5 architecture [27]

**Table 1.** Driving mode specifications

| No. | Mode Name | Specifications | | | | | | | Sensor Efficiency | Actuator Efficiency |
|---|---|---|---|---|---|---|---|---|---|---|
| | | conditioner | Lights | Engine | Cooling system | Wiper | Radars | Acceleration | | |
| 1 | Mode A | Off | Off | Off | Off | Off | Off | Off | 0% | 0% |
| 2 | Mode B | Off | Off | On | On | Off | On | Off | 40% | 30% |
| 3 | Mode C | Off | Off | On | On | Off | On | On | 50% | 50% |
| 4 | Mode D | On | Off | On | On | Off | On | On | 60% | 70% |
| 5 | Mode E | On | On | On | On | Off | On | On | 90% | 90% |
| 6 | Mode F | On | On | On | On | On | On | On | 100% | 100% |

**Table 2.** Sensors thresholds for selecting each driving mode

| Mode | Engine Temperature Co | Weather Temperature Co | Speed km/H | UV detector | Moisture | Accelerator m/sec2 |
|---|---|---|---|---|---|---|
| Mode A | 0-20 | 0-60 | 0-2 | 0-100% | 0-100% | 0-1 |
| Mode B | >50 | 0-25 | >5 | >20% | <90% | <10 |
| Mode C | >50 | 0-25 | >50 | >20% | <90% | >10 |
| Mode D | >50 | >25 | >50 | >20% | <90% | >10 |
| Mode E | >50 | >25 | >50 | <20% | <90% | >10 |
| Mode F | >50 | >25 | >50 | <20% | >90% | >10 |

**Table 3.** Dataset records for each driving mode

| Driving mode | No. of Records | No. of Valid Records | No. of Invalid Records | Validation Ratio |
|---|---|---|---|---|
| **Mode A** | 500000 | 500000 | 0 | 100% |
| **Mode B** | 500000 | 430000 | 70000 | 86% |
| **Mode C** | 500000 | 390000 | 110000 | 78% |
| **Mode D** | 500000 | 300000 | 200000 | 60% |
| **Mode E** | 500000 | 480000 | 20000 | 96% |
| **Mode F** | 500000 | 420000 | 80000 | 84% |
| **Total** | 3000000 | 2520000 | 480000 | 84% |

The software engineering guarantees the reliability, validity and flexibility of the proposed algorithms.

The MQTT broker has been adopted in monitoring the proposed data exchange algorithm performance between nodes as clients and broker server. The achieved results show that the investigated sensor network in electric car works in efficient manner, where over 1000 messages have been sent and the delivery time is less than 1 sec. These messages from six sensor node (clients) to the broker server under a common Quality of Service (QoS).

At the other hand, the proposed resource management algorithm uses the deep-learning model. Thus, the deep-learning model is tested to prove the validity of accuracy in terms of training and test modes. Figure 5 shows the training accuracy of the presented deep-learning model, while Figure 6 illustrates the testing accuracy of the deep-learning model. Both of training and testing accuracy and loss is changed and enhanced with the increasing number of epochs. This is due to the minimizing the error in building the weights for the training and testing output. The maximum obtained training accuracy is achieved after 100 epochs to be 99.2%, while the testing accuracy reaches the maximum value after 100 epochs to be 98.3%. These results prove the high efficiency of the introduced deep-learning model in classifying (selecting) the suitable driving mode.

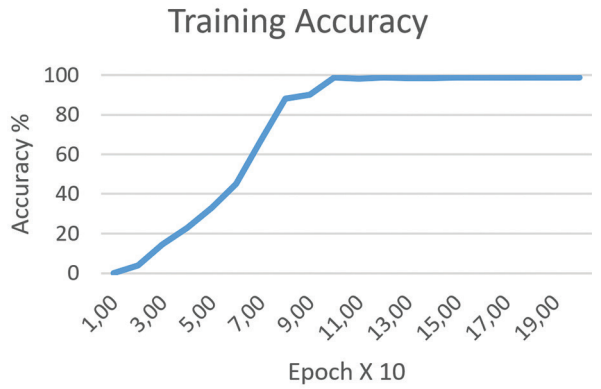


**Fig. 5.** Training accuracy vs. epochs

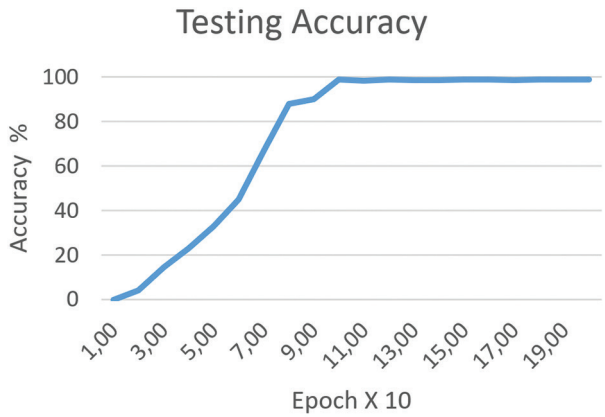


**Fig. 6.** Testing accuracy vs. epochs

In order to measure the saved energy using the proposed software engineering based resource management algorithm, the investigated system's driving modes are compared with the traditional electric car model in Figure 7. The traditional model consumes 15 kWh to cross 100 km distance. From this figure, it is appeared the superior performance of the proposed system in saving energy that can gain more than 8 kWh in Mode A, while this gain is reduced with the employed modes till reaching 1 kWh in Mode F. The last one is close to the traditional model due to the use of all car option, but the 1 kWh is gained from the use of proposed algorithms that manage the resources well.

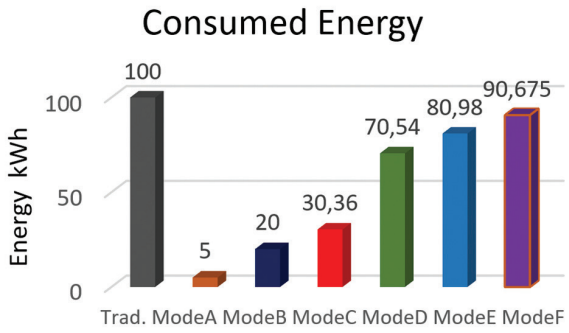


**Fig. 7.** The consumed energy vs. driving mode for 100 km distance

The consumed energy in kWh is computed using the following formula:

$$Energy = \frac{Total\ enrgy}{Speed} \times Distance \quad (2)$$

Where, Total energy means the available energy in electric car in kW, the Speed is measured by km/h, and the crossed Distance is in km. At the other hand, Figure 8 shows the saved storage capacity of the considered modes in comparison with the traditional electric car model. The traditional model is assumed to consume 100MB of storage for saving data of sensor readings and controller signals. The achieved saving in capacity is varied from 9-95 MB for driving distance of 100 km. The enhancement in the proposed system is the results of employing the proposed data exchange and resource management in efficient way throughout the considered driving modes.

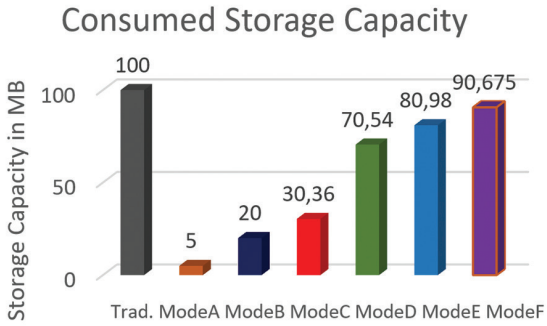


**Fig. 8.** The consumed storage capacity vs. driving mode for 100 km distance

To ensure the satisfied performance of the proposed system in selecting the suitable driving mode, Table 4 explains the training accuracy ratio of successful choosing of the mode. Each driving mode has trained (by injecting the sensor reading within the related thresholds) 100 times. It is clearly shown that the obtained accuracy ratios are involved in the testing accuracy of deep-learning model with 98.8%.

**Table 4.** Training accuracy for injected readings over the driving modes

| Driving Mode | Number of Training | Successful Selecting | Failed Selecting | Accuracy Ratio |
|---|---|---|---|---|
| Mode A | 100 | 98 | 2 | 98% |
| Mode B | 100 | 99 | 1 | 99% |
| Mode C | 100 | 98 | 2 | 98% |
| Mode D | 100 | 97 | 3 | 97% |
| Mode E | 100 | 98 | 2 | 98% |
| Mode F | 100 | 99 | 1 | 99% |

## 6. CONCLUSIONS

A resource management system for electric cars was proposed based on software engineering modelling. This system adopted two main algorithms: data exchange and resource management. The first one combined the software engineering model and MQTT protocol in order to enhance the performance in data exchanging between sensor nodes and controller. The second algorithm tackled the problem of reducing the consumed energy and storage size by employing the suitable driving mode based on the sensor readings. It used the deep-learning model in selecting the best driving mode depending on the fed sensor readings. The deep-learning model was tried and validated using the prepared dataset, obtained from the employed sensor network. The achieved results showed the superior efficiency performance for the proposed system. The MQTT broker server was used for monitoring and evaluating the data exchange algorithm. While the saved energy and storage capacity were measured in the applying of the resource management algorithm. In addition, the deep-learning was tested in terms of accuracy for training and validation. A hundred test sample have been considered in evaluating the proposed system for each driving mode and the results proved that the accuracy was over 98%.

## 7. REFERENCES


[1] Union of Concerned Scientists, "Electric Vehicle Survey Findings and Methodology", www.ucsusa.org/EVsurvey2019 (accessed: 2022)

[2] J. Sanguesa, V. Torres-Sanz, P. Garrido, F. Martinez, J. Marquez-Barja, "A Review on Electric Vehicles: Technologies and Challenges", Smart Cities, Vol. 4, 2021, pp. 372-404.

[3] X. Sun, Z. Li, X. Wang, C. Li, "Technology Development of Electric Vehicles: A Review", Energies, Vol. 13, No. 90, 2020, pp.1-29.

[4] A. Guizani, M. Hammadi, J.-Y. Choley, Th. Soriano, M. Abbes, M. Haddar, "Electric vehicle design, modelling and optimization", Mechanics & Industry, Vol. 17, No. 405, 2016, pp. 1-10.

[5] E. Grunditz, "Design and Assessment of Battery Electric Vehicle Powertrain, with Respect to Performance, Energy Consumption and Electric Motor Thermal Capability", Chalmers University of Technology, Sweden, PhD Thesis, 2016.

[6] J. Valladolid, D. Patino, G. Gruosso, C. Correa-Flórez, J. Vuelvas, F. Espinoza, "A Novel Energy-Efficiency Optimization Approach Based on Driving Patterns Styles and Experimental Tests for Electric Vehicles", Electronics, Vol. 10, No. 1199, 2021, pp. 1-23.

[7] M. Yasir, M. Croock, "Cyber DoS attack-based security simulator for VANET", International Journal of Electrical and Computer Engineering, Vol. 10, No. 6, 2020, pp. 5832-5843.

[8] J. Schauffele, T. Zurawka, "Automotive Software Engineering Principles, Processes, Methods, and Tools", 1st Edition, SAE Permissions, 2003.

[9] Y. Dajsuren, M. Brand, "Automotive Systems and Software Engineering", 1st Edition, Springer, 2019.

[10] M. Fahmideh, A. Ahmad, A. Behnaz, J. Grundy, W. Susilo, "Software Engineering for Internet of Things: The Practitioners' Perspective", IEEE Transactions on Software Engineering (in press)

[11] J. Jiang, Q. Jiang, J.Chen, X. Zhou, Sh. Zhu, T.Chen, "Advanced Power Management and Control for Hybrid Electric Vehicles: A Survey", Wireless Communications and Mobile Computing, Vol. 2021, 2021, pp. 1-12.

[12] M. Vajedi, M. Chehrehsaz, N. Azad, "Intelligent power management of plug-in hybrid electric vehicles, part II: real-time route based power management", International Journal of Electric and Hybrid Vehicles, Vol. 6, No. 1, 2014, pp. 68-86.

[13] A. Ali, D. Söffker, "Towards Optimal Power Management of Hybrid Electric Vehicles in Real-Time: A Review on Methods, Challenges, and State-Of-The-Art Solutions", Energies, Vol. 11, No. 476, 2018, pp. 1-12.

[14] M. Yasir, M. Croock, "Software engineering based self-checking process for cyber security system in VANET", International Journal of Electrical and Computer Engineering, Vol. 10, No. 6, 2020, pp. 5844-5852.

[15] P. Polverino, I. Arsie, C. Pianese, "Optimal Energy Management for Hybrid Electric Vehicles Based on Dynamic Programming and Receding Horizon", Energies, Vol. 14, No. 3502, 2021, pp. 1-11.

[16] S. Ihmood, H. Abid, H. Radhi, "Management of Energy sources of hybrid electric vehicles using degree of hybridization and Sequential Approximate Optimization", Journal of Mechanical Engineering Research and Developments, Vol. 44, No. 6, 2021, pp. 305-315.

[17] Z. Lei, D. Sun, Y. Liu, J. Li, P. Zhao, "Simulation and Analysis of Energy Consumption for Plug-in Hybrid Electric Vehicles Based on Driving Cycle", Proceedings of the 5th IFAC Conference on Engine and Powertrain Control, Simulation and Modeling E-COSM, Changchun, China, 20–22 September 2018, pp. 394-399.

[18] S. Adhikari, "Real-time Power Management of Parallel Full Hybrid Electric Vehicles", University of Melbourne, Australia, PhD Thesis, 2010.

[19] S. K. Narayanappa, "Hybrid Energy Management System of EV Using Grid to Vehicle System", International Journal of Electrical Engineering & Technology, Vol. 10, No. 1, 2019, pp. 30-38.

[20] D. Zhu, E. Pritchard, S. Dadam, V. Kumar, Y. Xu "Optimization of Rule-Based Energy Management Strategies for Hybrid Vehicles Using Dynamic Programming", Combustion Engines, Vol. 184, No. 1, 2021, pp. 3-10.

[21] B. Zhou, "Hybrid Electric Vehicle Energy Management Strategy with Consideration of Battery Aging", Michigan Technological University, USA, Master Thesis, 2020.

[22] J. N. Long, "Integrating Electric Vehicles into Software Engineering Project Based Education", American Society for Engineering Education, 2012.

[23] S. Chakraborty, M. Lukasiewycz, C. Buckl, S. Fahmy, "Embedded Systems and Software Challenges in Electric Vehicles", Proceedings of the Design, Automation & Test in Europe Conference & Exhibition, Dresden, Germany, 12-16 March 2012, pp. 1-6.

[24] S. Maase, R. Hoed, "EV Charging Data Management, five issues to solve", Proceedings of the 32nd Electric Vehicle Symposium, National French Pavilion, France, 19-22 May 2019, pp. 1-12.

[25] D. Pevec, J. Babic, V. Podobnik, "Electric Vehicles: A Data Science Perspective Review", Electronics, Vol. 8, No. 1190, 2019, pp. 1-30.

[26] S. Ahmed, R. Al-Hamdani, M. Croock, "Enhancement of Student Performance Prediction Using Modified K-nearest Neighbor", TELKOMNIKA, Vol. 18, No. 4, 2020, pp. 1777-1783.

[27] Y. LeCun, L. Bottou, Y. Bengio, P. Haffner, "Gradient-based learning applied to document recognition," Proceedings of the IEEE, Vol. 86, No. 11, 1998, pp. 2278–2324.

# Vehicular Wireless Communication Standards: Challenges and Comparison

Review Paper

**Muhammad Uzair**
Electrical Engineering Department,
Faculty of Engineering, Islamic University of Medina,
Medina, Saudi Arabia
uzair91@hotmail.com, muzair@iu.edu.sa

***Abstract*** *– Autonomous vehicles (AVs) are the future of mobility. Safe and reliable AVs are required for widespread adoption by a community which is only possible if these AVs can communicate with each other & with other entities in a highly efficient way. AVs require ultra-reliable communications for safety-critical applications to ensure safe driving. Existing vehicular communication standards, i.e., IEEE 802.11p (DSRC), ITS-G5, & LTE, etc., do not meet the requirements of high throughput, ultra-high reliability, and ultra-low latency along with other issues. To address these challenges, IEEE 802.11bd & 5G NR-V2X standards provide more efficient and reliable communication, however, these standards are in the developing stage. Existing literature generally discusses the features of these standards only and does not discuss the drawbacks. Similarly, existing literature does not discuss the comparison between these standards or discusses a comparison between any two standards only. However, this work comprehensively describes different issues/challenges faced by these standards. This work also comprehensively provides a comparison among these standards along with their salient features. The work also describes spectrum management issues comprehensively, i.e., interoperability issues, co-existence with Wi-Fi, etc. The work also describes different other issues comprehensively along with recommendations. The work describes that 802.11bd and 5G NR are the two potential future standards for efficient vehicle communications; however, these standards must be able to provide backward compatibility, interoperability, and co-existence with current and previous standards.*

***Keywords***: *Intelligent Transportation System (C-ITS); LTE (C-V2X); IEEE802.11p (DSRC), IEEE 802.11bd, 5GNR-V2X, ITS-G5*

## 1. INTRODUCTION

Autonomous vehicles (AVs) are the future of transportation mobility due to their increased traffic safety, fuel efficiency, better use of infrastructure, and other promising features. These AVs use different vehicular networks (one of the applications of Mobile ad-hoc networks- MANETs) to communicate with each other due to their high speed, short communication time, and highly dynamic topologies [1]. However, many of these standards (networks) are not able to meet the requirements, i.e., ultra-high reliability, ultra- low latency, etc., of vehicular communications. Therefore, new protocols, mechanisms, and standards are required to guarantee the highest reliability and interoperability among different vehicular networks, i.e., cooperative intelligent transportation system (C-ITS), etc., for safe and reliable driving [2]. Different types of wireless communications (also known as V2X communication) may be performed by a vehicle with different entities as shown in Fig.1. [3].

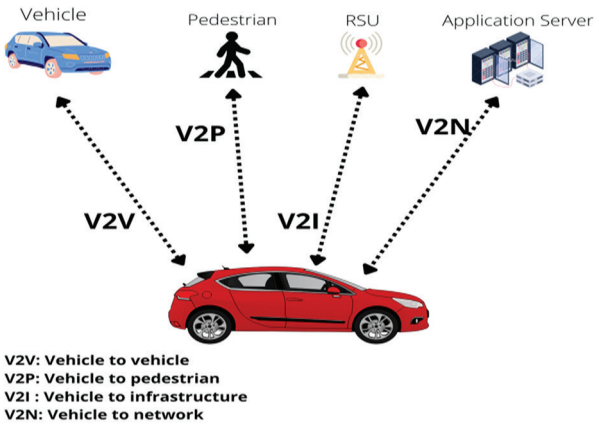


**Fig. 1.** Vehicle-to-everything (V2X) [3]

Sensors are heavily used in vehicles to assist human drivers to perform various applications as sensors are not prone to tiredness, deflection, or sentiment like humans. However, sensors have also limited sight as humans. Therefore, vehicles equipped with sensors are also

unable to coordinate efficiently with other vehicles in highly mobile environments [4]. However, C-ITS have no such issues and can also be used to reduce traffic jamming, traffic accidents, and other transportation-related environmental issues. CC-ITS also provides cooperative collision warning, traffic management, infotainment, etc., which makes autonomous vehicles (AVs) capable to share their driving information, ultimately making transportation safer and more reliable [4]. Two primary messages, i.e., cooperative awareness message (CAM) and decentralized environmental notification message (DENM), etc., are used to provide information related to speed, location, and other features of C-ITS [4, 5]. The basic set of C-ITS applications is shown in Fig.2. [3].

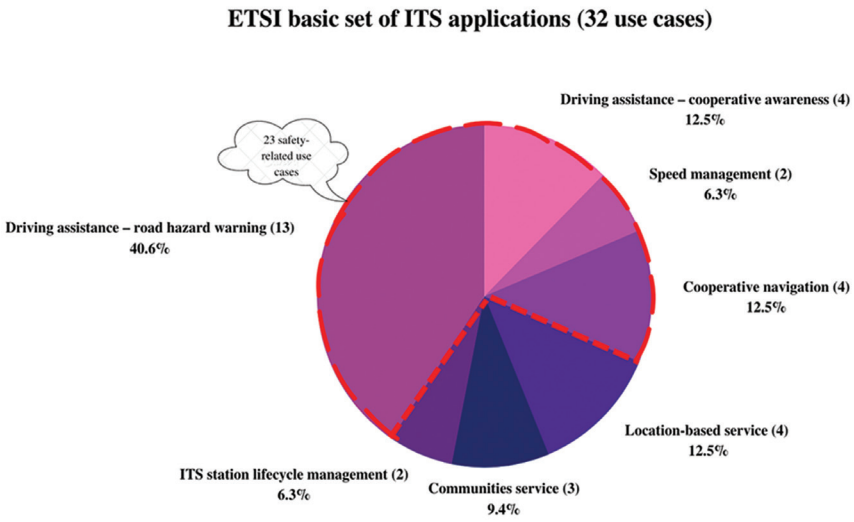


**Fig. 2.** ITS applications defined by ETSI (European Telecommunications Standards Institute) [3]

Traditional Wi-Fi-based approaches cannot be used for V2X communications as they have many challenges such as high power consumption, packet delivery rate issues and high latency, etc. Also, traditional Wi-Fi standards do not support high mobility applications, which is one of the fundamental requirements for vehicle communication. To overcome these shortcomings/challenges, many standards have been developed to support ITS applications such as Dynamic short-range communication (DSRC), long-term evolution-LTE (C-V2X), 5G NR-V2X, etc. [6]. However, which technology is best for V2X is another issue. No one would like to ride a car that uses technology not compatible with a technology used by a nearby moving car. Similarly, if the government standardizes one specific technology, it would stop the potential benefits of other technologies. It is also very difficult for the industry and the community to elicit all the possible benefits of new technology in the early stages of development. Therefore, delays may occur in choosing the best communication technology among vehicles which will ultimately also delay the commercial deployment of AVs [6, 7]. The evolution of V2X communication is shown in Fig.3. [8].

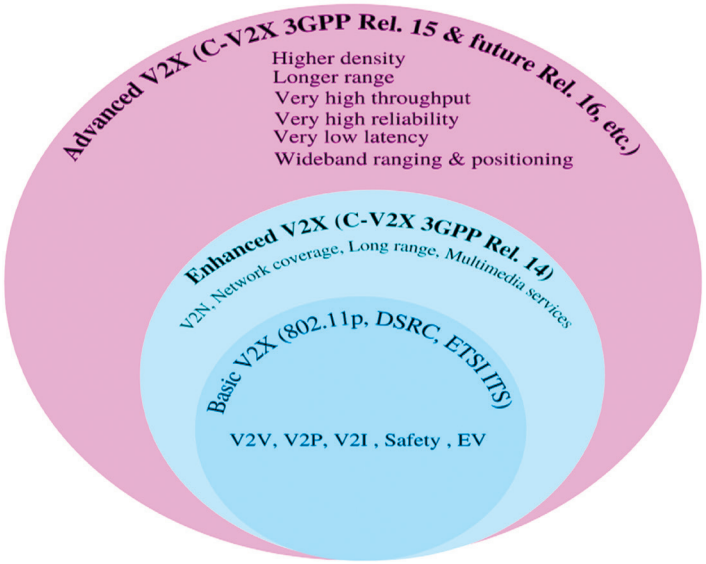


**Fig. 3.** V2X Evolution [8]

The existing V2X communication systems, i.e., IEEE 802.11p (DSRC), intelligent transportation systems (ITS-G5) & LTE (C-V2X), etc., have many issues and challenges. Similarly, the advanced V2X systems, i.e., IEEE 802.11bd, 5G NR-V2X, etc., also have many issues. The existing literature generally describes the features of these standards only. The existing literature also does not describe the issues/challenges and/or comparison between these standards or discuss challenges/comparison for any two standards only [4, 5, 9, 10, 11, 12, 13, 14]. However, this work comprehensively provides an overview of the different issues/challenges faced by these standards. This work also comprehensively provides a comparison among these communication standards along with their salient features. The overall structure of this work is shown in Fig.4.

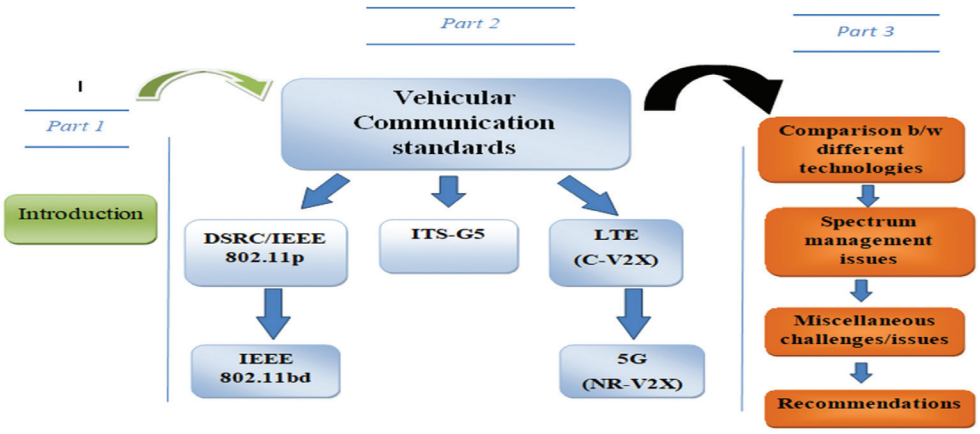


**Fig. 4.** The overall organization of the research

The paper is arranged as follows. Section II presents the V2X standards. Section III presents a comparison between DSRC (IEEE 802.11p) & LTE (C-V2X). Section IV presents a comparison between IEEE 802.11bd & 5GNR (NR-V2X). Section V presents a comparison between IEEE 802.11p (DSRC) & IEEE 802.11bd. Section VI presents a comparison between LTE (C-V2X) & NR-V2X. Section VII presents a comparison between IEEE WAVE (DSRC) & ITS-G5. Section VIII presents a comparison between ITS-G5 & LTE (C-V2X). Section IX presents spectrum management issues. Section X describes other challenges/issues. Section XI presents recommendations. Section XII presents the conclusion.

The next section presents the vehicular communication standards.

## 2. VEHICULAR COMMUNICATION STANDARDS

Different vehicular communication standards have been developed in recent years such as DSRC, ITS-G5, LTE (C-V2X), IEEE 802.11bd, 5G NR-V2X, etc. DSRC, ITS-G5, and LTE (C-V2X) operate at a 5.9 GHz unlicensed band. DSRC protocol is developed in the United States and the intelligent transportation system (ITS-G5) protocol is developed by the European telecommunications standards institute (ETSI), respectively. Similarly, C-V2X (a long-term evolution (LTE) based radio access technology (RAT) which facilitates LTE equipped vehicles to function even without cellular infrastructure) has been developed by the 3rd generation partnership project (3GPP). A generalized vehicular communication protocol stack used by DSRC, ITS-G5, and LTE is shown in Fig.5. [2, 10].

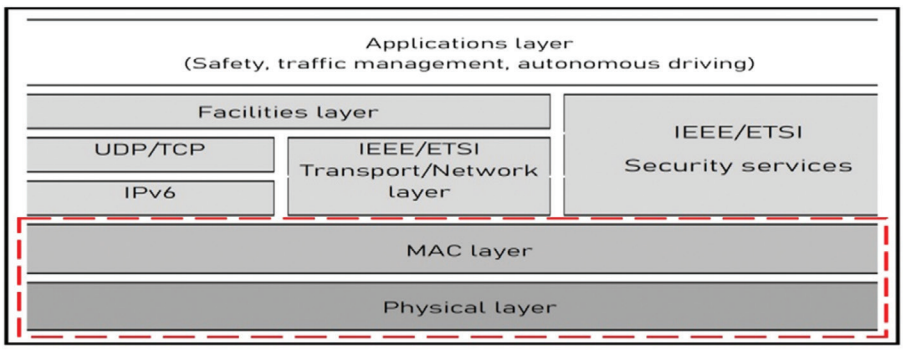


IEEE: Institute of Electrical and Electronics Engineers
ETSI: European Telecommunication Standard Institute
UDP: User Datagram Protocol
TCP: Transmission Control Protocol
MAC: Medium Access Control

**Fig. 5.** Generalized vehicular communication protocol stack [2]

The figure shows that the difference between these standards lies at MAC and PHY layers. DSRC and ITS-G5 use Wi-Fi, whereas LTE uses cellular-based access technology. Moreover, DSRC and ITS-G5 use different access mechanisms in the PHY layers [10, 15]. The next section describes the DSRC protocol.

### 2.1. DEDICATED SHORT RANGE COMMUNICATIONS (DSRC) - IEEE 802.11P

It is the de-facto standard for V2X communication based on the IEEE 802.11p (modified version of IEEE 802.11) and 1609 Wireless Access in Vehicular Environment (WAVE) protocols in the United States. The protocol stack for DSRC is shown in Fig.6. [5].

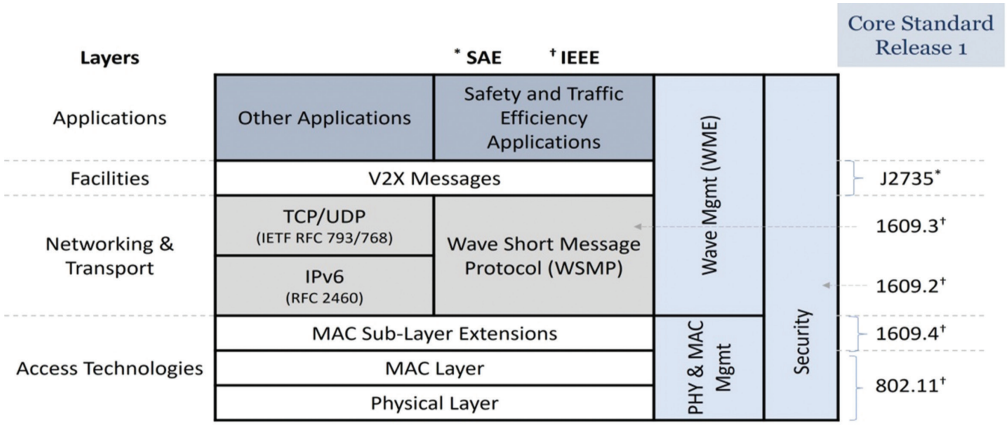


**Fig. 6.** Protocol stacks & related core standards for DSRC in the USA [5]

The work for DSRC was started in 2004 by the IEEE task group *p* and was approved in 2010. DSRC was the only available V2X technology for a long time. DSRC operates in the 5.9 GHz band ITS applications. The standard supports low latency V2X communications in high mobility scenarios. The standard also supports platooning (i.e., better fuel efficiency and carbon dioxide emissions, etc.) and provides reliable traffic management, i.e., traffic lights, emergency services, etc. Municipal/state governments and auto manufacturers have invested a lot of money to develop this standard and it is ready for deployment as it addresses the most challenging V2X requirements. Any other technology that can fulfill the same requirements would again require huge testing and investment [2, 12, 16].

#### 2.1.2. Issues/challenges

The DSRC has many issues. It is appropriate for short-range messaging, however, it does not provide a strong connection, very high reliability, and very low latency, especially in high mobility environments. DSRC also suffers low data rates, poor scalability, and packet losses when the vehicle's density is high. The standard also needs broader compatibility, merger, and coexistence, i.e., the ability to support safety services, etc. [5, 17].

The next section describes the Long term evolution-LTE (C-V2X) protocol.

### 2.2. Long term evolution - LTE (C-V2X)

Initially, there was an assumption that cellular technology does not provide vehicular safety applications as it requires low latency, especially at high speed as the messages have to go through the infrastructure. However, the 3GPP developed LTE. In this standard, direct communication among devices was achieved by using proximity services (ProSe). This was done in 3GPP-Release 14 & Release 15 (modes 3 and 4), based on the PC5 interface with or without any involvement of evolved node B (eNB) [10, 12]. The standard uses two different types of communications: network communications which use the Uu interface (radio interface between user equipment & enodeB) and direct communications which use a side link channel over the PC5 interface as shown in Fig.7. [14].

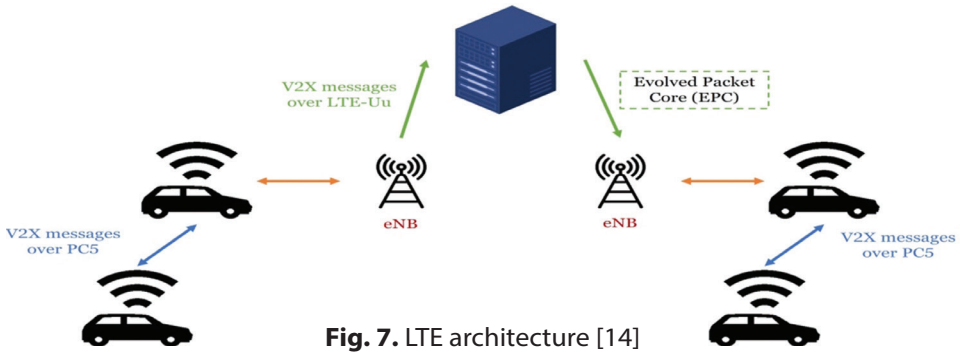


**Fig. 7.** LTE architecture [14]

Licensed spectrum is used for network communications, while evolved node B (eNodeB) is used to send messages to the vehicle's user equipment (UEs). For direct communication, messages are communicated at 5.9 GHz (unlicensed spectrum). Moreover, modes 3 and 4 (D2D transmission modes) support low-latency vehicular applications by allocating resources in different ways. In mode 3, resources are allocated by eNodeB, while mode 4 allocates resources autonomously without using eNodeB. Therefore, LTE operates at licensed and unlicensed spectrum [2, 12].

#### 2.2.1. C-V2X (LTE-release 14) issues

**a) V2I/I2V related issues**

Cellular technology is generally suitable for non-safety-related uses. Similarly, the performance of LTE networks is not clear when the network traffic is very high, especially when roaming conditions for many network operators is not clear. This issue can be solved by using a point-to-multipoint interface, i.e., Multimedia Broadcast/Multicase Service (eMBMS). However, eMBMS is typically designed to support static scenarios, e.g., crowd watching a football match in a stadium. Moreover, handovers and cooperation between mobile network operators (MNOs) are also not well defined due to the presence of data traffic from other applications which might affect I2V applications [5, 18].

**b) V2V-related issues**

The use of cellular technology for safety-related applications experiences many challenges. Unicast LTE networks cannot handle too much data when some V2V applications produce continuous traffic among vehicles, as cellular networks do not provide high data bandwidth at a low latency across all coverage areas. Although, messages with low bandwidth, i.e., decentralized environmental notification messages (DENM), are supported by the cellular networks at very low latency. However, cellular systems are not capable of supporting these messages under all conditions [18, 19].

**c) Timeline for C-V2X**

The 5G NR-V2X will be included in Release 16 and onwards (i.e., referred to as 5G) as shown in Fig.8. [20]. By the time, the cellular community addresses all LTE issues, other technologies (e.g., 802.11p) would be already in use and would create tough competition for 5G NR-V2X [18, 19].

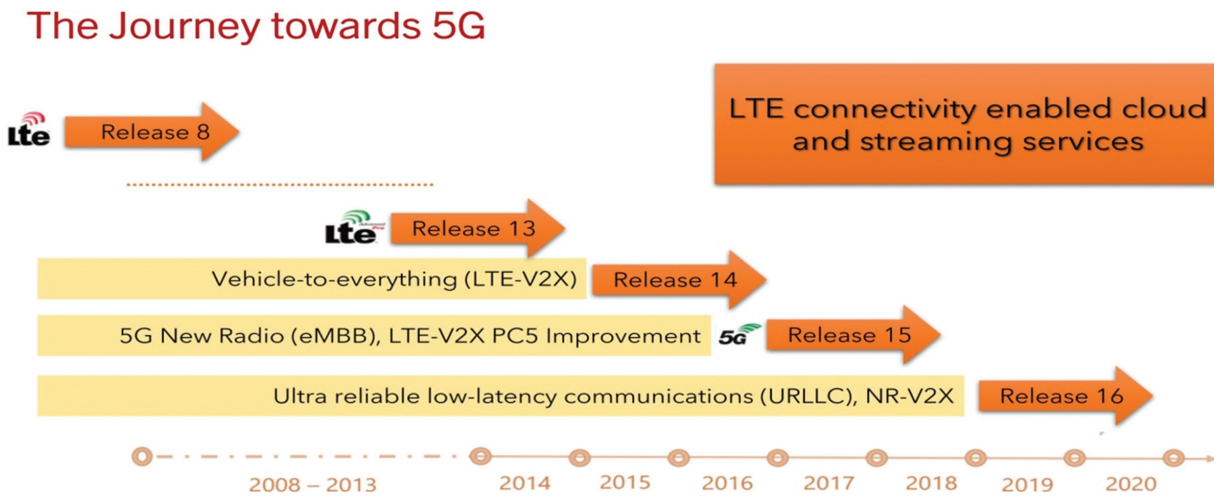


**Fig. 8.** A journey towards 5G [20]

**d) Safety and privacy considerations**

The subscriber Identity Module (SIM) card is used for network authentication by cellular networks for the user's

security. However, in the absence of a network, SIMs may not work for network-assisted V2X communication, and 3GPPP has not addressed this issue yet. Similarly, privacy is a growing concern for everyone and there is major opposition to cloud-based systems with this technology. However, privacy is more secure in IEEE 802.11p/bd as there is no cloud system [18, 19].

**e) Cellular infrastructure issues**

Existing cellular infrastructure does not support many V2X applications as these applications require low latency in high mobility and/or high congestion scenarios. Therefore, improvements and expansion are required for cellular infrastructure. On the other hand, roadside units (RSUs) can be deployed in IEEE 802.11p/bd along with existing infrastructure (traffic lights and traffic signs, etc.) which will reduce costs for near and long-term deployment [18].

**f) Standardization issues**

It is very difficult for cellular networks to fulfill all the technical and standardization requirements of V2X due to bandwidth issues. However, in IEEE 802.11p/bd, the standard only operates at 5.9 GHz once everything is according to the standards/requirements, i.e., no requirement of subscriptions and roaming agreements, etc. [18, 21].

**g) C-V2X security architecture issues**

Control functions are provided by eNB and mobility management entity (MME) in LTE. Although efficient, this design does not provide a robust approach for credential management, privacy, and anonymity of involved entities. Moreover, there is limited support for many other functions such as positioning, maneuver changes, platoon formations, etc. Similarly, the safety requirements in LTE applications (e.g., periodic transmission after every 100 msec) are not efficient compared to aperiodic transmission by using large and variable-sized packets [18, 19, 22].

**h) Other issues/challenges**

There are also many other issues/challenges in Relesae14 such as a high Doppler shift of 2700 Hz, which creates a channel variation even within a sub-frame at a relative speed of 500 Km/hr at 6 GHz; reliability of channel estimation is also very difficult at very high frequency, e.g., there is an offset of up to 1800 Hz at 6 GHz; channel inter-leaver issue exists because of the reuse of other LTE uplink severely impacts the performance of side link data channel in RB/modulation coding scheme. Moreover, the solutions provided are incompatible with Rel-15; the transport block-sized table used in Rel-15 is incompatible with Rel-14; Mode-4 in Rel-14 suffers from high latency and the solution provided in Rel-15 is not compatible with Rel-14; users may miss the safety messages due to half-duplex problem. The solution is only available with 5G NR instead of Release 15. This issue is also not present in ETSI ITS-G5 due to the principle of "listen-before-talk"; LTE is also very sensitive to frequency offsets, e.g., a small subcarrier spacing of 15 kHz, especially at 2 or 3 GHz region is not compatible in the 5.9 GHz band. However, in 5G NR, 3GPP is planning to "unlock" the subcarrier spacing according to the deployment; selecting a suitable modulation scheme (e.g., SC-FDM or OFDM) and changes in signal structure (e.g., additional pilots for better channel estimation) are other issues with Release 14 which need to be solved [5, 18, 19, 21, 22].

To address all the above-mentioned issues would require new approaches and designs requiring time and money [18]. The next section describes the Intelligent Transportation System (ITS-G5) protocol.

## 2.3. INTELLIGENT TRANSPORTATION SYSTEM (ITS-G5)

This protocol operates in the 5 GHz frequency band and is developed by ETSI. It uses the same PHY layer as in 802.11p, however, it defines different algorithms for channel access [11]. The protocol stack for the ITS-G5 is shown in Fig.9. [5].

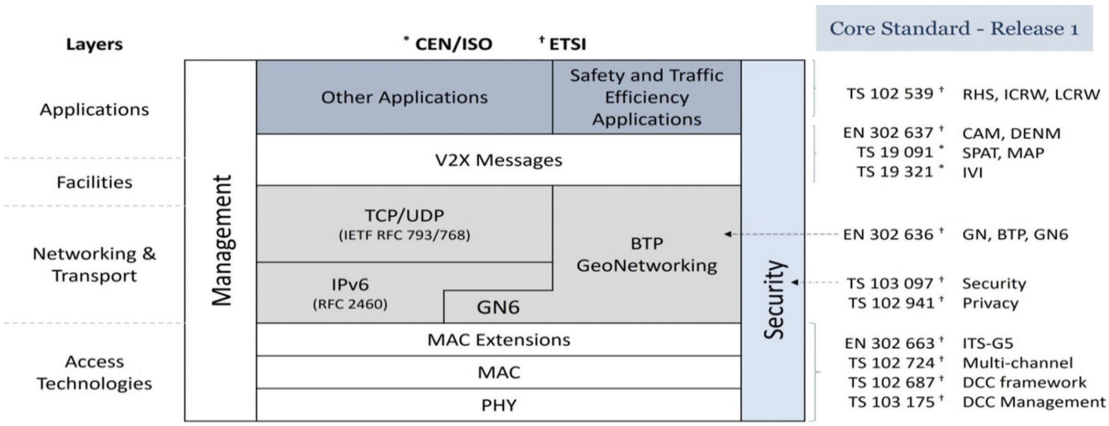


**Fig.9.** Protocol stacks & related core standards for C-ITS (Europe) [5]

### 2.3.1. ETSI (ITS-G5) issues

The performance, i.e., end-to-end delay, packet error rates, etc., of the ITS-G5 systems is not well defined under high node density scenarios. Similarly, decentralized congestion control in ITS-G5 introduces local and global oscillation of the state machine. Moreover, the number of received cooperative awareness messages (CAMs) reduces considerably at a high penetration rate, which ultimately reduces the number of known neighbors [23].

It is very difficult to say which standard (DSRC, LTE, and ITS-G5) is better. Currently, DSRC has the advantage as the 5.9 GHz band in the United States is reserved for DSRC for more than a decade now. Until unless, the LTE inventors can convince government regulators that LTE is a technically superior and more flexible alternative than 802.11p, the mandate for 802.11p seems imminent. In Europe, the EU plans to roll out the ITS-G5 system very soon. However, ITS-G5 also intends to use 802.11p as the basis of the radio standard for safety applications. Similarly, the Chinese government is ready to mandate LTE by using the 5905-5925 MHz spectrum. This is important as it would provide minimal standards differences worldwide. In the US, the legislation timeframe for mandating V2V communication is set for 2023 [3].

However, the above-mentioned standards (DSRC, LTE, and ITS-G5) provide vehicle safety applications up to 99% reliability & 100 ms latency only, however, AV

driving requires reliability and latency up to 99.99% & 3 ms. Therefore, to meet this challenge, IEEE Task Group 802.11bd (TGbd-enhanced version of DSRC) was formed in Jan. 2019. Similarly, 3GPP is also developing New Radio (NR-V2X) for its Rel. 16 (enhanced version of LTE-V2X), i.e., building on the top of 5G [2, 12].

The next section describes the IEEE 802.11bd (Enhanced version of IEEE 802.11p-DSRC) protocol.

### 2.4. IEEE 802.11BD (ENHANCED VERSION OF IEEE 802.11P-DSRC)

To meet the requirements of V2X communications and to accomplish the challenges faced by the different standards mentioned above, the work has started to develop the IEEE 802.11bd standard to provide high throughput and low latency, etc. [2]. In this standard, various improvements such as low-density parity-check (LDPC) coding, space-time block coding (STBC), midambles, etc., have been achieved at the PHY and MAC layer protocols of IEEE 802.11n, 802.11ac, and 802.11ax [2]. This standard also improves orthogonal frequency division multiplexing (OFDM) sub-carrier spacing, forward error correction (FEC) coding, channel estimation, etc. Moreover, better spectral efficiency is achieved as compared to 802.11p by using efficient orthogonal frequency-division multiple access (OFDMA) numerologies. However, the reduced sub-carrier spacing affected by channel variations is still an issue [2, 22, 24].

#### 2.4.1. Issues/challenges

There are many issues with the 802.11bd standard which are described below.

**a) Interoperability**

Interoperability is a critical requirement that 802.11bd must satisfy. For interoperability, 802.11bd & 802.11p must be able to decode each other messages as many auto manufacturers are already installing 802.11p in their AVs [12].

**b) Backward compatibility**

At least, one mode of 802.11bd must be interoperable with 802.11p for backward compatibility. Design of the PHY and MAC layers of 802.11bd, i.e., space-time block coding, etc., face many constraints due to the interoperability and backward compatibility requirements. Many changes have been made in the frame format to address this issue [12, 24].

**c) Coexistence**

Coexistence requires 802.11p devices to detect 802.11bd frames as valid frames instead of decoding and vice versa. Coexistence is required when 802.11bd devices send messages only for 802.11bd (not 802.11p). However, in situations where both devices are present, 802.11bd devices can also send messages using only the 802.11p frame format, i.e., even when there is no 802.11p device [12].

**d) Fairness**

There are many issues of fair and equal access to the physical transmission channel, especially when both 802.11bd and 802.11p equipment are operating in the same vicinity [12].

The next section describes the 5G New Radio (5G NR-V2X) protocol.

### 2.5. 5G New Radio (5G NR-V2X)

5G is the future of cellular networks. Therefore, 3GPP is working toward the development of the NR-V2X standard to fulfill ultra-reliable and ultra-low latency requirements, i.e., Rel. 16 (enhanced version of LTE-V2X) as shown in Fig.10. [25].

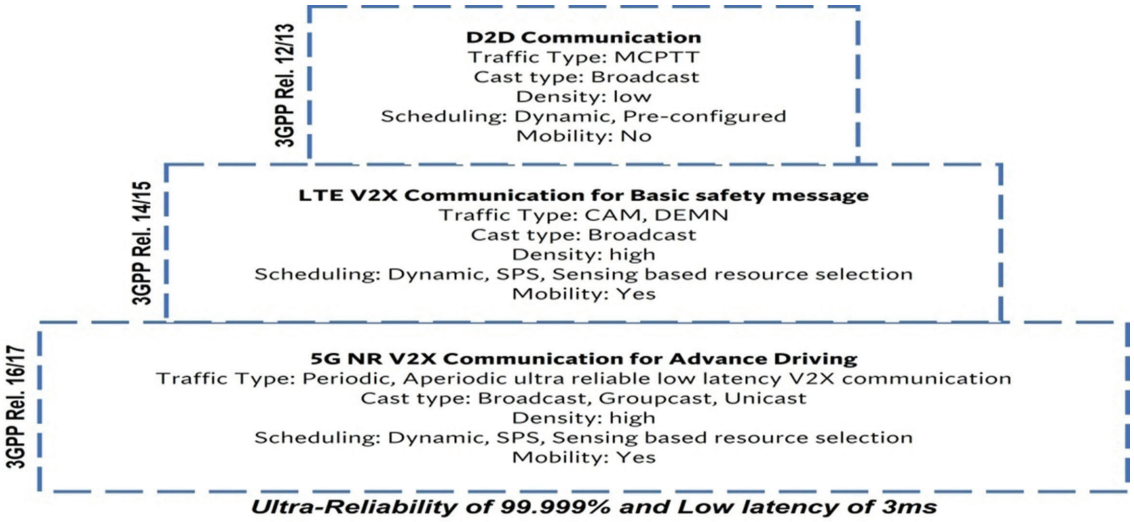


**Fig.10.** 3GPP Side link Evolution [25]

As compared to LTE, NR-V2X is a function-based architecture that mainly provides service-based access to all involved entities as shown in Fig.11. [25].

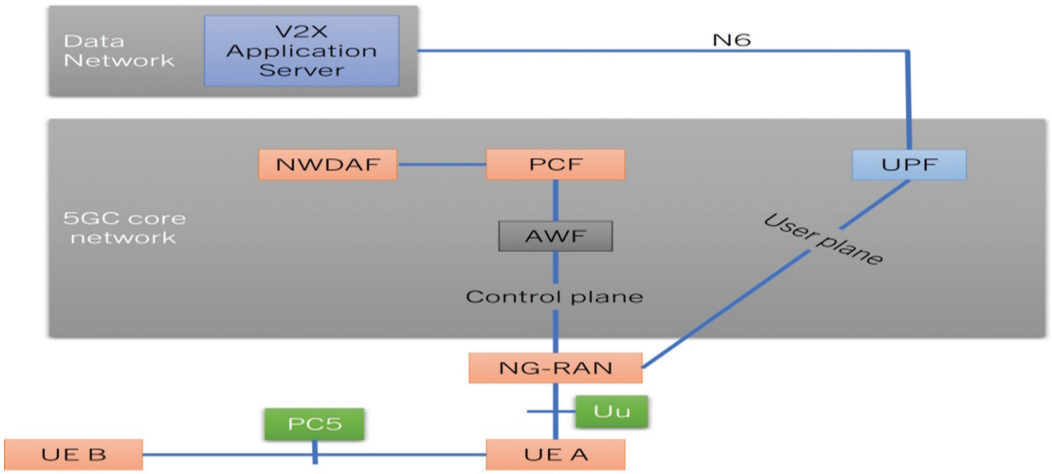


**Fig.11.** Release 16 V2X architecture within 5G system architecture [25]

The standard uses flexible numerologies, agile frame structure, mm-Wave bands, better channel recovery, and advanced multiple access techniques. It also provides side link communication via the PC5 interface to provide immediate dissemination of vehicles' planned maneuvers. Similarly, NR-V2X will also provide preemptive resource scheduling for critical messages, adaptive retransmissions, and support of unicast & groupcast communications [2, 12, 26, 27]. The standard also uses both DFT-spread-OFDM (DFT-s-OFDM) and OFDM as compared to LTE, which is more suitable for high throughput and wide-bandwidth operations with low complexity. For low-budget devices, DFT-s-OFDM provides high efficiency because of its low peak to average power ratio (PAPR). The standard also uses scalable OFDM numerologies which allow the standard to choose between different subcarrier spacing from 15 to 480 kHz. All of the above-mentioned features make NR-V2X more reliable, scalable, and throughput efficient as compared to LTE [28].

### 2.5.1. Issues/challenges

**a) Security attacks and threats**

Security is one of the key issues for NR-V2X. LTE is highly vulnerable to attacks if it is used in NS-5G (Non-Standalone) mode. Similarly, NR-V2X also requires additional security when used in the NS-5G V2X mode for different scenarios (which do not exist for LTE) such as service-based accessibility and edge-based authentications, etc. [29].

**b) Irregular placement of gNB**

Irregular placement of gNB (counterpart of eNB (tower) & MME of LTE) may cause possible attacks on NR-V2X, especially for authentication and authorization of vehicles. Certificate-based security is provided in semi-autonomous mode or a secure connection is achieved between roadside units (RSUs) and original equipment manufacturer (OEM) to address this issue. However, in fully autonomous mode, the smooth transit between gNBs may be hindered by certificate-based solutions [12, 25].

**c) Cell coverage**

Cell coverage, network layout, planning, and handover are other areas that may be exploited by the attackers in both intra and inter modes. Although, a lower number of roadside units (RSUs) are used by LTE and NR, however, issues related to universal availability and access management are still there. Similarly, there is no architecture available to provide dynamic RSUs. NR securities also have complex and expensive backward operations for V2X applications [25, 30].

**d) Excessive service initiations**

Many services can be initiated by an attacker, if he gets access to security reflex functions (SRF).

**e) Security reflex function (SRF) positioning**

Optimization of the SRF function is another issue in different scenarios. In some scenarios, SRF functions must be placed near original equipment manufacturers (OEM) to have direct control of vehicles by the OEM. However, it violates the principles of edge computing [25, 29].

**f) Accurate sensor readings**

In all situations, accurate data regarding the vehicle needs to be retrieved by sensors for location and trajectory-based key generations.

**g) Credential theft**

New approaches are required for the accurate identification of vehicles to avoid any kind of threats to infrastructure (KX), especially in the case of a fake call from vehicles (KV) [25, 30].

**h) Configuration attacks**

For NS-5G-V2X, configuration attacks are very critical. The receiving entity may be misleading to take wrong decisions by using V2V/V2P broadcasts by the attackers. These attacks may further create routing attacks and session hijacking [25].

**i) Perfect forward secrecy**

Forward secrecy is violated while capturing a vehicle or doing signature replication by NR, which may enhance credential threats of vehicles to physical threats [29].

**j) Insider threats & zero-day attacks**

These vulnerabilities are the major reason for the privacy and anonymity issues, which may expose the entire network to other entities further enhancing attacks [31].

**k) Privacy protection for unicast & multicast messages over PC5**

New identifier(s) (layer 2 identifiers - L2 IDs) are used to update request messages from the user equipment (UE) in case of unicast messages over PC5. L2 IDs can be made blind by an attacker by using long-term V2X IDs and may create track and linkability issues. Similarly, long multicast sessions may create L2 ID tracking in the groupcast, i.e., SA3 WG multicast [25].

**l) Issues of eV2X unicast messages over PC5**

A man-in-the-middle attack may happen while initiating a direct communication by UE via broadcast to all UEs and interested UEs may reply to establish a unicast communication. This may further lead to eavesdropping on signaling, data traffic, etc. [25].

**m) Issues of identifier conversion in group communication**

Mapping or configuration is used by UE in the conversion procedure to find out the destination L2 ID. This conversion should be secure; otherwise, an attacker may get access to UE group memberships [25].

**n) Setting up multicast security**

A man-in-the-middle attack may happen to L2 signaling and UEs may receive wrong or no multicast information at all. As there is no security setup for multicast (groupcast) communication at present [25].

**o) UE service authorization and revocation issues**

The overall security of all services may be under threat, if service authorization and revocation are not safe over the PC5 [25].

**p) Cross-RAT (radio access technology) PC5 control authorization indication**

There is no secure procedure for cross-RAT PC5 control authorization, i.e., control of the cellular network for LTE and/or NR side link (via LTE Uu or NR Uu). This may create severe security issues [25].

**q) Other miscellaneous issues**

There are many other issues/challenges such as ciphertext attacks, these may happen as sensory information is shared without encryption; fresh keys and synchronized patterns should be used to avoid issues such as a replay or de-synchronous attacks; side-channel attacks are difficult to find which may put the entire network under threat by affecting only the vehicle or gNB; locations of certain entities/functions, involving gNB, session management function (SMF), access and mobility function (AMF), etc., are other key issues for the security of NR [25, 30, 31].

Different V2X standards have been discussed in the previous section presenting their brief features, along with their comprehensive challenges and issues.

The next section presents the comparison between 802.11p & LTE.

## 3. COMPARISON BETWEEN IEEE 802.11P (DSRC) & LTE (C-V2X)

Both standards support various basic vehicular safety applications such as road awareness, traffic situations, emergency vehicle notifications, etc.

### 3.1. READINESS

IEEE 802.11p is ready to use, while LTE is in its advanced stages with an advantage of the already deployed infrastructure. 802.11p is a mature technology and LTE is the latest technology, and comparative analyses between these are not widely available. A comparison among these technologies is shown in Fig.12. [18].The key difference is that 802.11p uses direct communication, while LTE depends on the presence of the network [18].

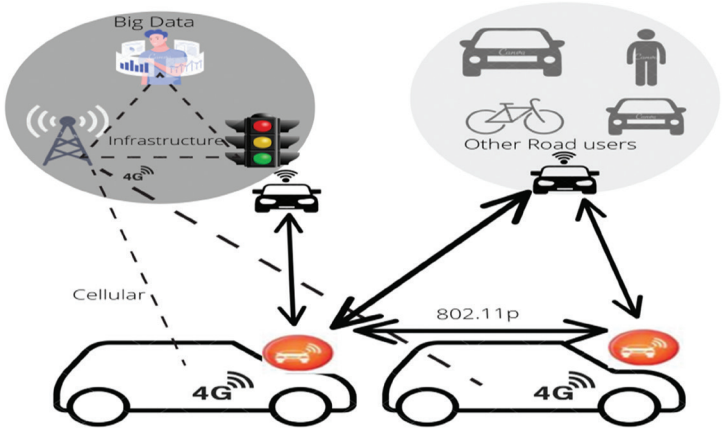


**Fig.12.** Comparison between IEEE 802.11p & LTE [18]

### 3.2. LATENCY

Both technologies provide a latency of around 100 milliseconds for low vehicular density scenarios. However, in a high vehicular density scenario, DSRC performance rapidly deteriorates because of packet collisions. Packet collision happens due to simultaneous transmissions and hidden node issues. This issue can be partially addressed by using congestion control approaches [12].

### 3.3. HIGHER LINK BUDGET

The *side link* mode 4 of LTE performs better than DSRC in terms of a higher link budget. Similarly, *side link* mode 3 of LTE provides efficient utilization of the spectrum. Although, mode 4 provides frequency re-use, the re-use distance is reduced as traffic density increases reducing the performance of LTE [12].

### 3.4. DELIVERY RATE

Both standards are not capable of providing consistent high data rate transmissions for advanced autonomous driving applications. However, the performance of LTE is better than 802.11p due to the improved PHY layer. Similarly, 802.11p does not provide optimal congestion control mechanisms such as LTE [21].

### 3.5. PACKET RECEPTION RATIO

At low data traffic, LTE-V2V supports a better packet reception ratio (e.g., up to 10%) as compared to 802.11P. Similarly, LTE-V2V provides a lower update

delay for longer distances (up to 500 meters) as compared to 802.11p (approximately 250 meters) [32].

### 3.6. RANGE

The field trials show that LTE can support reliable communication for distances longer than 1.2 km at a relative speed greater than 430 km/h compared to 802.11p, especially in mode 3 [2, 33].

### 3.7. MISCELLANEOUS COMPARISONS

Several other comparisons can be made. Such as the comparison that LTE mode 3 performs better than 802.11p & LTE mode 4 because of the better knowledge of node positions and allocations; LTE-V2V mode 4 performs better than 802.11p, especially at larger distances with high density, but with longer update delay; LTE is generally better than 802.11p for standard and non-standard application layer codes, but 802.11p with 16QAM-3/4 is preferable at higher channel load; LTE mode 3 is collision-free; LTE is better than 802.11p on highways, but less in urban areas; LTE provides longer range, enhanced reliability and consistent performance during traffic congestions as compared to 802.11p; the future of LTE is 5G due to better co-existence with other technologies [2, 21, 33, 34, 35].

### 3.8. IMPORTANT NOTES

Existing literature reveals that LTE performance is better than 802.11p in terms of additional link budget, better resistance to interference, better non-line-of-sight (NLOS) capabilities, and mainly due to the already deployed infrastructure. However, factors such as mobility management, cost, consistency, safety, and scalability are yet to be further evaluated, especially by using different modulation and coding scheme (MCS) strategies as these factors generally penalize 802.11p without proper evaluation [12, 21, 28]. A comparison between LTE and DSRC is shown in Fig.13. [18]. In the cellular case, proper management of the network interference is achieved via full control of direct communication, while in the case of DCRS, a fast execution happens due to the use of the random access protocol, however, wireless resources are used inefficiently.

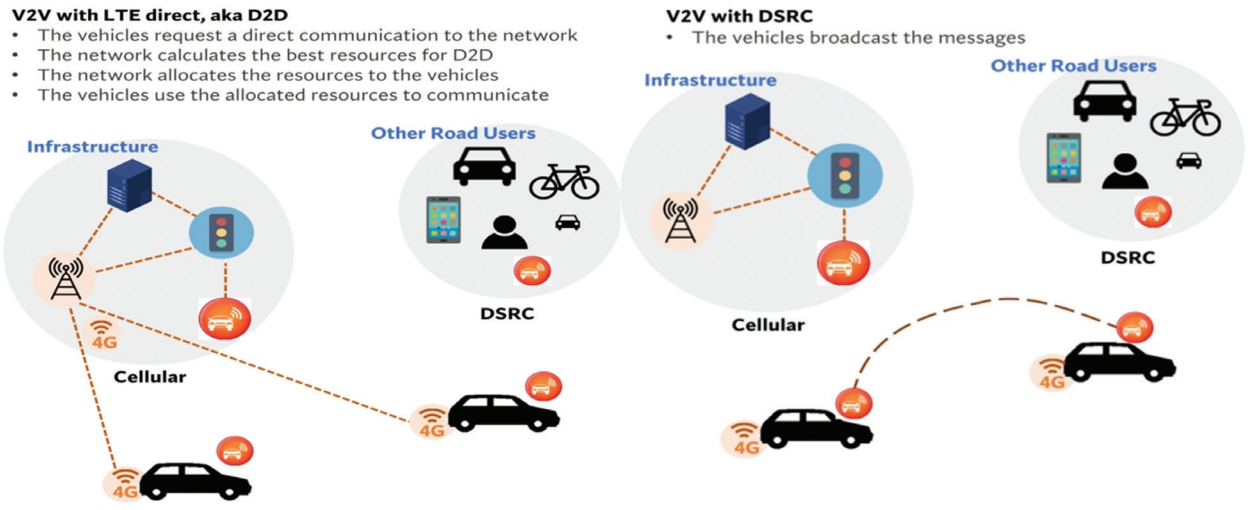


**Fig.13.** LTE advantages over IEEE 802.11p [18]

The next section presents comparisons between 802.11bd & 5G NR.

## 4. COMPARISON BETWEEN IEEE 802.11BD & 5G NR-V2X

Both standards provide reliable end services, lower latency, and high throughput. However, their design approach is considerably different.

### 4.1. BACKWARD COMPATIBILITY

IEEE802.11bd is backward compatible with 802.11p, i.e., devices from both standards can communicate with each other while using the same channel. However, in 5G NR, vehicles using NR can communicate with LTE by using a dual radio system, i.e., one for each technology [4, 12].

### 4.2. TRANSMISSION RELIABILITY

For the PHY performance, NR-V2X provides better transmission reliability. However, Doppler shifts are a major issue for 802.11bd. Although, mid ambles and extended range preamble significantly improve the performance of 802.11bd, however, NR-V2X is still better due to better channel estimation techniques, lower code rates, and DFT-s-OFDM.

### 4.3. PACKET ERROR RATES

This error happens in 802.11bd even at high signal-to-noise ratios due to the high Doppler shift for PHY performance [33]. Similarly, more advanced control applications such as the cooperative adaptive cruise control (CACC) system need further investigation for 802.11bd [24].

### 4.4. TRANSMISSION LATENCY

NR provides better transmission latency than 802.11bd due to the use of the mini slot option. However, NR outperforms LTE when the minimum latency requirement is less than 1 ms.

### 4.5. DATA RATE

NR provides a four times higher data rate for a packet size of 100 bytes and a 7 Mbps higher data rate for a packet size of 1500 bytes as compared to 802.11bd [24].

### 4.6. PACKET INTER-ARRIVAL TIME

For this feature, NR is better than 802.11bd due to lower code rates [24].

### 4.7. PACKET RECEPTION RATIO (PRR)

Taking 90% PRR as a threshold, both LTE & NR are better than 802.11bd because of their very low coding

rate. For 100 & 1500 bytes packet size, NR performs better than other standards by providing a higher range. This performance can be further improved by the hybrid automatic repeat request (HARQ) mechanism [24].

### 4.8. DOPPLER SHIFT

NR-V2X takes care of the Doppler shifts in a better way and outperforms 802.11bd by providing better reliability.

Based on the above discussion, NR performance is better in terms of reliability, latency, data rate, and packet inter-arrival time as compared to 802.11bd. However, many other challenging issues regarding these technologies need to be further investigated, especially the design of PHY and MAC layers.

The next section presents comparisons between 802.11p & 802.11bd.

## 5. COMPARISON BETWEEN IEEE 802.11P & IEEE 802.11BD

### 5.1. TRANSMISSION LATENCY

IEEE 802.11bd has a low transmission latency as compared to 802.11p because of higher-order modulation & coding schemes and more data carriers. With packet sizes of 100 & 1500 bytes, 802.11bd achieves 0.1 ms and 0.388 ms transmission latency, respectively [36].

### 5.2. DATA RATE

IEEE 802.11bd provides a peak data rate of approximately 0.3 Mbps & 8 Mbps for 100 &1500 bytes of packet sizes as compared to 8021.11p because of better channel estimation and coding scheme.

### 5.3. HIGH DOPPLER SCENARIOS

IEEE 802.11bd provides better performance in high Doppler scenarios as compared to 802.11p [12].

### 5.4. GAIN COMPARISON

Simulation results show that 802.11bd provides a gain of 3-8 dB instead of 0.5-1.7 dB achieved by 802.11p at a block error rate of $10^{-1}$. Similarly, 802.11bd can provide an additional 1-3 dB gain at a block error rate of $10^{-1}$ by using the parity-based interoperability mechanism [24].

### 5.5. PACKET ERROR RATE

IEEE 802.11bd provides a gain of 8 dB as compared to 802.11p in terms of packet error rate.

The above discussion shows that 802.11bd is better than 802.11p in every aspect. The next section presents comparisons between LTE & NR-V2X.

## 6. COMPARISON BETWEEN LTE (C-V2X) & 5G NR-V2X

### 6.1. DATA RATE

5G NR provides a data rate better than LTE, i.e., 16 & 13 Mbps for 100 & 1500 bytes of packet sizes, because

of less control overhead and better bandwidth efficiency [12].

### 6.2. GAIN

Simulation results show that NR provides much better gain due to 60 kHz sub-carrier spacing compared to LTE, which uses 15 kHz spacing, especially at relatively higher velocities, i.e., 500 *kmph*.

In summary, by using flexible NR numerologies which provide larger sub-carrier spacing and superior link-level performance, NR significantly outperform**s** LTE in every aspect including transmission, latency, reliability, throughput, packet reception ratio, packet error rate, etc. Under highway scenarios, NR almost meets the desired performance requirements for vehicular communication. [24].

The next section presents comparisons between IEEE WAVE (DSRC) & ITS-G5.

## 7. COMPARISON BETWEEN IEEE WIRELESS ACCESSES IN VEHICULAR ENVIRONMENTS (WAVE) (DSRC) & ETSI (ITS-G5)

A similar, however, not identical approach is used by ETSI in Europe and IEEE WAVE in North America to achieve the required vehicular communications. Both standards are based on 802.11p which operates at 5.9 GHz. However, both standards use different ways to access the available channels, i.e., WAVE uses enhanced distributed channel access (EDCA) subsystems, and ITS-G5 uses models consisting of state machines. Generally, the performance of both systems for many parameters such as end-to-end delay, packet error rates, inefficient channel utilization, etc., is not up to the standard, especially in high node scenarios. Although, ITS-G5 with decentralized congestion control (DCC) may access channels conservatively, however, it performs better than WAVE in most cases**.** Similarly, ITS-G5 performs better than WAVE for packet delivery rates at higher penetration rates, however, approximately only 40% of AVs are detectable by radio receivers at short distances [5, 11, 37**].**

The next section presents comparisons between ITS-G5 & LTE.

## 8. COMPARISON BETWEEN ITS-G5& LTE (C-V2X)

### 8.1. READINESS

ITS-G5 is an advanced version of the Wi-Fi standard, while most of the available LTE data are based on numerical simulations. For LTE, different performance classes will be available in the future due to different releases (Rel-14, Rel-15, etc.), which will also create an unfair situation for customers, as Rel-15 cars will have more advanced features as compared to Rel-14 cars [7]. Generally, we can say that LTE (especially Rel-14)) is not ready yet as compared to ITS-G5 as the testing has not been done according to the required standards [38].

### 8.2 COMPATIBILITY

LTE Rel-15 is not backward compatible with Rel-14, and Rel-14 may be obsolete even before deployed. Similarly, 5G NR technology is not backward compatible with LTE Rel-15 & Rel-14. Therefore, LTE implementation will always be equipped with previous versions in case it relies on services from previous releases, e.g., basic safety messages [7, 38].

### 8.3 RANGE COMPARISON

Real-time results show that generally, LTE suffers more losses as compared to ITS-G5 in range comparison. However, LTE has a better range in low node concentration due to data rate differences. For high node concentration, ITS-G5 outperforms LTE because of better resource scheduling.

### 8.4 HIGH MOBILITY ENVIRONMENT

ITS-G5 provides high mobility even for long distances by using a turbo-codec compared to LTE, which does not provide the same performance at high speed even with advanced block-based codecs (like LDPC) as these codecs cannot be decoded per symbol [38].

### 8.5 DATA RATE

LTE performs better than ITS-G5 for the same data rate. Moreover, LTE outperforms ITS-G5 when user density is less than 150 users per $km^2$, however, performance deteriorates more severely as congestion increases [10].

### 8.6 LATENCY

Generally, ITS-G5 provides better latency than LTE. Overall, which systems perform better depends on user density and operating range [10].

### 8.7 END-TO-END DELAY

The E2E delay of ITS services is affected by the handover procedure. However, association and authentication procedures are disabled in ITS-G5, which is an advantage of ITS-G5 over LTE (mode 3).

### 8.8 OTHER COMPARISONS

ITS-G5 is designed for V2X, whereas LTE (mode 3) is also used for other applications such as video streaming and VoIP. Similarly, undefined communication profiles for LTE, unrealistic timing requirements, non-clarities regarding the number of supported vehicles along with latency issues are additional challenges that have not been evaluated yet. These challenges also prove that LTE is still in the developing stage compared to ITS-G5.

Table.1. presents a generalized comparison of 802.11p, LTE, 5G-NR & 802.11bd [8]

**Table.1.** Comparison of DSRC, LTE, 5G-NR & 802.11bd [8]

| Key Elements | DSRC/IEEE802.11p | C-V2X (LTE) | NR-V2X (Release 15, 16) | IEEE 802.11bd |
|---|---|---|---|---|
| Operations beyond networks | Yes | Yes | Yes | Yes |
| Vehicle to Vehicle operation | Yes | Yes | Yes | Yes |
| Safety-related messages | Yes | Yes | No* | Yes |
| Vehicle to pedestrian operation | Yes | Yes | Yes | Yes |
| Vehicle to infrastructure operation | Limited | Yes | Yes | Yes |
| Multimedia services | No | Yes | Yes | Yes |
| Network coverage | Limited | Yes | Yes | Yes |
| Global economies of scale | No | Yes | Yes | Yes |
| Regulatory/testing efforts | Yes | Limited | No | No |
| Very high throughput | No | No | Yes | Yes |
| Very high reliability | No | No | Yes | Yes |
| Wideband ranging and positioning | No | No | Yes | Yes |
| Very low latency | No | No | Yes | Yes |

*Rel-15 supports all basic safety messaging as Rel-14.
Rel-16 has all features such as Rel-14 & 15 and will support advanced cases by using 5G NR-V2X.

The next section presents the spectrum management issues related to vehicular wireless communication.

## 9. SPECTRUM MANAGEMENT ISSUES

### 9.1. HETEROGENEOUS V2X NETWORKS (INTEROPERABILITY CHALLENGES)

Multiple V2X radio access technologies (RATs) may drive different vehicles simultaneously in the same region very soon. However, LTE and DSRC are two different technologies and are not compatible with each other. A true perspective of V2X communications cannot be obtained if vehicles with different technologies are not compatible with each other [2, 12, 39].

### 9.2. COEXISTENCE OF DSRC & WI-FI

Studies show that the MAC protocols of Wi-Fi & DSRC are considerably similar. However, the current coexistence mechanism may make it more difficult for Wi-Fi users to operate with the same spectrum. Especially, in urban areas, a large number of vehicles equipped with DSRC will always make it difficult for Wi-Fi devices to get access to the spectrum. Moreover, Wi-Fi operation at 5.9 GHz (unlicensed) should only be permitted if it does not create interference with V2X technologies. Coexistence between DSRC & Wi-Fi can potentially be obtained by changing different parameters in the current Wi-Fi standards instead of using conservative back-off mechanisms. DSRC transmitters can only get a high chance of channel access with a larger contention window size and/or spacing between frames of Wi-Fi. The MAC protocol of 802.11bd is also almost the same as 802.11p, which means that the coexistence of DSRC & Wi-Fi may also be appropriate for the coexistence of 802.11bd &Wi-Fi [39, 40].

### 9.3. COEXISTENCE OF LTE & WI-FI

The MAC protocol of LTE is considerably different from Wi-Fi. Similarly, LTE & Wi-Fi coexistence has not been properly evaluated and the coexistence of DSRC & Wi-Fi cannot be used as a standard for LTE & Wi-Fi coexistence. Therefore a cohesive coexistence approach is required due to the different MAC protocols of DSRC & LTE. The developed approach must also be forward compatible, i.e., LTE & Wi-Fi approach must also be compatible with 5G NR & Wi-Fi coexistence [39, 41]. However, there are still many issues that need to be addressed and are described below:

#### 9.3.1.

For the signal range between -62 dBm and -82 dBm, LTE and Wi-Fi cannot detect each other signals. Therefore, a new mechanism should be designed to detect signals in this range. The performance of LTE and Wi-Fi systems can also decrease up to 40 %, if the SINR is above 10 dB [39].

#### 9.3.2.

LTE-WLAN Aggregation (LWA) effectively minimizes interference between LTE & Wi-Fi as they access channels differently. However, interference while finding data routing between LTE and Wi-Fi radio is still an issue. Similarly, changing traffic situations along with changing the number of Wi-Fi equipment is also a challenge to design efficient flow routing algorithms [39, 42].

#### 9.3.3.

Multefire devices are in the early stage of development and the effect of their transmissions on the Wi-Fi system, especially concerning Wi-Fi & Wi-Fi coexistence still needs further investigation. Similarly, MulteFire devices also get interference from LTE-U (unlicensed LTE systems) and LAA (License Assisted Access) systems due to similar channel access parameters. Therefore, the performance of MulteFire devices needs further evaluation, especially in the presence of unlicensed LTE technologies [39].

#### 9.3.4.

The back-off mechanism in LBT (listen-before-talk) has a significant impact on the balanced sharing of the spectrum between LTE and Wi-Fi. Therefore, more research is required for optimal LBT schemes in the presence of unlicensed LTE devices [39, 40]].

### 9.4. INTERFERENCE FROM ADJACENT BANDS

V2X RAT technologies are also affected by adjacent bands. In the US, wireless local area networks use the lower side of the 5.9 GHz band. The Federal Communications Commission (FCC) in the US has also proposed to use unlicensed Wi-Fi operations in the 6 GHz band, i.e., the upper side of the 5.9 GHz band. In such scenarios, if a Wi-Fi device is using a nearby channel of a V2X receiver, the noise floor may be elevated, which will reduce the overall performance as the separation between Wi-Fi & ITS channels is less [39, 41].

### 9.5. COEXISTENCE OF LTE & NR-V2X

NR may coexist with LTE without any backward compatibility due to the use of multiple numerologies. Therefore, designing an efficient coexistence approach is very important. However, studies suggest that the two technologies can coexist by using frequency division multiplexing (FDM) and/or time-division multiplexing (TDM) in separate channels [2, 12].

#### 9.5.1. Coexistence issues while using FDM

In this mechanism, transmissions may overlap in time while using two different radio access technologies. Similarly, if two different radios are used, and if the frequency channels are not sufficiently apart, interference may occur. Furthermore, if the same band (5.9 GHz band) is used, then the overall power radiated by automobiles may be constrained due to defined vehicle regulations, which may also split the power across the two terminals affecting the QoS [2, 12].

#### 9.5.2. Coexistence issues while using TDM

The transmissions occur at different channels and different timings in TDM, however, latency is still an issue for critical messages as the interference of NR may be off when a latency-sensitive message is created. Similarly, time synchronization between LTE & NR is another issue while using TDM. Furthermore, if LTE & NR channels are not sufficiently apart and NR transmits in this case, then sensing cannot be done by LTE due to a half-duplex problem, affecting the LTE sensing-based resource reservation algorithm [2, 12].

### 9.6. COEXISTENCE ISSUES OF DIFFERENT COMMUNICATION TYPES & PERIODICITIES

QoS requirements may be different for different messages, i.e., broadcast, groupcast, unicast, etc., even transmitted by the same user equipment (UE) in NR. Furthermore, these messages may be periodic or aperiodic. Periodic messages can use LTE *sidelink* mode 4 resource reservation algorithms for out-of-coverage situations, while aperiodic unicast may use different transmission approaches creating different issues. One approach is to solve this issue by using a pre-emption mechanism [2, 12, 40].

### 9.7. COEXISTENCE ISSUES OF DSCR & CELLULAR NETWORKING

Many issues need to be solved before DSRC-cellular coexistence can be achieved efficiently. These issues generally arise while deploying dynamic vehicular topology which uses small cell deployment for the next-generation cellular networks because of the requirements of effective network selection techniques.

### 9.8. COEXISTENCE ISSUES OF HETEROGENEOUS WIRELESS SYSTEMS AT 5 GHZ BANDS

Accurate design is required to efficiently detect the signals in the 5.35-5.47 GHz band Wi-Fi access points (APs). Similarly, hidden node problems in the 5.25-5.35 GHz & 5.47-5.725 GHz ranges (due to dynamic frequency selection, and implementation only at AP), and 5.35-5.47 GHz range (due to non-collocated transceivers) are still an issue [19, 39, 43].

### 9.9. OTHER ISSUES

Safe mechanisms are required to develop for the security of every user in any V2X standard when it coexists with Wi-Fi systems.

The next section presents different other miscellaneous issues/challenges.

## 10.MISCELLANEOUS ISSUES & CHALLENGES

### 10.1. MILLIMETER-WAVE COMMUNICATIONS AND BEAMFORMING

Millimeter-wave (mmWave) provides high throughput at 30-300 GHz band for transmission and can also

be reused with less interference. NR & 802.11bd want to use mmWave in the 60 GHz range to accommodate more users. Moreover, multiple antennas can also be used due to the small antenna size with narrowly focused beams (beamforming) to overcome many other challenges, i.e., increasing signal strength and effective range, etc. However, mmWaves are highly attenuated and can only be used for short-range, i.e., 1km. Therefore, multiple hops may be required, which may increase transmission delays. Short wavelength is also sensitive to weather conditions and blocking objects. Moreover, fast-moving communicating nodes also make it difficult to use beamforming in V2X applications [2, 12, 16].

### 10.2. BACKWARD COMPATIBILITY WITH NEW STANDARDS

New standards should be backward compatible with previous standards, and protocols should be developed to enable seamless interoperability between new and previous standards. If not, there will be numerous vehicles of different standards and interoperability will be a challenge [2].

### 10.3. AUTONOMOUS/FOG-BASED RESOURCE ALLOCATION

Resource allocation, i.e., time slots in 802.11bd & resource blocks in LTE, etc., is very critical, particularly, when vehicle applications will increase in the future. For efficient communication, a robust autonomous resource allocation scheme (e.g., SB-SPS) or fog RSUs (roadside units) will be required in the future [2].

### 10.4. MULTI-VENDOR APPLICATION SUPPORT (MVAS)

Multiple vendors will provide V2X communications inside a vehicle for different applications. Therefore, multi-vendor application support (MVAS) is a key requirement for V2X. Efficient designing of layouts, software-defined networking (SDN), network function virtualization (NFV), etc., are required for MVAS.

### 10.5. AUTONOMOUS ALGORITHM SAFETY (AAS)

Vulnerability is another source of cyber attacks, especially at level 5 (fully autonomous). Therefore, features such as channel security, session management, camouflage detections, risk mitigation, etc., need to be efficiently provided by AAS [2].

### 10.6. NETWORK CONTROL & SAFETY (NCS)

The tradeoff between network control and safety has a substantial effect on the accomplishment and security of the network for V2X, i.e., attaining MVAS and AAS, as NCS takes care of all security-related issues. Similarly, finding anomalies and avoiding zero-day vulnerabilities are other issues that need to be efficiently analyzed.

### 10.7. ROGUE DEVICES

Rogue devices **(**which can disable dynamic frequency selection or interrupt functions in the presence of other systems**)** need to be detected, identified, and adjudicated. Moreover, all of these operations should be automatic and less expensive so that they can be easily implemented [39].

### 10.8. HALF DUPLEXING ISSUE

4G and 5G devices cannot perform the sensing procedure while the device is transmitting due to the constraint of half duplexing. Similarly, the transmissions sent by neighboring vehicles during the same TTI (transmission time interval) cannot be received, even by using different radio base stations [27].

### 10.9. ORTHOGONALITY ISSUE

The orthogonality issue exists in the frequency domain. Therefore, interference due to in-band emission (IBE) is always present for messages sent at the same TTI, even when nominally orthogonal resources are used [27].

### 10.10. HANDOVER ISSUES IN LTE & 5GNR

Due to the higher range provided by a large number of available base stations, cellular network technology can be used for V2X continuous network operations in all scenarios with a minimum number of handovers. However, handover management may be a problem with the next-generation cellular technology due to the smaller BS coverage range, especially when network capacity needs to be increased [15].

### 10.11. NETWORK CHOICE

A little bit of an increase in performance or quality of experience may not prompt a user to change his current network provider to another technology. For example, a user may prefer to remain connected to a BS (which provides a whole highway coverage range) rather than to connect scattered RSUs (which provide non-overlapping coverage ranges along the highway) for slightly better QoS.

### 10.12. FAIRNESS ISSUES

Fairness issues may also arise in a scenario for vehicles that do not use a dual interface for DSRC & cellular network access, especially for network selection and handover decisions according to the vehicle's preferences. Similarly, for delay-sensitive V2X applications, the computational complexity of the algorithms will be different for different networks. Therefore, it will be safe and secure if the same technology is used by a large

number of vehicles, especially for safety broadcast messages which must be received within the defined time limit.

### 10.13. SECURITY ISSUES REGARDING UNICAST & MULTICAST

The unicast and groupcast modes are enhanced for NR-based PC5. Unicast mode over PC5 uses control plane signaling over two layers (V2X layer and AS layer). Similarly, for security and privacy protection, the groupcast is used by the application layer and UE configuration provisioning for vehicle communications. However, several other issues such as security of eV2X unicast messages over PC5, security of identifier conversion in group communication, multicast security setup, etc., need further research [25].

Based on the previous discussion, the next section presents recommendations.

## 11. RECOMMENDATIONS

### 11.1.

Some standards**,** e.g., LTE., already have a large deployed infrastructure as compared to other standards, i.e., DSRC, 802.11bd, etc. However, the performance of these standards on large-scale operations is not proven. If LTE/5G proves better and cheaper in the future than other standards on a large scale, then holding off until more information is available about other standards so that the industry can make a decision seems to be a practical (or at least risk-averse) strategy. On the other hand, standardizing DSRC/802.11bd without properly analyzing LTE/5G can be a mistake. Moreover, if LTE/5G does not prove to be good, then mandating DRSC/802.11bd or any other standard will not be too late. Of course, some costs have to pay due to the time factor, however, it will be less costly than making the opposite mistake [16].

### 11.2.

C-ITS demands backward compatibility, interoperability, and advanced design for standardizing ITS. Therefore, a hybrid communication approach will be more efficient for the security and safety of the V2X. Therefore, such protocols should be developed that can provide seamless communications with high throughput and low latency in a heterogeneous environment while using any standard, i.e., DSRC, LTE, NR, etc. Another option is to use only one standard (either DSRC or LTE) in an AV for a short period [2, 12].

### 11.3. BACKUP

There should always be a backup mechanism in case of vehicle disconnections from the central controller, which should be achieved by better collaboration among different service providers.

### 11.4.

802.11bd and 5G NR are the two potential future standards for vehicle communications. However, spectrum management issues and operational challenges must be pro-actively solved for the efficient co-existence of these two standards.

### 11.5.

Spectrum management issues need more research to attain seamless interoperability and coexistence among different V2X technologies for secure and efficient operations.

### 11.6.

Security and safety are the critical aspects of concern when considering the widespread adoption of AVs by the community. Therefore, safe, secure, and reliable algorithms should be developed for efficient V2X communication.

### 11.7.

All of the above management issues/challenges must be addressed before standardizing any technology to provide secure V2X communications for vehicular technology.

## 12. CONCLUSION

An efficient and reliable communication standard is required for the communication of AVs with all other entities and their operations. Existing work generally discusses the features and certain performance comparisons of the existing vehicular communication standards without comprehensively describing the drawbacks of these standards. Existing literature also does not provide a comparison between these standards and generally discusses a comparison between two standards only. However, this work comprehensively describes different issues/challenges and comparisons between these standards along with their salient features.

The first contribution of the work is the comprehensive description of the different issues/challenges of these standards, along with their salient features. The second contribution of the work is the presentation of the comparisons among different standards. Another contribution is the detailed description of the spectrum management issues of these technologies. The work also comprehensively presents several miscellaneous challenges to these technologies. In the end, the paper also proposes recommendations that must be taken into account for an efficient V2X communication standard.

The work concludes that theoretically LTE is better than DSRC and does not require large infrastructure investments as compared to DSRC, however, it is still not proven in a large-scale operation. The work also describes that 802.11p, LTE, and ITS-G5 standards are not

able to meet the requirements for a reliable and efficient vehicular communication standard, i.e., ultra-high reliability, ultra-low latency, etc. However, two new standards, i.e., 802.11bd and 5G NR-V2X, are the two potential vehicle communication standards as they can meet the requirement of V2X communication, however, issues such as backward compatibility, interoperability, and co-existence with other standards need further evaluation. The work describes that generally, 5G NR performs better than 802.11bd in most of the technical parameters. However, 5G NR and 802.11bd are still in the developing stages. The work also describes that solving spectrum management issues is very critical, especially in the case of co-existence with Wi-Fi and interoperability issues, etc. Similarly, many other challenges such as compatibility, security, highly dynamic vehicular environment, etc., are very important before standardizing any technology.

The work emphasizes that standardizing any one technology without properly analyzing comparative technologies can be a mistake. Delaying is not a big issue when done to investigate an efficient standard. Similarly, standardizing two technologies at the same time in one geographical area can also be very challenging, especially in terms of interoperability, and spectrum management issues. Additionally, implementation cost, road maintenance issues, compatibility, performance in real large-scale environments, etc., must also be evaluated before standardizing any technology. AVs cannot be successful until a secure, safe, and reliable vehicle communication technology is available. Therefore, all the issues related to a standard must be solved before implementation; otherwise the maximum benefits of V2X communication cannot be obtained.

## 13. REFERENCES:


[1] F. Arena, G. Pau, "An Overview of Vehicular Communications", Future Internet, Vol. 11, No. 2, 2019, pp. 27-54.

[2] S. Zeadally, M. Javed, E. Hamida, "Vehicular Communications for ITS: Standardization and Challenges", IEEE Communications Standards Magazine, Vol. 4, No. 1, 2020, pp. 11-17.

[3] M. Slovick "DSRC vs. C-V2X: Looking to Impress the Regulators", Endeavor business Media, Canada, Electronic design, Technical Report, 2017.

[4] W. Anwar, A. Trabi, N. Franchi, G. Fettweis, "On the Reliability of NR-V2X and IEEE 802.11bd", Proceedings of the IEEE 30th Annual International Symposium on Personal, Indoor and Mobile Radio Communications, Istanbul, Turkey, 8-11 September 2019, pp. 1-7.

[5] A. Festag, "Standards for vehicular communication-from IEEE 802.11p to 5G", E & I Elektrotechnik und Informationstechnik, Vol. 132, No. 7, 2015, pp. 409–416.

[6] B. Howel, "Who will determine the communications standards for the future autonomous vehicles", https://www.aei.org/technology-and-innovation/who-will-determine-the-communications-standards-for-the-future-of-autonomous-vehicles/ (accessed:2020)

[7] A. Turley, K. Moerman, A. Filippi, V. Martinez, "C-ITS: Three observations on LTE-V2X and ETSI ITS-G5-A comparison", NXP semiconductors, Arizona, USA, Technical Report CITSCOMPWP REV 0, 2018.

[8] "Cellular V2X Communications Towards 5G", 5G Americas White Paper, USA, Technical Report, 2018

[9] Z. Xu, X. Li, X. Zhao, M. Zhang, Z. Wang," DSRC versus 4G-LTE for Connected Vehicle Applications: A Study on Field Experiments of Vehicular Communication Performance", Journal of Advanced Transportation, Vol. 2017, No. 2, 2017, pp. 273-283.

[10] V. Mannoni, V. Berg, S. Sesia, E. Perraud, "A Comparison of the V2X Communication Systems: ITS-G5 and C-V2X", Proceedings of the IEEE 89th Vehicular Technology Conference, Kuala Lumpur, Malaysia, 28 April - 1 May 2019, pp. 1-5.

[11] D. Eckhoff, N. Sofra, R. German, "A performance study of cooperative awareness in ETSI ITS G5 and IEEE WAVE", Proceedings of the 10th Annual Conference on Wireless On-demand Network Systems and Services, Banff, Alberta, 18-20 March 2013, pp. 196-200.

[12] G. Naik, J. Park, "IEEE 802.11bd & 5G NR V2X: Evolution of Radio Access Technologies for V2X Communications", IEEE Access, Vol. 7, No. 3, 2019, pp. 169-184.

[13] T. Shimizu, H. Lu, J. Kenney, S. Nakamura, "Comparison of DSRC and LTE-V2X PC5 Mode 4 Performance in High Vehicle Density Scenarios", Proceedings of the ITS World Congress, Singapore, 21-25 October 2019, pp.1-10.

[14] M. Karoui, A. Freitas, G. Chalhoub, "Performance comparison between LTE-V2X and ITS-G5 under

realistic urban scenarios", Proceedings of the IEEE 91st Vehicular Technology Conference, Antwerp, Belgium, 25-28 May 2020, pp. 1-7.

[15] K. Abboud, H. Omar, W. Zhuang, "Interworking of DSRC and Cellular Network Technologies for V2X Communications: A Survey", IEEE Transactions on vehicular technology, Vol. 65, No. 12, 2016, pp. 485-497.

[16] A. Lautenbach, N. Nowdehi, T. Olovsson, R. Zaragatzky, "A Preliminary Security Assessment of 5G V2X", Proceedings of the IEEE 89th Vehicular Technology Conference, Kuala Lumpur, Malaysia, 28 April-1 May 2019, pp. 1-7.

[17] G. Karagiannis, O. Altintas, E. Ekici, G. Heijenk, B. Jarupan, K. Lin, T. Weil, "Vehicular Networking: A Survey and Tutorial on Requirements, Architectures, Challenges, Standards and Solutions", IEEE Communications survey & Tutorials, Vol. 13, No. 4, 2011, pp. 155-172.

[18] A. Filippi, K. Moerman, G. Daalderop, P. D. Alexander, F. Schober, W. Pfliegl, "Why 802.11p beats LTE and 5G for V2x", A White paper by NXP Semiconductors, Cohda Wireless, and Siemens, Germany, 2016.

[19] "Cellular-V2X Technology Overview", Qualcomm Technologies, Inc. San Diego, CA, U.S.A, Technical Report 80-PE732-63 Rev. B, 2019.

[20] M. Flament, "Automotive advanced use cases using NR-V2X", 5G Automotive Association, Berlin, Germany, Technical report, 2019.

[21] A. Bazzi, G. Cecchini, M. Menarini, B. M. Masini, A. Zanella, "Survey and Perspectives of Vehicular Wi-Fi versus Sidelink Cellular-V2X in the 5G Era", Future Internet, Vol. 11, No. 6, 2019, pp. 463-483.

[22] C. Campolo, A. Molinaro," Multichannel Communications in Vehicular Ad Hoc Networks: A Survey", IEEE Communications Magazine, Vol. 5, No. 4, 2019, pp. 973-987.

[23] "V2X Technology Functional and Performance Benchmark Testing Key Findings", 5GAA Automotive Association, USA, Technical Report, P-190033, 2018.

[24] W. Anwar, N. Franchi, G. Fettweis, "Physical Layer Evaluation of V2X Communications Technologies: 5G NR-V2X, LTE-V2X, IEEE 802.11bd, and IEEE 802.11p", Proceedings of the IEEE 90th Vehicular Technology Conference, Honolulu, HI, USA, 22-25 September 2019, pp. 1-7.

[25] K. Ganesan, D. Karamp, A. Kunz, "5G V2X Architecture and Radio Aspects", Proceedings of the IEEE Conference on Standards for Communications & Networking, Granada, Spain, 28-30 October 2019, pp. 1-6.

[26] X. Wang, S. Mao, M. X. Gong, "An overview of 3GPP cellular vehicle to- everything standards," GetMobile, Mobile Computing Communication, Vol. 21, No. 3, 2017, pp. 19-25.

[27] C. Campolo, A. Molinaro, F. Romeo, A. Bazzi, A. Berthet, "5G NR V2X: On the Impact of a Flexible Numerology on the Autonomous Sidelink Mode", Proceedings of the IEEE 2nd 5G World Forum, Dresden, Germany, 30 September - 2 October 2019, pp. 102-107.

[28] V. Sharma, I. You, N. Guizani, "Security of 5G-V2X: Technologies, Standardization and Research Directions", IEEE Network, Vol. 5, No. 34, 2020, pp. 306-314.

[29] M. Condoluci, L. Gallo, L. Mussot, A. Kousaridas, P. Spapis, M. Mahlouji, T. Mahmoodi, "5G V2X System-Level Architecture of 5GCAR Project", Future Internet, Vol. 6, No. 2, 2019, pp. 155-173.

[30] K. Serizawa, M. Mikami, K. Moto, H. Yoshino," Field Trial Activities on 5G NR V2V Direct Communication Towards Application to Truck Platooning", Proceedings of the IEEE 90th Vehicular Technology Conference, Honolulu, HI, USA, 22-25 September 2019, pp.1-10.

[31] L. Hobert, A. Festag, I. Llatser, L. Altomare, F. Visintainer, A. Kovacs," Enhancements of V2X Communication in Support of Cooperative Autonomous Driving", IEEE Communications Magazine, Vol. 3, No. 1, 2015, pp. 525-625.

[32] F. Arena, G. Pau, A. Severino, "A Review on IEEE 802.11p for Intelligent Transportation Systems", Journal of Sensor and Actuator Networks, Vol. 9, No. 2, 2020, pp. 122-144.

[33] X. Wu, S. Subramanian, R. Guha, R.White, K. Lu, A. Bucceri, T. Zhang, "Vehicular Communications Us-

ing DSRC: Challenges, Enhancements, and Evolution", IEEE Journal on selected areas in communications/supplement, Vol. 31, No. 9, 2013, pp. 433-447.

[34] J. Kenney, "Dedicated Short-Range Communications (DSRC) Standards in the United States", Proceedings of the IEEE, Vol. 99, No. 7, 2011, pp. 657-672.

[35] J. Hu, S. Chen, L. Zhao, Y. Li, J. Fang, B. Li, Y. Shi," Link level performance comparison between LTE V2X and DSRC", Journal of communications and information networks, Vol. 2, No. 2, 2017, pp. 101-112.

[36] V. Khairnar, K. Kotecha, "Performance of Vehicle-to-Vehicle Communication using IEEE 802.11p in Vehicular Ad-hoc Network Environment", International Journal of Network Security & Its Applications, Vol.5, No.2, 2013, pp. 223-238.

[37] D. Jiang, L. Delgrossi, "IEEE 802.11p: Towards an International Standard for Wireless Access in Vehicular Environments", Proceedings of the IEEE Vehicular Technology Conference, Marina Bay, Singapore, 11-14 May 2008, pp.1-10.

[38] R. Sattiraju, D. Wang, A. Weinand, H. Schotten, 'Link Level Performance Comparison of C-V2X and ITS-G5 for Vehicular Channel Models", Proceedings of the IEEE 91st Vehicular Technology Conference, Antwerp, Belgium, 25-28 May 2020, pp.1-8

[39] G. Naik, J. Liu, J. Park, "Coexistence of Wireless Technologies in the 5 GHz Bands: A Survey of Existing Solutions and a Roadmap for Future Research", IEEE Communications Surveys & Tutorials, Vol. 20, No. 3, 2018, pp. 1777-1798.

[40] Chen B, Gao Y, Zhang J, "Coexistence of LTE-LAA and Wi-Fi on 5 GHz with corresponding deployment scenarios: A survey", IEEE Communications. Surveys Tutorials, Vol. 19, No. 1, 2017, pp. 545-557.

[41] J. Lansford, B. Kenney, P. Ecclesine, "Coexistence of unlicensed devices with DSRC systems in the 5.9 GHz ITS band", Proceedings of the IEEE proceeding on Vehicular Network Conference, Boston, MA, USA, 25-28 October 2013, pp. 9–16.

[42] H. B. Hafaiedh, I. El Korbi, L. A. Saidane, A. Kobbane,"LTE-U and WiFi coexistence in the 5 GHz unlicensed spectrum: A survey", Proceedings of the **International Conference on Performance Evaluation and Modeling in Wired and Wireless Networks,** Paris, France, 28-30 November 2017, pp. 1-8.

[43] M. Kees, J. Vincent, T. Andrew, "How re-allocating the 5.9 GHz band could affect road safety, DSRC, C-V2X and implications of the proposed spectrum changes", Document no. V2XFCCWP REV 0, NXP USA, Inc. 2020

# Design and Development of High Torque, Compact and Energy Saver IPMSM Motor for Hydraulic Applications

Case Study

**Rupalee S. Ambekar**
Bharati Vidyapeeth (Deemed to be University) College of Engineering, Pune
Faculty of Engineering, Department of Electrical Engineering
Pune-Satara Road, Pune-411043, INDIA
pawar.roopali@gmail.com

***Abstract*** *– The Permanent Magnet Synchronous Motor (PMSM) is widely used for various applications. It is the highly efficient motor as there are no field copper losses. The electrical energy is supplied to the motor through generator and the generator size depends upon the motor output. The efficiency of motor is the factor which will affect the size of the generator. This paper contributes the research work for the design of 35 kW, 440 V, 1000 rpm, 8 pole Synchronous Motor with Interior mounted Permanent Magnets (IPMSM) for the Hydraulic application. The designed IPMSM motor has efficiency of 98 % and can be used in place of 3-phase Induction Motor for the hydraulic application. The simulation is done in Ansys RMxprt fulfilling the required characteristics of Hydraulic application.*

***Keywords****: ansys software, energy saver, generator size, IPMSM, optimum design, RMxprt, skewing*

## 1. INTRODUCTION

An effective and efficient design methodology of Permanent Magnet Synchronous Motor (PMSM) is possible by dividing the rotor design into Induction Motor (IM) and PMSM design. The proposed design approach can then be validated by comparing the calculated results with the simulation results [1]. The design parameters of PMSM for required applications are core diameter, core length, number of poles & conductors, types of slots and materials [2]. The demagnetizing effect on limiting the ampere conductors per meter weakens the flux and use of Permanent Magnets (PM) makes the PMSM costlier. But, PMSM is widely used due the high efficiency and reliability [3]. Short end connections in Interior Permanent Magnet (IPM) machines makes its construction simple and also improves the performance [4].The starting torque and efficiency are the important factors for the optimum design of rotor [5]and in this study IPMSM machine is analyzed for different speed ranges and observed that the efficiency, torque and torque angle varies with the speed. Change in rotor geometry improves the efficiency of Line Start Permanent Magnet Motor (LSPMM) and increases the air gap flux [6, 7]. The performance and the main dimensions of the machine depend upon the type of magnetic material [8]. The PMSM performance can be improved by major considerations of stator and rotor structure and the development would avoid the importation [9]. The motor performance and the geometry can also be improved by using different stator configurations, magnet shape and rotor structure [10, 11]. The proposed IPMSM is analyzed by changing the stator outside diameter from 400 mm to 420 mm, selecting bridge type rotor construction. The motor performance and geometry are optimized with changed no-load and full load parameters. The distribution of magnetic field in PM motor scan be estimated by analytical approach [12]. Differential evolution algorithm with stator and rotor performance and geometric parameters issued to develop the software which will optimize the machine design using Finite Element Analysis [13]. Magnetization and the air gap between the magnets and the inter-poles influence the magnetic flux density and the counter emf [14]. The estimated values of EMF, Inductance and magnetic circuit by conventional calculations are validated with FEM analysis and experimental results [15]. It is found that the design of the Permanent Magnet Synchronous Generator can be optimized and verified by FEM analysis. The performance of the permanent magnet machines can be improved with different rotor geometry and can also be cost effective with ferrite magnet [16]. On comparison with different rotor geometry having same magnet volume, the rotor geometry with radial and circumferential magnetized magnet gives high flux density in air gap [17]. The air gap flux, flux linkages and hence the back emf may deviates from the analytical results due to the inaccuracies in manufacturing [18].

**Table 1.** Proposed Solutions as per Literature Review

| Sr. No. | Analysis Type | Advantages | Disadvantages |
|---|---|---|---|
| 1 | Limiting the ampere conductors per meter | It is widely used due the high efficiency and reliability [3] | Weakens the flux and use of Permanent Magnets (PM) makes the PMSM costlier [3] |
| 2 | Short end connections in Interior Permanent Magnet (IPM) machines | makes its construction simple and also improves the performance [4] | The air gap flux, flux linkages and hence the back emf may deviates from the analytical results due to the inaccuracies in manufacturing [4] |
| 3 | Change in rotor geometry | improves the efficiency of Line Start Permanent Magnet Motor (LSPMM) and increases the air gap flux [6, 7] | The air gap flux, flux linkages and hence the back emf may deviates from the analytical results due to the inaccuracies in manufacturing [18] |
| 4 | type of magnetic material | It affects the performance and the main dimensions of the machines [8] | The air gap flux, flux linkages and hence the back emf may deviates from the analytical results due to the inaccuracies in manufacturing |
| 5 | Use of different stator configurations, magnet shape and rotor structure | The motor performance and the geometry can be improved [10, 11] | The air gap flux, flux linkages and hence the back emf may deviates from the analytical results due to the inaccuracies in manufacturing |
| 6 | Magnetization and the air gap between the magnets and the inter-poles | influences the magnetic flux density and the counter emf [14] | The air gap flux, flux linkages and hence the back emf may deviates from the analytical results due to the inaccuracies in manufacturing |
| 7 | Different rotor geometry | Improves the performance of the permanent magnet machines and can also be cost effective with ferrite magnet [16] | The air gap flux, flux linkages and hence the back emf may deviates from the analytical results due to the inaccuracies in manufacturing |

The objective of this work is to design and develop the high torque, compact and energy saver Interior Permanent Magnet Synchronous Motor(IPMSM)for hydraulic application. To analyze and compare the results obtained by RMxprt with the calculated results. The design is then validated with the features of the machine and the requirements of the application.

The fundamentals of rotating machines, design calculations of AC and DC machines and the design software Ansys (RMxprt) are the basic requirements of this study.

The interior permanent magnet synchronous motor is recommended for Hydraulic application based on its advantages. It is proposed in place of the existing induction motor of 40 kW, 415 V, 69 A with a power factor of 0.86 and full load efficiency of 94 %. The required full load torque for the 1500 rpm speed and 40 kW power rating is 255 Nm and the input to the motor is the 100 kVA generator output. The induction motor frame size is 225 M (Medium) with a stator Outer Diameter (OD) of 400 mm. The proposed IPMSM is made compact by reducing the stack length, using the Interior mounted permanent magnets with the same stator outer diameter (OD). The proposed machine is analyzed for different speed ranges from 500 rpm to 2500 rpm as per the operating characteristics of axial hydraulic pump. It is analyzed for different voltages as 220 V, 440 V, 690 V, for different stator OD as 410 mm, 420 mm and also analyzed with different power rating as 30 kW, 32.5kW, 35kW, 37.5kW and 40kW. Finally, the optimum design is achieved which is compact and energy saver as it will reduce the generator size.

## 2. STATEMENT OF THE EXISTING SYSTEM

The existing motor is 40 kW, 415 V, 50 Hz, 69 Amp., 3-phase Induction motor with power factor of 0.86 and full load efficiency of 94 %. The full load torque is 255 Nm as per the given speed and power rating. The generator of 100 kVA is used to give supply to the motor.

As per the operating characteristics of Pump Model 4046 the power consumption at 1450 rpm and at maximum pressure and displacement is 32 kW, Maximum torque on the shaft is 350 Nm, Maximum permissible load on drive shaft is 1500 N and speed rating is 500 to 2500 rpm. For safety, power rating should be taken as 35 kW and generator size required is as per Table 2 for different power factor of generator by calculations.

Pump Model 4046 is a variable displacement axial piston pump which can operate at high pressure with low noise level and suitable for hydraulic oils having lubricating characteristics. The length of the stroke of the pumping piston affects the actual displacement and the position of the swashing plate determines the length of the stroke.

The pump supply voltage is 220 V AC with a tolerance of ± 10 % and frequency is 50 Hz as per the insulation class 'H' and connector protection degree of IP 65.

**Table 2.** Generator kVA for 35 kW motor output with different Power Factor (PF)

| Motor Output. Power (kW) | Motor Efficiency | Motor Input Pin | Generator Input | Generator PF | Generator kVA |
|---|---|---|---|---|---|
| 35 | 0.98 | 35.71 | 39.572 | 0.8 | 49.465 |
| | | | | 0.75 | 52.763 |
| | | | | 0.7 | 56.532 |
| | | | | 0.65 | 60.880 |
| | | | | 0.6 | 65.954 |

The 40 kW IPMSM can also run with the 62.5 kVA generator if power factor of the generator is good. The generator size required is as per Table 3 with different power factor of generator by calculations.

**Table 3.** Generator KVA for 40 kW motor output with different Power Factor (PF)

| Motor Output. Power (kW) | Motor Efficiency | Motor Input Pin | Generator Input | Generator PF | Generator kVA |
|---|---|---|---|---|---|
| 40 | 0.98 | 40.816 | 45.225 | 0.8 | 56.532 |
| | | | | 0.75 | 60.301 |
| | | | | 0.7 | 64.608 |
| | | | | 0.65 | 69.578 |
| | | | | 0.6 | 75.376 |

Motor Efficiency = 98 % and Assumed: Drive Efficiency = 95 % Generator Efficiency = 95 %

The best suitable motor for the same application of lifting is PMSM which have the advantages over Induction motor as of higher efficiency, higher power density, higher torque density and better dynamic performance.

## 3. DESIGN ANALYSIS

The design analysis is verified with different parameters as follows:

1) As per the pump details, the speed range is 500 rpm to 2500 rpm, so the same machine is analyzed for different speed ranges and observed that there are changes in frequency, frictional losses, no load line current, no load input power and all full load parameters such as line voltage increases, line current decreases, thermal and electric loading decreases, frictional and iron losses increases, copper losses decreases which decreases the total loss. Efficiency increases up to speed of 1500 rpm and afterwards decreases with further increase in speed. Torque and torque angle decrease with increase in speed as shown in Figure 1.

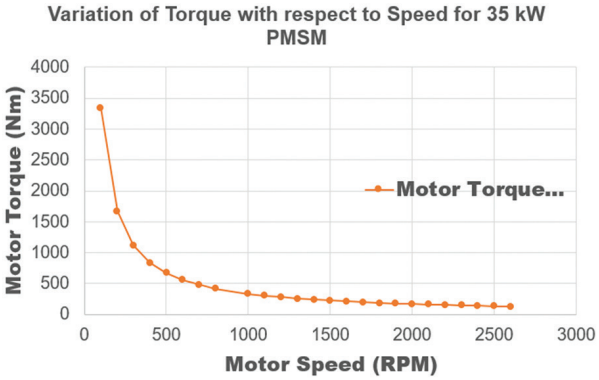


**Fig. 1.** Variation of Torque with speed

2) If the power rating is changed from 35 kW to 55 kW then there is change in torque as shown in Figure 2 for 1500 rpm IPMSM and Figure 3 for the speed range of 500 rpm to 2500 rpm.

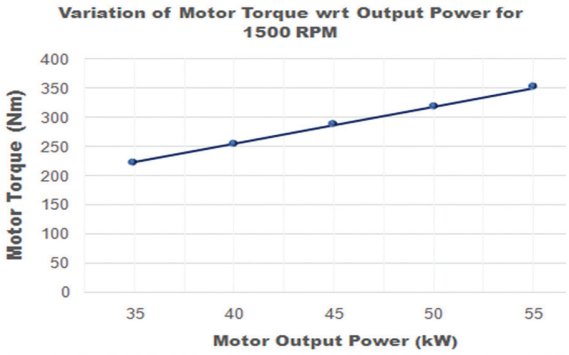


**Fig. 2.** Variation of torque w. r. t. output power for 1500rpm IPMSM

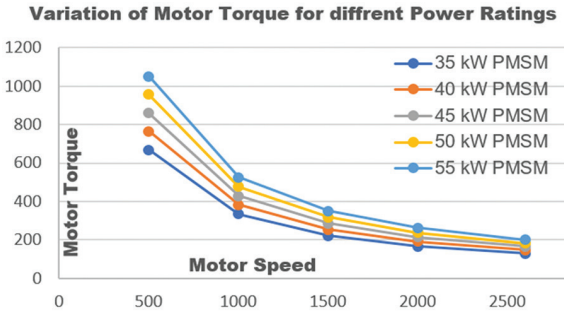


**Fig. 3.** Variation of motor torque for different power ratings

3) The same machine with a power rating ranges from 35 kW to 55 kW is analyzed for different voltage ratings as 690 V, 440 V, 220 V and observed the changes in i) no. of conductors per slot: it is doubled ii) no. of wires per conductors: reduced by half with increase in voltage iii) Steady state parameters: reactive inductances reduced with the increase in voltage, armature phase resistance increases with increase in voltage. iv) No load line current, no load input power. v) Full load parameters. It is presented in Figure 4.

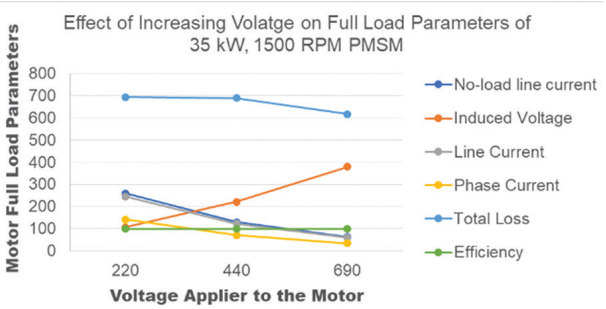


**Fig.4.** Effect of Stator voltage on full load parameters of 35 kW, 1500 rpm IPMSM

To attain the requirement of 350 Nm torque and speed of 1500 rpm, the power rating is 55 kW and power rating can be reduced by reducing the speed.

4) The effect of stator outside diameter is also analyzed by changing the diameter from 400 mm to 420 mm. The no-load and full load parameters changed with large deviation from 400 mm to 410 mm but from 410 mm to 420 mm the slight deviation is observed as shown in Figure 5.

The best suitable motor for the same application of lifting is IPMSM which have the advantages over Induction motor as of higher efficiency, higher power density, higher torque density and better dynamic performance.

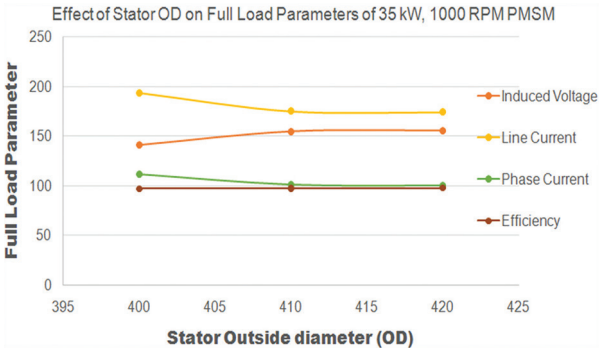


**Fig. 5.** Effect of Stator OD on full load parameters of 35 kW, 1000 rpm IPMSM

## 4. FINANCIAL IMPLICATIONS

The proposed IPMSM motor with better performance, high power per unit volume will make the generator compact and hence there would be saving in fuel consumption and electricity bill.

**Justification:**
For Diesel Generator:
Energy and fuel consumption Calculations

Electrical Energy and oil fuel cost associated to 67 kVA generator for existing 3-phase Induction Motor is as follows:

For 67 kVA generator the generator active power with power factor of 0.8 is 54 kW. The total energy consumption, total fuel consumption and electricity bill per month is estimated as shown in Table 4 and 5 respectively for 54 kW& 40 kW generator input.

**Table 4.** Generator Energy Consumption

| Generator input (kW) | Hours/day | Energy Consumption (kWH) | Liter/kWH |
|---|---|---|---|
| 54 | 10 | 540 | 0.4 |
| 40 | 10 | 400 | 0.4 |

If the machine power rating is changed to 35 kW then the energy consumption, total fuel consumption and electricity bill per month for generator input as 40 kW is estimated as shown in Table 4 and 5.

Hence the generator rating is reduced to 50 kVA which reduces the operating cost.

**Table 5.** Total Consumption of fuel and electricity bill

| Total Consumption of fuel (Liter) | Cost of Fuel/ Liter (Rs.) | Electricity Bill/ Day (Rs.) | Electricity Bill/ Month (Rs.) |
|---|---|---|---|
| 216 | 67 | 14, 472/- | 4,34,160/- |
| 160 | 67 | 10,720/- | 3,21,600/- |

## 5. PROPOSED SYSTEM

### 5.1 DESIGN CONSIDERATIONS

#### a) SPECIFICATION OF INTERIOR PERMANENT MAGNET SYNCHRONOUS MOTOR

The Interior Permanent Magnet Synchronous Motor is compact in size, the installation and maintenance of permanent magnet is easy and it improves the system efficiency. The selected machine has the following specification:

| | |
|---|---|
| Type of Operation: | Motor |
| Type of Mechanical Load: | Constant Power |
| Output Power(kW): | 35 |
| Applied Voltage (V): | 440 |
| Number of Poles, p: | 8 |
| Speed (RPM): | 1000 |
| Frequency (Hz): | 66.67 |
| Loss due to Friction (W): | 18 |
| Rotor location: | Inner |
| In service Temperature (°C): | 75 |

The total loss and no-load line current of the proposed IPMSM get reduced with the increase in voltage. Hence the 440 V rating is selected and optimized design is achieved with the 440 V voltage rating. The performance of the motor is improved and cost of the motor is therefore reduced.

The proposed design specification of the motor then helps to decide the stator and rotor main dimensions.

#### b) STATOR CONSTRUCTION

Design calculations are carried out with given rating of the motor and some assumptions. The following are the stator core dimensions and type of the core material.

| | |
|---|---|
| Stator Slots Number: | 48 |
| Stator OD (mm): | 400 |
| Stator ID (mm): | 270 |
| Stator Core Length (mm): | 90 |
| Stator Core Stacking Factor: | 0.95 |
| Steel Type: | M19_24G |
| Designed Wedge Thickness (mm): | 5.11966 |
| Parallel Branches: | 1 |
| Conductors per Slot: | 10 |
| Skew Width (Number of Slots): | 2 |

With these stator core data, the following results have been obtained:

| | |
|---|---|
| Top Tooth Width (mm): | 6.59375 |
| Bottom Tooth Width (mm): | 5.83885 |
| Average Coil Pitch: | 6 |
| Number of Wires per Conductor: | 99 |
| Wire Diameter (mm): | 0.724 |
| Stator Slot Fill Factor (%): | 70.3924 |
| Coil Half-Turn Length (mm): | 257.529 |
| Wire Resistivity (ohm.mm^2/m): | 0.0217 |

Figure 6 presents the stator with semi-enclosed slots.

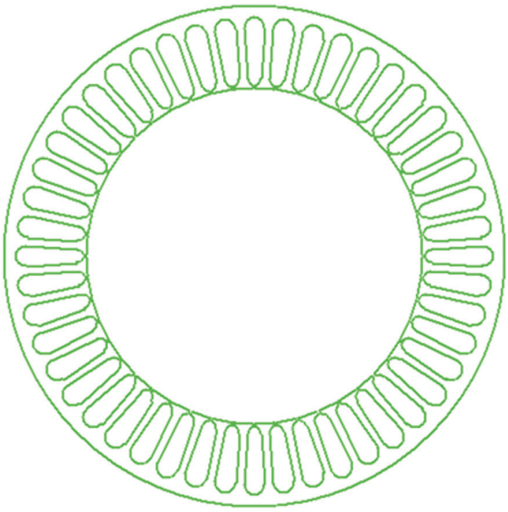

**Fig. 6.** Stator with semi-enclosed slot

**WINDING ARRANGEMENT**

The 3-phase, 2-layer winding can be arranged in 6 slots as below and shown in Figure 7.

| | |
|---|---|
| Angle per slot (elec. degrees): | 30 |
| Phase-A axis (elec. degrees): | 105 |
| First slot center (elec. degrees): | 0 |

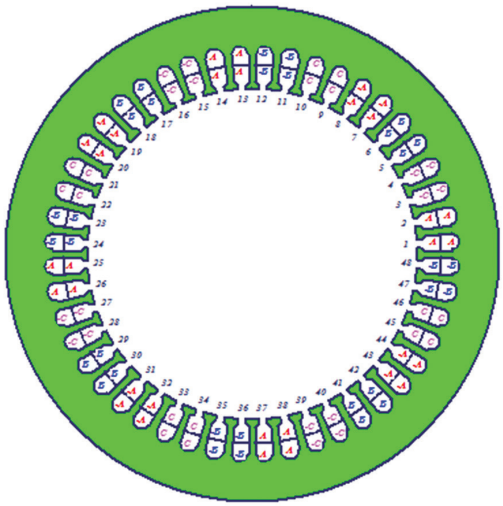

**Fig. 7.** Stator Winding Layout

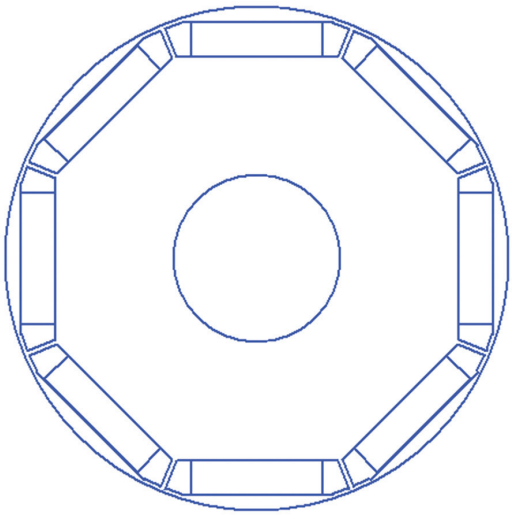

**Fig. 8.** Bridge Type Magnet Rotor

**c) ROTOR CONSTRUCTION**

On the basis of stator core dimensions, it is possible to estimate the rotor core dimensions &to decide the type of rotor magnet structure. Estimated rotor core dimensions and type of core material, magnet material are as follows:

| | |
|---|---|
| Air Gap (mm): | 0.5 |
| ID (mm): | 90 |
| Length (mm): | 90 |
| Iron Core Stacking Factor: | 0.95 |
| Steel Type: | M19_24G |
| Bridge (mm): | 2 |
| Rib (mm): | 3 |
| Pole Embrace (Mechanical): | 0.8 |
| Pole Embrace (Electrical): | 0.748 |
| Max. Magnet Thickness (mm): | 18 |
| Magnet Width (mm): | 70 |
| Magnet Type: | NdFe35 |

**a) MATERIAL CONSUMPTION**

With the stator and rotorcore data, the material consumption is calculated and the results are as follows:

| | |
|---|---|
| Copper Weight of Armature (kg): | 44.83 |
| Weight of Permanent Magnet (kg): | 6.71 |
| Weight of Armature Core Steel (kg): | 20.09 |
| Weight of Rotor Core Steel (kg): | 24.71 |
| Total Net Weight (kg): | 96.35 |
| Consumption of Armature Core Steel (kg): | 68.778 |
| Consumption of Rotor Core Steel (kg): | 37.449 |

The total net weight and size of the motor depends upon the volume of the motor. The volume is estimated by main dimensions of the motor. The main dimensions are stator bore diameter and stator core length.

### b) STEADY STATE PARAMETERS

The steady state parameters have been calculated after optimizing the design. The steady state parameters are d & q axis inductances, leakage inductance and armature phase resistance.

| | |
|---|---|
| Stator Winding Factor: | 0.965926 |
| D-Axis Reactive Inductance Lad | (H):0.00103 |
| Q-Axis Reactive Inductance Laq | (H):0.01383 |
| D-Axis Inductance L1+Lad (H): | 0.002065 |
| Q-Axis Inductance L1+Laq (H): | 0.014898 |
| Armature Leakage Inductance L1 (H): | 0.00103342 |
| Slot Leakage Inductance Ls1 (H): | 0.00048239 |
| End Leakage Inductance Le1 (H): | 0.00015713 |
| Harmonic Leakage Inductance Ld1 (H): | 0.000393896 |
| Zero-Sequence Inductance L0 (H): | 0.00103342 |
| Armature Phase Resistance R1 (H): | 0.0219383 |
| Armature Phase Resistance at $20^0$C (ohm): | 0.0180461 |

### c) NO LOAD DATA

The performance of the motor is based upon the no load line current, no load input power and cogging torque. These no-load parameters are affected by the magnetic flux density and Ampere Turns (ATs).

| | |
|---|---|
| Stator-Teeth Flux Density (Tesla): | 2.04552 |
| Stator-Yoke Flux Density (Tesla): | 2.19373 |
| Rotor-Yoke Flux Density (Tesla): | 0.295285 |
| Air-Gap Flux Density (Tesla): | 0.633033 |
| Magnet Flux Density (Tesla): | 0.775206 |
| Stator-Teeth By-Pass Factor: | 0.0654571 |
| Stator-Yoke By-Pass Factor: | 0.0496894 |
| Rotor-Yoke By-Pass Factor: | 7.79752e-06 |
| Stator-Teeth Ampere Turns (A.T): | 2011.23 |
| Stator-Yoke Ampere Turns (A.T): | 3657.92 |
| Rotor-Yoke Ampere Turns (A.T): | 0.924299 |
| Air-Gap Ampere Turns (A.T): | 263.784 |
| Magnet Ampere Turns (A.T): | -5923.41 |
| Leakage-Flux Factor: | 1.08676 |
| Correction Factor for Magnetic Circuit Length of Stator Yoke: | 0.26853 |
| Correction Factor for Magnetic Circuit Length of Rotor Yoke: | 0.753369 |
| No-Load Line Current (A): | 194.217 |
| No-Load Input Power (W): | 871.026 |
| Cogging Torque (Nm): | 1.47273e-12 |

The no load line current is minimum and cogging torque is minimized by skewing the stator slots. The flux density in air gap is maximum and it is as per the choice.

### d) FULL LOAD DATA

| | |
|---|---|
| Maximum Line Induced Voltage (V): | 140.448 |
| Root-Mean-Square Line Current (A): | 189.108 |
| Root-Mean-Square Phase Current (A): | 109.285 |
| Armature Thermal Load (A2 /mm3): | 165.821 |
| Specific Electric Loading (A/mm): | 61.8416 |
| Armature Current Density (A/mm2): | 2.68138 |
| Frictional and Windage Loss (W): | 18 |
| Iron-Core Loss (W): | 195.697 |
| Armature Copper Loss (W): | 786.03 |
| Total Loss (W): | 999.727 |
| Output Power (W): | 34875 |
| Input Power (W): | 35874.7 |
| Efficiency (%): | 97.2133 |
| Synchronous Speed (rpm): | 1000 |
| Rated Torque (Nm): | 333.031 |
| Torque Angle (degree): | 76.8727 |

The proposed IPMSM on full load gives the satisfactory results as shown above. The full load torque and the output power is as per the requirements and the efficiency is improved by different ways as discussed in section 3 of design analysis.

### e) PERFORMANCE ANALYSIS

The design is optimized and the results are obtained for the different core diameter and length, tooth and slot dimensions and rotor geometry.

**Table 6.** IPMSM Optimized Design Sheet

| Specification | Value |
|---|---|
| Operation Type: | Motor |
| Mechanical Load Type | Constant Power |
| Power Output (kW) | 35 |
| Voltage (V) | 440 |
| Number of Poles | 8 |
| Speed (rpm) | 1300 |
| Stator slots No. | 48 |
| OD of Stator (mm) | 380 |
| ID of Stator (mm) | 250 |
| Length of Stator Core (mm) | 90 |
| No. of Conductors per slot | 10 |
| ID of Rotor (mm) | 90 |
| Rotor Structure Type | Bridge |
| Type of Magnet | NdFe 35 |
| Line Current on No-Load (A) | 142.065 |
| Input Power on No-Load (W) | 797.553 |
| No-Load Air Gap Flux Density (Tesla) | 0.761 |

| Specification | Value |
|---|---|
| Cogging Torque | 2.1148e-12 |
| Line Voltage (V) | 208.986 |
| RMS Line Current (A) | 133.703 |
| RMS Phase Current (A) | 77.7342 |
| Armature Thermal Load (A2/mm3) | 136.465 |
| Specific Electric Loading (A/mm) | 47.5067 |
| Total Loss (W) | 815.153 |
| Power Output (W) | 34840.1 |
| Power Input (W) | 35655.2 |
| Efficiency (%) | 97.71 |
| Synchronous Speed (rpm) | 1300 |
| Rated Torque (Nm) | 255.922 |
| Torque Angle (degree) | 70.2798 |

The cogging torque is reduced by skewing the stator slots. The curve shown in Fig. 9 and indicates the zero-cogging torque for different air gap positions. Here the stator slots are skewed by two slots so that the cogging torque is reduced to zero value.

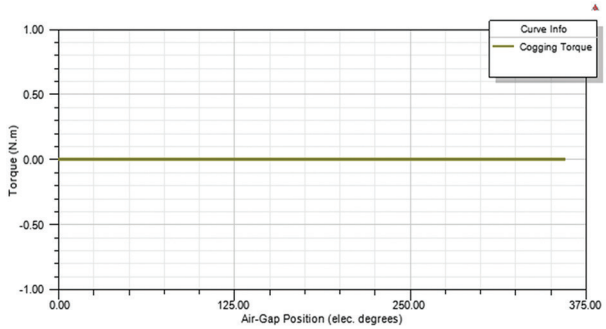


**Fig. 9.** Cogging Torque

The skewing of the stator slots by two slots optimized the $B_{gmax}$ as shown in Fig. 10.

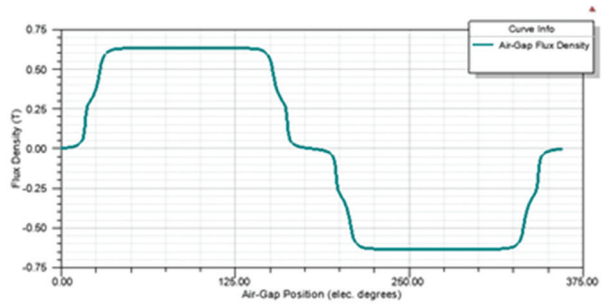


**Fig. 10.** Flux Density in Air gap

The sinusoidal nature of the phase currents and line currents as presented in Fig. 11 indicates the normal working of the motor on full load.

The skewing of the stator slots also improves the phase voltage as shown in Fig. 12 which is sinusoidal in nature.

The stability of the system depends upon the power torque angle characteristics of the motor. The curve shown in Fig. 13 indicates the satisfactory operation on the motor.

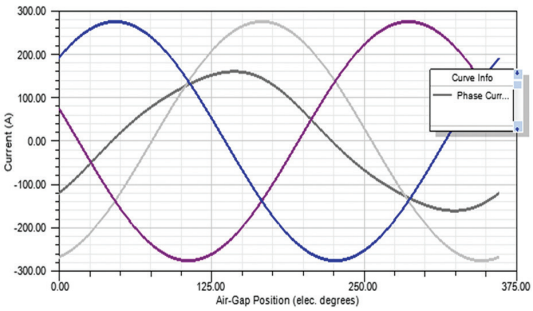


**Fig. 11.** Phase and line Currents

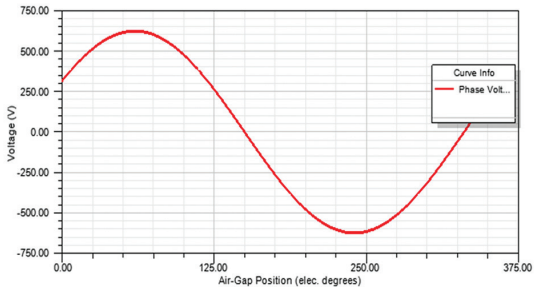


**Fig.12.** Phase Voltage

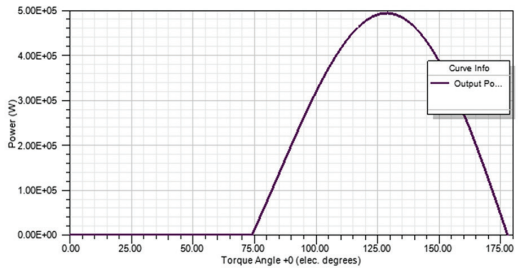


**Fig. 13.** Output Power and Torque Angle Characteristics

The curve of induced phase voltage with respect to the air gap positions is shown in Fig. 14 and indicates the better performance of the motor as the induced phase voltage is almost sinusoidal in nature.

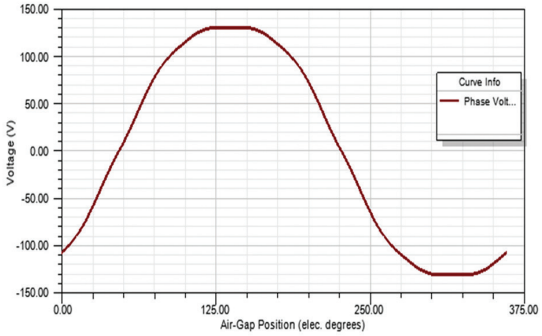


**Fig. 14.** Induced phase voltage at rated speed with respect to the air gap

## 6. COMPARISON OF PERFORMANCE

The performance of the IPMSM machine can be compared with the 3-Phase Induction motor for the same power rating but to the higher side of 55 kW. The data of the 3-phase induction motor is available and the PMSM is analyzed for the same rating using RMxprt.

**Table 7.** Comparison of Performance

| Parameters | 3-Phase Induction Motor | PMSM |
|---|---|---|
| Power Rating (kW) | 55 | 55 |
| Full Load Current (Amp) | 110 | 63 |
| Speed (RPM) | 1500 | 1500 |
| Losses (Copper) (W) | 2500 | 282.153 |
| Losses (Total) (W) | 3760 | 713.935 |
| %Efficiency | 93.6 | 98.71 |
| Frame Size | 225 M | 225 M |
| Stack Length (mm) | Not exactly Known, but it could be large in length | 110 mm |

The performance of both the machines can be compared on the basis of the different losses in the motor. The following table shows the percentage of the losses due to the motor components.

**Table 8.** Comparison of Losses

| 3-Phase Induction Motor | | PMSM | |
|---|---|---|---|
| Motor Component Loss | Total Loss % | Motor Component Loss | Total Loss % |
| Stator copper Losses, $I^2 R_1$ | 37% | Armature copper Losses, $I^2 R_1$ | 39% |
| Rotor copper Losses, $I^2 R_2$ | 18% | Rotor copper Losses, $I^2 R_2$ | 00% |
| Magnetic Core Losses | 20% | Magnetic Core Losses | 57% |
| Friction and Windage Losses | 9% | Friction, Windage and Stray Load Losses | 4% |
| Stray Load Losses | 16% | | |

It is observed from the comparison of the performance and losses that the

- PMSM is Highly Efficient with reduced full load current and increased full load voltage.
- PMSM is compact in size as instead of rotor winding permanent magnets are used. The stack length for the required output gets reduced.
- As the efficiency if High, it will act as a Energy Saver.

## 7. CONCLUSION

This paper presented the design of (IPMSM) Interior Permanent Magnet Synchronous Motor and the analysis shows that the motor is compact in size, have high efficiency, constant full load torque and adjustable speed up to rated speed.

The final rating of the motor is 35 kW, 1000 rpm, 440 V, 8 Pole, 100 Hz frequency, rated torque 333 N-m, torque angle 70° and maximum output power is 37 kW. Volumetric ratios are 1) armature copper to core = 2.02 2) Armature copper to steel = 0.99 3) Armature copper to Magnet = 6.64 as per the finite element analysis and design calculations.

The existing 3-phase Induction Motor is larger in size and can be replaced by PMSM for the same frame size but with reduced weight and stack core length.

The Adjustable Speed Permanent Magnet Synchronous Motor with better dynamic performance is proposed. The analytical results verify that the satisfactory performance can be achieved with the proposed machine.

The proposed IPMSM has minimum total loss, improved efficiency and maximum torque as per kW and speed rating of the motor. The full load and no-load parameters are optimized by analyzing the machine for different voltage ratings, power ratings and stator outside diameters.

The proposed motor is compact in size as NdFe permanent magnets with bridge type structure is used and cost effective, saves energy as reduced generator rating is used which reduces the operating cost.

When compared with the 3-Phase Induction Motor, the Proposed PMSM has several advantages as follows:

1) No excitation losses
2) Simplified Construction
3) Improved Efficiency
4) Fast Dynamic Performance
5) High Torque or Power per unit volume

## 8. REFERENCES


[1] D. Karthigha, A. Patel, "Design and Analysis of Permanent Magnet Synchronous Generator for Wind Energy Conversion System using Ansoft-Maxwell", International Journal of Advance Research and Innovative Ideas in Education, Vol. 3, No. 4, 2017, pp. 2024-2038.

[2] Z. Q. Zhu, W. Q. Chu, Y. Guan, "Quantitative Comparison of ElectromagneticPerformance of Electrical Machines forHEVs/EVs", CES Transactions on Electrical Machines and Systems, Vol. 1, No. 1, 2017.

[3] G. Pellegrino, A. Vagati, B. Boazzo, P. Guglielmi, "Comparison of Induction and PM Synchronous Motor Drives for EV Application Including Design Examples", IEEE Transactions on Industry Applications, Vol. 48, No. 6, 2012.

[4] B. M. Dinh, "Optimal Rotor Design of Line Start Permanent Magnet Synchronous Motor by Genetic Algorithm", Advances in Science, Technology and Engineering Systems Journal, Vol. 2, No. 3, 2017, pp. 1181-1187.

[5] A. Nekoubin, "Design a Line Start synchronous Motor and Analysis Effect of the Rotor Structure on the Efficiency", World Academy of Science, Engineering and Technology International Journal of Electrical and Computer Engineering Vol. 5, No. 9, 2011.

[6] EI K. A. N. Tun, T. Tin, "Design of Conventional Permanent Magnet Synchronous Motor used in Electric Vehicle", International Journal of Scientific Engineering and Technology Research, Vol. 3, No. 16 2014, pp. 3289-3293.

[7] B. N. Chaudhari, S. K. Pillai, B. G. Pernandes, "ENERGY EFFICIENT LINE START PERMANENT MAGNET SYNCHRONOUS MOTOR", Proceedings of IEEE TENCON '98. IEEE Region 10th International Conference on Global Connectivity in Energy, Computer, Communication and Control, New Delhi, India, 17-19 December 1998.

[8] P. S. Shindeand, A. G. Thosar, "Design of Permanent Magnet Synchronous Motor", International Journal of Scientific & Engineering Research, Vol. 6, No. 1, 2015.

[9] A. S. Arora, G. Singh, "Review of Design and Performance of Permanent Magnet Synchronous Motor", International Journal of Industrial Electronics and Electrical Engineering, ISSN: 2347-6982 Vol. 3, No. 10, 2015.

[10] W. Wang, R. Fu, Y. Fan, "Electromagnetic Parameters Matching of Permanent Magnet Synchronous Motor for Hybrid Electric Vehicles", 2018, IFAC International Federation of Automatic Control, pp. 407-414.

[11] L. Jian, K. T. Chau, Y. Gong, C. Yu, W. Li, "Analytical Calculation of Magnetic Field in Surface-Inset Permanent Magnet Motors", IEEE Transactions on Magnetics, Vol. 45, No. 10, 2009.

[12] Divya, Visalakshi, Vijayalakshmi, "Design Optimization of PM AC MachinesUsing Differential Evolution andComputationally Efficient-FEA", International Journal of Advanced Research in Electrical, Electronics and Instrumentation Engineering, Vol. 3, No. 4, 2014.

[13] A. Rahideh, T. Korakianitis, "Analytical Magnetic Field Distribution of Slotless Brushless MachinesWith Inset Permanent Magnets", IEEE Transactions on Magnetics, Vol. 47, No. 6, 2011.

[14] A. J. Sorgdrager, R.-J. Wang, A. J. Grobler, "Design procedure of a line-start permanent magnet synchronous machine", Proceedings of the 22nd South African Universities Power Engineering Conference, 9 October 2014.

[15] S. Paitandi, M. Sengupta, "Design, Fabrication and Parameter Evaluation of aSurface Mounted Permanent Magnet Synchronous Motor", Proceedings of the IEEE International Conference on Power Electronics, Drives and Energy Systems, Mumbai, India, 16-19 December 2014.

[16] S. Nanda, M. Sengupta, "Design, Fabrication and Analytical Investigations ona Permanent Magnet Synchronous Generator", Proceedings of the IEEE International Conference on Power Electronics, Drives and Energy Systems, Mumbai, India, 16-19 December 2014

[17] B. N. Chaudhari, B. G. Fernandes, "Permanent Magnet Synchronous Motor for General Purpose Energy Efficient Drive", IEEE Power Engineering Society Winter Meeting. Conference Proceedings, Singapore, 23-27 January 2000.

[18] R. Ambekar, S. Ambekar, "Design investigation for continual torque operative performanceof PMSM for vehicle", Sådhanå, Vol. 45, No. 120, 2020.

# A Cost-Effective Method for Power Factor Metering Systems

Case Study

**Ahmed M. T. Ibraheem Al-Naib**
Northern Technical University,
Technical Engineering College, Department of Electrical Power Technology Engineering, Mosul, Iraq
ahmed_alnaib2018@ntu.edu.iq

**Bashar Abdullah Hamad**
Northern Technical University,
Technical Engineering College, Department of Electrical Power Technology Engineering, Mosul, Iraq
bashar.hamad@ntu.edu.iq

***Abstract*** *– The power factor (PF) is an important measurement in an AC electrical system that indicates how much power is utilized to accomplish productive work by a load and how much power is consumed. As a result, it's one of the primary causes of excessive energy costs and power outages. This paper aims to present a simple, cost- effective, and accurate PF metering and monitoring system implemented using an Arduino microcontroller with a novel methodology different from other papers. The proposed method is to design the software code instead of using external components of Zero-Crossing Detectors (Z-CDs) for both voltage (V) and current (I) signals, and instead of using Exclusive-OR (X-OR) gates also. Determining the phase-angle and PF in an efficient manner can be useful in many approaches to electrical systems: 1-for synchronization of parallel connections of alternators; 2-for directional protection systems; 3-for PF correction and load management; and 4-for designing watt/energy meters. Using the Proteus 8 Professional (ISIS program), the proposed designed circuit was simulated for more verification. The simulation and experimental findings are presented to validate the proposed metering system's effectiveness.*

***Keywords****: Power factor, phase-angle, Zero-Crossing Detectors, Microcontroller, Wattm eter.*

## 1. INTRODUCTION

Technology is developing at a fast pace, and so is energy consumption. There is an immediate necessity for us to exceed from electro-dynamic meters to digital meters that calibrate them efficiently. Because of the mechanical components in the meter, the commonly used electro-dynamic meters are subject to variations in temperature and time. They're additionally sensitive to flux variation and its dependency. Accurate measurement of the PF for electrical energy is becoming a developing topic among researchers since it distributes electrical energy at an acceptable cost. The cost of electrical energy rises as a result of power losses in transformers, transmission lines, and loads [1, 2]. Due to its versatile features and rich library functionalities, the Arduino is gaining traction in this field (i.e., measurement devices and monitoring systems). It is robust, fast, and user-friendly all at the same time. Many methods for measuring, monitoring, and detecting defects in electrical systems based on microcontrollers have been employed. [3]. There are many previous studies and research on metering the PF: The authors of [4] created a PF measurement circuit prototype. A Z-CD (based on operational amplifiers of the LM358-type) is employed. The logical signals obtained from the detector are fed into the PIC16F877 microcontrollers. PIC16F877 performs the conversion of the difference between the V and I logical signals of the load into time in seconds and angle in degrees, as well as calculates the PF. On the LCD panel is displayed the PF measurement value. The authors of [5] designed and built a single-phase PF meter using an Arduino Nano-type. Two operational amplifiers (LM358) were used as Z-CDs for both V and I signals. Both logical signals from the Z-CDs are sent to the Exclusive-OR (X-OR) gate (4030). The information gotten by the X-OR gate is sent to Arduino for calculation of the phase-shift (Θ) and the corresponding PF using cos (Θ) and the results are displayed on the 16×2 LCD. The authors of [6] have designed an automotive PF correction system that always measures and displays the instant value of PF. If the PF deviates from the specified limits, then the switching of capacitors is done

automatically. If the PF is not set within the limits, the information regarding this will be sent to the industry manager through the Internet of Things (IOT) for necessary actions. The major components that were used in this system are the Potential (PT) and Current Transformer (CT), two UA741 op-amps, a 7486 XOR gate IC, the Arduino Uno, the relay module, power capacitors, a 16 x 2 LCD display, an ESP8266 Wi-Fi module, and various kinds of electrical loads. The authors of [7] present a multi meter to measure electric parameters like real power, reactive power, and PF of different loads where data processing is FPGA based. The meter includes an ADS1220, which is a 24-bit ADC interfacing with an FPGA (Artix 7), which provides V and I digital samples. The main problem with this method is that it requires an external ADC, which adds to the complexity and cost of the whole thing. The author [8] used the Arduino Mega type for calculating the PF and activating the relays that connect the capacitor banks to the load in parallel as an automatic PF correction. A PT and a CT were used to step down and measure the V and I of the load. The V and I waveforms obtained from PT and CT were sent to the Z-CD circuits, which contain LM324 operational amplifiers to change the waveform of the V and I from sinusoidal to square. The outputs of the Z-CD circuits are fed to the XOR (3040) gate, which produces a series of pulses. The amplitude and width of these pulses are then calibrated to obtain the phase angle between V and I. The author [9] measured the PF with Arduino. A ZMPT101B AC voltage sensor and a non-invasive SCT-013-050 split core CT were used. Op-Amps (LM324N) were utilized for Z-CDs on the I and V signals. The XOR gate (IC4030) output will determine whether there is a phase shift between V and I or not, comparing the time delay for each input value. Table 1 lists the advantages and disadvantages of the proposed metering method compared with the traditional method for determining the PF.

**Table 1.** Comparison between the existing solution method and the proposed method for metering PF

| Existing solution in [4 - 9] | Proposed method |
|---|---|
| Use an external component that works as a Z-CD for both V and I signals | Eliminate using external components such as Z-CDs |
| Use an external component (X-OR gate) to find out the phase-angle between both the V and I signals. | Eliminate using external X-OR gate |
| High cost | Low cost |
| High complexity | Low complexity |
| Restricted to a sinusoidal waveforms | Restricted to a sinusoidal waveforms |

## 2. DISPLACEMENT PF METERING METHOD

When both voltage and current have a sinusoidal waveform, the PF value equals the cosine of the angle between them and can be known as the displacement PF. The traditional method for determining the displacement PF depends on using external circuits for Z-CDs for both V and I signals and an external X-OR gate (see Fig 1: a). First, the Z-CD circuits, which are based on operational amplifiers, convert the sine wave signals coming from VT and CT with different amplitudes to logical signals (V & I), and then these two logical signals are applied to the X-OR gate to find out the phase-angle between them, as shown in Fig. 1: b. [1, and 10].

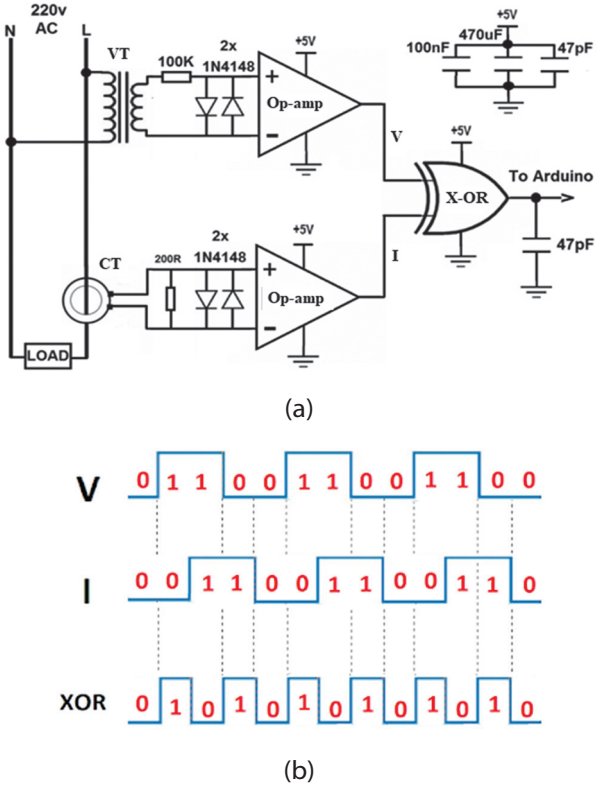


(a)

(b)

**Fig. 1.** Circuit diagram of PF determination

When the load type is resistive, the X-OR gate output is LOW logic because both V and I waveforms begin and end at the same time, but when the load type is inductive or capacitive, the X-OR output is HIGH logic because there is a phase-shift between V and I. By measuring the duration time (dt) difference between the V and I waveforms (XOR output ON-time in seconds) and putting it in equation (1), the Arduino can find the PF.

$$PF = \cos(f * dt * 360). \quad (1)$$

Where: f : frequency (Hz) of the supply voltage.

## 3. PF ANALYSIS UNDER NON-SINUSOIDAL WAVEFORMS

The displacement PF methods may present unacceptable errors under non-sinusoidal voltages and current waveforms. In general, the definition of the PF under non-sinusoidal waveforms is as the ratio between the active power (P) and the apparent power (S), as the current waveform distortion prevents accurately detecting the zero crossing points and the phase displacement of the current with respect to the voltage. So the calculation of P and S requires consideration. These calculations

are estimated according to the instantaneous values of the current (Ii) and voltage (Vi) measured on the load, so this method is known as the instantaneous power calculation method. Based on these quantities, it is possible to calculate the rms current ($I_{rms}$), the rms voltage ($I_{rms}$), P, S, and then the PF, according to (2)–(6) equations [11-14]:

$$I_{rms} = \sqrt{\frac{\sum_{i=1}^{n} I_i^2}{n}} \quad (2)$$

$$V_{rms} = \sqrt{\frac{\sum_{i=1}^{n} V_i^2}{n}} \quad (3)$$

$$P = \frac{1}{n}\sum_{i=1}^{n} V_i * I_i \quad (4)$$

where n is the number of samples.

$$S = V_{rms} * I_{rms} \quad (5)$$

$$PF = \frac{P(W)}{S(VA)} \quad (6)$$

## 4. PROPOSED METHODS FOR MEASURING THE PF

The circuit diagram of the proposed system is simply composed of voltage and current transformers, signal conditioning circuits for V and I signals, an Arduino, and a 4 x 20 LCD, as presented in Fig. 2. In this work, there are abridgments in using external electrical elements compared to Fig. 1, which saves installation time and space in the prototype. It also does not increase the cost and complexity of the system.

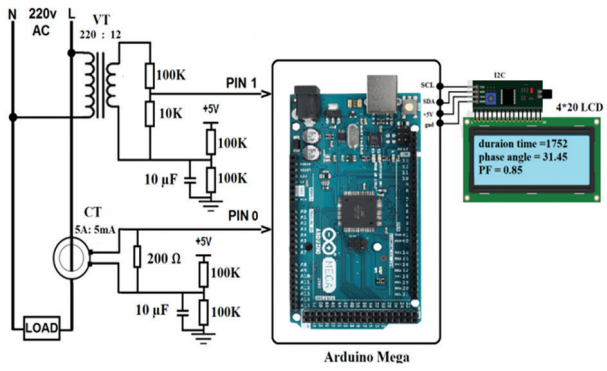


**Fig. 2.** Circuit diagram of the proposed system

The AC supply voltage of 220 volts is stepped down to 12 volts AC via a VT. This 12 volt signal is divided and stepped down into a 1.5 volt sine wave signal by a voltage divider circuit. The AC voltage (1.5 volts) alternates from positive to negative values with respect to ground (0 volt). However, the analog inputs of the Arduino require positive voltage values. So a 2.5 volt DC offset is applied to the input sine wave signal. As a result, the whole input sine wave can be sensed at the positive threshold (0 – 5 volts). The V signal remains positive because it will now swing above and below 2.5 volts. The Arduino can read the entire sine wave signal through its analog input (pin A1). The I signal flowing through the load is retrieved through a CT, which has a 5 A: 5 mA rating. A shunt resistor (also called a burden resistor) converts the I signal into a voltage form that represents the properties of the current sine wave. As in the V signal, a DC offset voltage of 2.5 volts is applied to the sine wave signal so that the reference point is lifted up and the entire sine wave can be read in analog mode (pin A0) within its operative range (0-5 volts).

## 5. DESIGN FLOW OF THE SYSTEM

The design flow of the system software implementation is an important part of this system. The microcontroller is programmed to calculate the PF and display it on the LCD. The flowchart for the PF measurement is shown in Fig. 3.

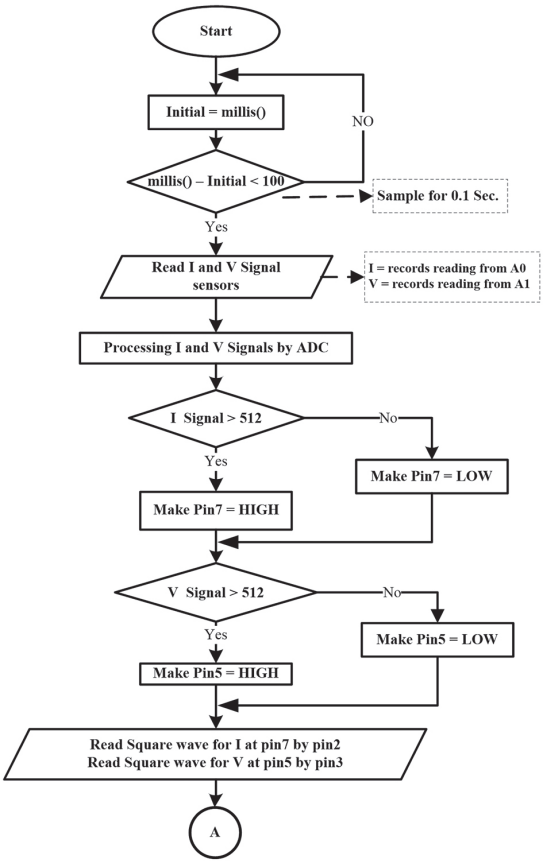


(a) Flowchart of the Z-CD algorithm,

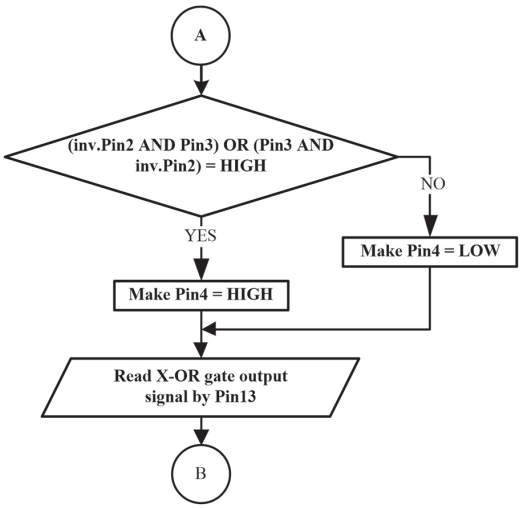


(b) Flowchart of the X-OR algorithm,

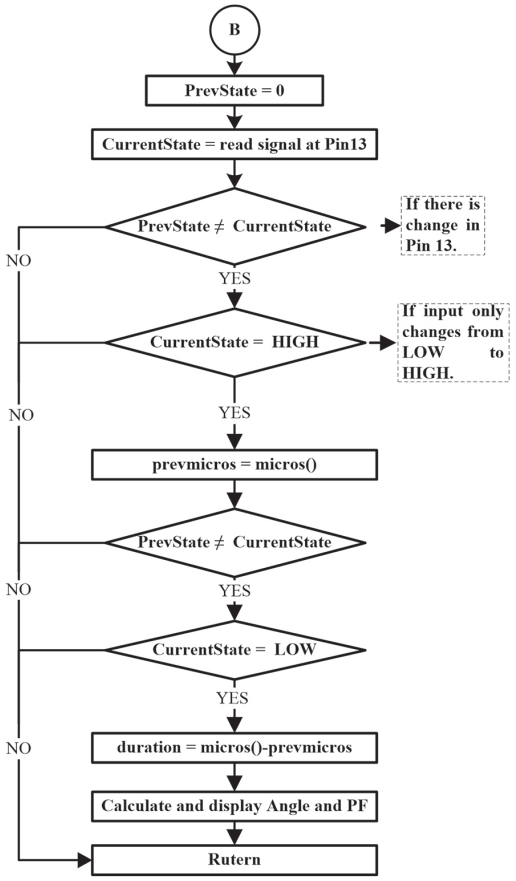


(c) Flowchart for time duration & PF determination

**Fig. 3.** Flowchart of the proposed PF measuring System

Instead of using an external component of the Z-CDs, the offsetting signals of V and I are converted to square waves via the proposed Arduino code by comparing these signals with defined values (bias level, which represents zero level). Fig. 3 (a): Using the proposed code of the Z-CD algorithm, the Arduino generates a HIGH state signal at pin 7 and pin 5 when the I and V signals exceed this defined value (512 bits, which is equal to the 2.5 volt value at the analog input of the Arduino, which is also equal to the value 0A at the secondary side of CT and 0 volt at the secondary side of VT). Also, the Arduino generates a "low state" signal when the signal is lower than this defined value. In other words, by the code, the Arduino will produce a high-logic square wave signal (5 volts) at the positive half-cycle of both V and I signals, and for the negative half-cycle, the square wave will have low logic (0 volts).

Instead of using an external component of the X-OR gate, this gate is implemented programmatically via Arduino code, as shown in Fig. 4 according to the flowchart of the X-OR gate implementation shown in Fig. 3 (b). The implementation code depends on the equivalent circuit of the X-OR gate function, which is shown in Fig. 5. The output signal of the X-OR gate (ON-time) represents the time difference between the V and I waveforms. Fig. 3 (c) represents the flowchart for determining this duration time. Finally, the mentioned equation 1 was programmed to find the PF.

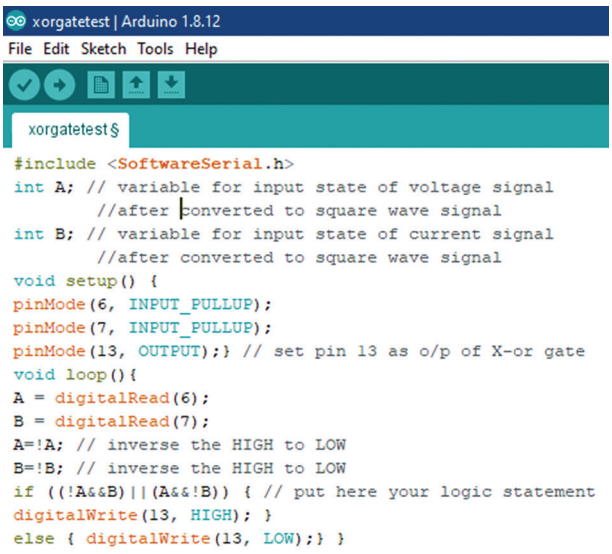


**Fig. 4.** Software implementation code of the X-OR gate

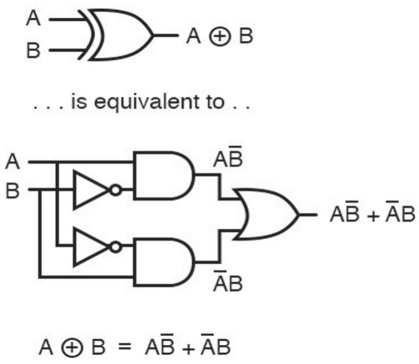


**Fig. 5.** Equivalent circuit of X-OR gate

## 6. SIMULATION CIRCUIT OF THE PROPOSED SYSTEM

The proposed measuring system shown in Fig. 2 was simulated as shown in Fig. 6 using the Proteus 7 Professional.

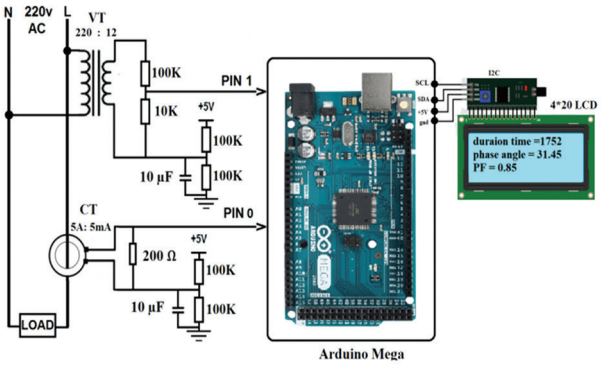


**Fig. 6.** Simulation circuit diagram of the proposed PF metering system

## 7. SIMULATION RESULTS

The proposed design is tested at various sorts of loads (resistor and inductor). Figure 7 shows the wave-

forms of the V and I signals (a:1 and b:1 blue and yellow, respectively) of a resistive and inductive load and their square waveforms (green and red, respectively), which are considered as input signals to the X-OR gate. The second figure (a:2 and b:2) shows the output signal from the X-OR gate, which represents the phase difference between the V and I signals. Figures (a:3 and b:3) (serial monitor), which show the instantaneous values of the duration time, phase-angle, and PF.

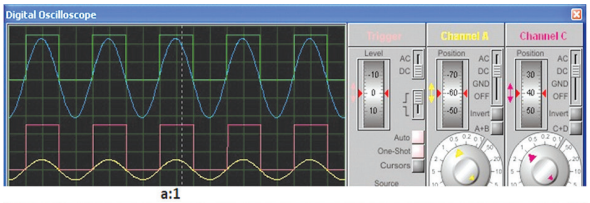


a:1

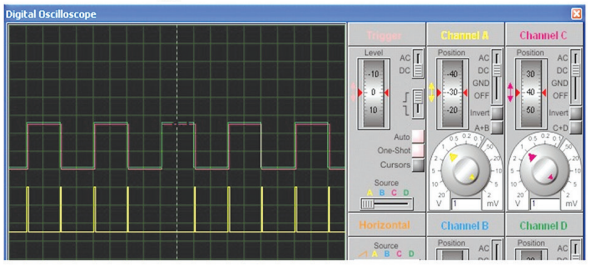


a:2

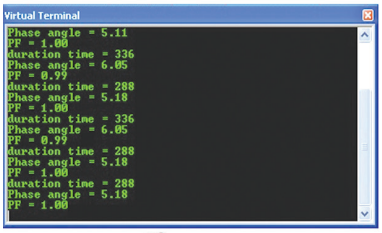


a:3

(a) Resistive load

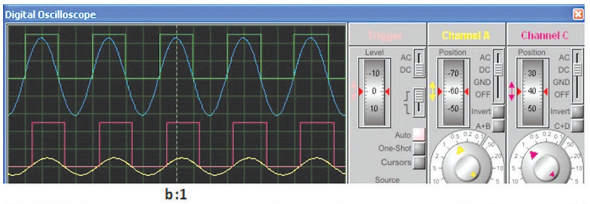


b:1

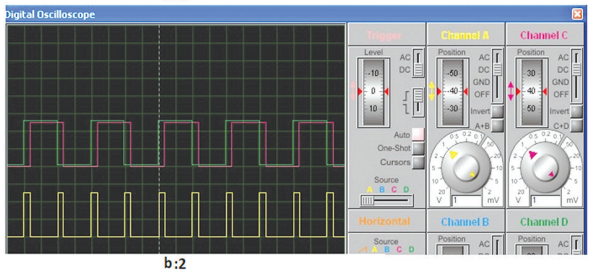


b:2

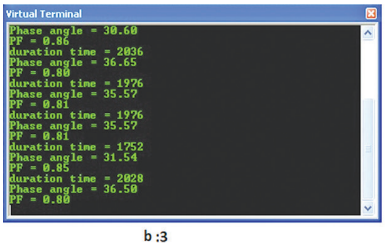


b :3

(b) Inductive load

**Fig. 7.** Waveform of the proposed method

It's observed from Fig. 7 (a) that at resistive load, the time difference between the V and I waveform is very small, approximately zero, and so the phase-angle is very small, so the PF is unity. While in the inductive load in Fig. 7 (b), there is a clear time difference between the V and I signals which equal to 1.988 milliseconds (phase-shift equal to 34.35°) and so the PF is equal to 0.81.

## 8. EXPERIMENTAL RESULTS

Fig. 8 presents the prototype of the proposed circuit. Practically, the proposed design circuit is tested at various types of loads (resistive load using a tungsten filament bulb, and inductive load using an induction motor).

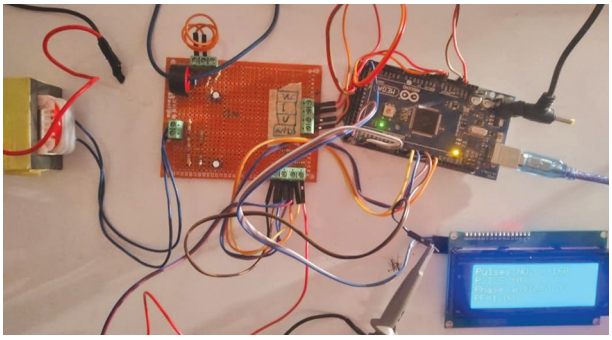

**Fig. 8.** Experimental setup of the proposed circuit

Fig. 9 shows the signals that are taken from the Arduino for both resistive (Fig. 9: a) and inductive load (Fig. 9: b). These waveforms are the square waveform of the V signal (yellow waveform), the square waveform of the load I signal (blue waveform), and the output of the X-OR (red waveform). The X-OR gate output will be HIGH logic when the inputs have a phase-shift between V and I signals and the time of this period represents the duration time.

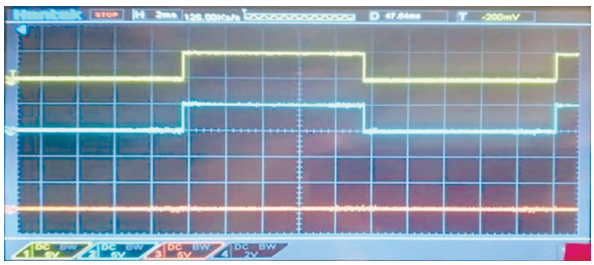

(a)

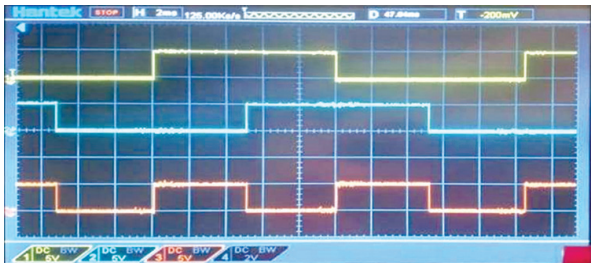

(b)

**Fig. 9.** Experimental Arduino waveforms of the proposed circuit

Fig. 10 presents the real-time measurement of the time duration, phase-shift, and PF on the LCD for both resistive and inductive loads.

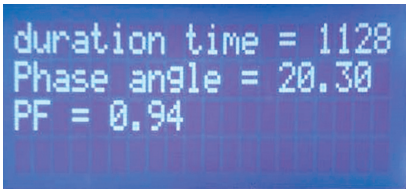


(a)

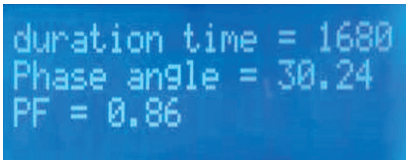


(b)

**Fig. 10.** Real-Time monitoring of the PF

## 9. CONCLUSIONS

The proposed work provides one of the simplest ways to measure and monitor the PF. This method eliminates the use of some external components such as Z-CD circuits and X-OR gates. Thus, the proposed design costs less due to the savings from the eliminated components, which also leads to a smaller size and volume. So, the market approach is possible, and a commercial version would be suitable and could easily integrate. The PF metering circuit has been designed and tested using the Proteus simulator before practical implementation. The proposed method of metering the PF is limited to linear loads only with a sinusoidal terminal voltage that draws a sinusoidal load current. So, for harmonics-rich non-linear loads, the instantaneous power calculation method can be adopted in future work. Also, practical implementation of this work can be done, and the measuring data can be monitored based on IOT devices such as Wi-Fi. In addition to designing and developing a PF correction via compensation for the lagging PF by adding relay and capacitor banks to the designed circuit, wattmeter, energy meter, digital phase sequence meter, and directional protection relay based on the proposed system.

## 10. REFERENCES

[1] S. V. Nemani, D. Shahi, I. K. Vibhav, "Design and Implementation of Digital Energy Meters with Power Factor Measurement and Load Indication Feature", Proceedings of the IEEE 8th Power India International Conference, Kurukshetra, India, 10-12 December 2018, pp. 1-6.

[2] S. R. Fahim, S. S. Avro, S. K. Sarker, "A novel fractional order power factor measurement", SN Applied Sciences, Vol. 1, 2019, p. 1611.

[3] J. A. Ahmed, M. T. Ahmed, A. Ibraheem, O. T. Mahmood, "Design of a Smart Control and Protection System for Three-Phase Generator Using Arduino", Proceedings of the The Fourth Scientific Conference for Engineering and Postgraduate Research, Baghdad, Iraq, 16-17 December 2019.

[4] S. Rustemli, M. Ates, "Measurement and Simulation of Power Factor using PIC16F877", PRZEGLĄD ELEKTROTECHNICZNY Journal, Vol. 2012, No. 6, 2012, pp. 290-294.

[5] A. A. Mukaila, I. Olugbemi, E. E. Sule, "Design and Construction of A Single-Phase Power Factor Meter", Electrical Science & Engineering, Vol. 2, No. 2, 2020, pp. 11-14.

[6] M. Pampalle S. Srikanth, V. C. J. Mohan, T. R. Babu, "IOT-Based Automatic Power Factor Correction Unit for Industries to Curtail the Retribution of Power Utility Companies", Proceedings of Smart Systems: Innovations in Computing, Vol. 235, 2021.

[7] K. Parimala, K. C. R. Nisha. "FPGA Based Power Quality Monitoring Using FFT Method For Single Phase Power Metering", Proceedings of the International Conference on Emerging Technological Trends, Kollam, India, 21-22 October 2016.

[8] B. Rija, M. K. Hussain, A. M. Vural. "Microcontroller Based Automatic Power Factor Correction for Single-Phase Lagging and Leading Loads", Engineering, Technology & Applied Science Research, Vol. 10, No. 6, 2020, pp. 6515-6520.

[9] O. Andrei et al. "IoT Power Monitoring Device Using Wi-fi and Arduino", Proceedings of the 9th International Conference on Modern Power Systems, Cluj-Napoca, Romania, 16-17 June 2021.

[10] C. M. Diniș et al. "Power Factor Measuring Device Using Microcontroller for Single-Phase Consumers", Proceedings of the International Conference on Applied Science, Vol. 1781, 2021, pp. 1-13.

[11] F. P. Marafao, S. M. Deckmann, J. A. G. Marafao. "Power Factor Analysis Under Non-sinusoidal and Unbalanced Systems", Proceedings of the 10th International Conference on Harmonics and Quality of Power, Vol. 1, 2002.

[12] D. Slomovitz, "Behavior of Power-factor Meters Under Non-Sinusoidal Current and Voltage", In-

ternational Journal of Electronics Theoretical and Experimental, Vol. 70, No. 4, 1991, pp. 827-838.

[13] P. P. Machado et al. "Power Factor Metering System Using Arduino", Proceedings of the IEEE Workshop on Power Electronics and Power Quality Applications, Bogota, Colombia, 31 May - 2 June 2017.

[14] T. S. Gunawan et al. "Development of Power Factor Meter Using Arduino", Proceedings of the IEEE 5th International Conference on Smart Instrumentation, Measurement and Application, Songkhla, Thailand, 28-30 November 2018

# INTERNATIONAL JOURNAL OF ELECTRICAL AND COMPUTER ENGINEERING SYSTEMS

Published by Faculty of Electrical Engineering, Computer Science and Information Technology Osijek,
Josip Juraj Strossmayer University of Osijek, Croatia.

## About this Journal

The International Journal of Electrical and Computer Engineering Systems publishes original research in the form of full papers, case studies, reviews and surveys. It covers theory and application of electrical and computer engineering, synergy of computer systems and computational methods with electrical and electronic systems, as well as interdisciplinary research.

## Topics of interest include, but are not limited to:

- Power systems
- Renewable electricity production
- Power electronics
- Electrical drives
- Industrial electronics
- Communication systems
- Advanced modulation techniques
- RFID devices and systems
- Signal and data processing
- Image processing
- Multimedia systems
- Microelectronics
- Instrumentation and measurement
- Control systems
- Robotics
- Modeling and simulation
- Modern computer architectures
- Computer networks
- Embedded systems
- High-performance computing
- Parallel and distributed computer systems
- Human-computer systems
- Intelligent systems
- Multi-agent and holonic systems
- Real-time systems
- Software engineering
- Internet and web applications and systems
- Applications of computer systems in engineering and related disciplines
- Mathematical models of engineering systems
- Engineering management
- Engineering education

## Paper Submission

Authors are invited to submit original, unpublished research papers that are not being considered by another journal or any other publisher. Manuscripts must be submitted in doc, docx, rtf or pdf format, and limited to 30 one-column double-spaced pages. All figures and tables must be cited and placed in the body of the paper. Provide contact information of all authors and designate the corresponding author who should submit the manuscript to https://ijeces.ferit.hr. The corresponding author is responsible for ensuring that the article's publication has been approved by all coauthors and by the institutions of the authors if required. All enquiries concerning the publication of accepted papers should be sent to ijeces@ferit.hr.

The following information should be included in the submission:

- paper title;
- full name of each author;
- full institutional mailing addresses;
- e-mail addresses of each author;
- abstract (should be self-contained and not exceed 150 words). Introduction should have no subheadings;
- manuscript should contain one to five alphabetically ordered keywords;
- all abbreviations used in the manuscript should be explained by first appearance;
- all acknowledgments should be included at the end of the paper:
- authors are responsible for ensuring that the information in each reference is complete and accurate. All references must be numbered consecutively and citations of references in text should be identified using numbers in square brackets. All references should be cited within the text;
- each figure should be integrated in the text and cited in a consecutive order. Upon acceptance of the paper, each figure should be of high quality in one of the following formats: EPS, WMF, BMP and TIFF;
- corrected proofs must be returned to the publisher within 7 days of receipt.

## Peer Review

All manuscripts are subject to peer review and must meet academic standards. Submissions will be first considered by an editor-in-chief and if not rejected right away, then they will be reviewed by anonymous reviewers. The submitting author will be asked to provide the names of 5 proposed reviewers including their e-mail addresses. The proposed reviewers should be in the research field of the manuscript. They should not be affiliated to the same institution of the manuscript author(s) and should not have had any collaboration with any of the authors during the last 3 years.

## Author Benefits

The corresponding author will be provided with a .pdf file of the article or alternatively one hardcopy of the journal free of charge.

### Units of Measurement

Units of measurement should be presented simply and concisely using System International (SI) units.

## Bibliographic Information

Commenced in 2010.
ISSN: 1847-6996
e-ISSN: 1847-7003

Published: semiannually

## Copyright



## Subscription Information

The annual subscription rate is 50€ for individuals, 25€ for students and 150€ for libraries.

## Postal Address

Faculty of Electrical Engineering,
Computer Science and Information Technology Osijek,
Josip Juraj Strossmayer University of Osijek, Croatia
Kneza Trpimira 2b
31000 Osijek, Croatia

# IJECES Copyright Transfer Form

(Please, read this carefully)

This form is intended for all accepted material submitted to the IJECES journal and must accompany any such material before publication.

**TITLE OF ARTICLE** (hereinafter referred to as "the Work"):

COMPLETE LIST OF AUTHORS:

The undersigned hereby assigns to the IJECES all rights under copyright that may exist in and to the above Work, and any revised or expanded works submitted to the IJECES by the undersigned based on the Work. The undersigned hereby warrants that the Work is original and that he/she is the author of the complete Work and all incorporated parts of the Work. Otherwise he/she warrants that necessary permissions have been obtained for those parts of works originating from other authors or publishers.

Authors retain all proprietary rights in any process or procedure described in the Work. Authors may reproduce or authorize others to reproduce the Work or derivative works for the author's personal use or for company use, provided that the source and the IJECES copyright notice are indicated, the copies are not used in any way that implies IJECES endorsement of a product or service of any author, and the copies themselves are not offered for sale. In the case of a Work performed under a special government contract or grant, the IJECES recognizes that the government has royalty-free permission to reproduce all or portions of the Work, and to authorize others to do so, for official government purposes only, if the contract/grant so requires. For all uses not covered previously, authors must ask for permission from the IJECES to reproduce or authorize the reproduction of the Work or material extracted from the Work. Although authors are permitted to re-use all or portions of the Work in other works, this excludes granting third-party requests for reprinting, republishing, or other types of re-use. The IJECES must handle all such third-party requests. The IJECES distributes its publication by various means and media. It also abstracts and may translate its publications, and articles contained therein, for inclusion in various collections, databases and other publications. The IJECES publisher requires that the consent of the first-named author be sought as a condition to granting reprint or republication rights to others or for permitting use of a Work for promotion or marketing purposes. If you are employed and prepared the Work on a subject within the scope of your employment, the copyright in the Work belongs to your employer as a work-for-hire. In that case, the IJECES publisher assumes that when you sign this Form, you are authorized to do so by your employer and that your employer has consented to the transfer of copyright, to the representation and warranty of publication rights, and to all other terms and conditions of this Form. If such authorization and consent has not been given to you, an authorized representative of your employer should sign this Form as the Author.

Authors of IJECES journal articles and other material must ensure that their Work meets originality, authorship, author responsibilities and author misconduct requirements. It is the responsibility of the authors, not the IJECES publisher, to determine whether disclosure of their material requires the prior consent of other parties and, if so, to obtain it.

- The undersigned represents that he/she has the authority to make and execute this assignment.
- For jointly authored Works, all joint authors should sign, or one of the authors should sign as authorized agent for the others.
- The undersigned agrees to indemnify and hold harmless the IJECES publisher from any damage or expense that may arise in the event of a breach of any of the warranties set forth above.

_____ _____

**Author/Authorized Agent** **Date**

**CONTACT**
**International Journal of Electrical and Computer Engineering Systems (IJECES)**
Faculty of Electrical Engineering, Computer Science and Information Technology Osijek
Josip Juraj Strossmayer University of Osijek
Kneza Trpimira 2b
31000 Osijek, Croatia
Phone: +38531224600,
Fax: +38531224605,
e-mail: ijeces@ferit.hr